Description of the Community Climate System Model Version 2 Sea Ice Model

by Bruce P. Briegleb[1] Cecilia M. Bitz[2]

Elizabeth C. Hunke[3] William H. Lipscomb[3] and Julie L. Schramm[1]

May 13, 2002

1 2 3

[1]National Center for Atmospheric Research, PO Box 3000, Boulder CO 80307 (NCAR is sponsored by the National Science Foundation)

[2]University of Washington

[3]T-3 Fluid Dynamics Group, Theoretical Division, Los Alamos National Laboratory, Los Alamos NM 87545

Abstract

Based on CSM1 simulations (Boville and Gent, 1998; Weatherly et al., 1998), the CCSM Polar Climate Working Group (PCWG) recommended a number of improvements to the sea ice component. The CCSM2 sea ice model satisfies all of those recommendations and includes additional parameterizations, representing a major improvement over the previous version. The model consists of: elastic-viscous-plastic (EVP) dynamics (Hunke and Dukowicz, 1997), which includes the effects of metric terms (Hunke and Dukowicz, 2002), energy conserving thermodynamics with a resolved vertical temperature profile and an explicit brine pocket parameterization (Maykut and Untersteiner, 1971; Bitz and Lipscomb, 1999), Lagrangian ice thickness distribution (Thorndike et al., 1975; Bitz et al., 2001), linear remapping for thickness space evolution (Lipscomb, 2001), mechanical redistribution due to rafting and ridging (Hibler, 1980), ice strength computed from energetics (Rothrock, 1975), lateral and bottom melt processes (McPhee, 1992), second order horizontal advection (Smolarkiewicz, 1984), and an albedo parameterization with implicit melt ponds. Five thickness categories adequately resolve newly formed, first year, consolidated, multiyear and ridged ice. Flux exchange with the atmosphere and ocean is evaluated over each thickness category and aggregated. The model uses 2D domain decomposition and time split thermodynamics and dynamics for efficient parallel performance. The code is written using standard MPI and Fortran 90 constructs, and runs efficiently on several platforms. Fundamental equations, numerical approximations/algorithms and output history fields are presented.

Acknowledgments

Recently, the name of CSM (Climate System Model) has been augmented to include another "C" for community, to emphasize the importance of cooperative efforts towards improving and using CCSM (Community Climate System Model). The efforts to improve the sea ice model certainly reflect this community aspect of CCSM. In addition to the authors of this document, the model development benefitted significantly from the contributions of Dick Moritz (UW), John Weatherly (CREL), Judy Curry (CU), Jinlun Zhang (UW), and from NCAR: Marika Holland, Gokhan Danabasoglu, Tony Craig, Brian Kauffman, Matthew Hecht, Peter Gent and Bill Large.

Contents

List of Figures

1 Introduction

The Community Climate System Model (CCSM) is a coupled climate model consisting of atmosphere, ocean, land, and sea ice components which exchange fluxes and states through a coupler. This model is making important contributions to knowledge about past, present, and future climates.

The polar regions are important to the climate system, as they represent the heat sink for energy absorbed in the tropics and transported through temperate latitudes. As such, they are as important in the overall climate system as the more widespread heat source regions of the tropics. It is the dynamic balance of heat source and sink in response to external forcing that determines both the basic climate state of the earth system, as well as its response to changing forcing.

An important component of the polar regions is sea ice, which acts as an insulator between atmosphere and ocean. Sea ice facilitates net heat lost to space at the poles and resulting cold air formation in the atmosphere and deep water formation in the ocean. A realistic representation of sea ice processes is essential for high quality global climate simulations.

The first version of the CCSM sea ice model (CSIM1) represented an initial step towards modeling of sea ice processes. The CSIM1 model included one ice thickness category with the following dependent variables: ice concentration, thickness, snow depth, surface temperature, ice temperature and velocity (Bettge et al., 1996). The thermodynamics was based on (Semtner, 1976) and the dynamics on the cavitating fluid rheology of (Flato and Hibler, 1992). Initial CSM1 coupled experiments resulted in some significant biases in Arctic ice thickness (Boville and Gent, 1998; Weatherly et al., 1998). While there was concern in the CCSM community over the biases in atmospheric and oceanic forcing in the coupled model, over the past two years the CCSM PCWG has identified a number of areas of needed improvement in the sea ice model itself. In particular, it was recommended that all of the following be implemented: (1) a plastic rheology with an elliptical yield curve, (2) enhanced sea ice thermodynamics, (3) an ice thickness distribution, (4) elimination of spurious polar convergence near the north pole, (5) an ice model on the same grid as the ocean model, (6) an efficient parallel version of the model and (7) an active ice only framework for testing the sea ice model. The CCSM2 sea ice model meets all of these recommendations.

To meet recommendation (1), the EVP dynamics of Hunke and Dukowicz (1997) was implemented, which adds to the basic viscous/plastic (VP) rheology of (Hibler, 1979) stress tensor equation an elastic term for elastic wave regularization. In the limit of large viscosities, the EVP solutions asymptote to the VP solutions. The similarity of simulations with EVP and VP dynamics for identical forcing has been demonstrated (Hunke and Zhang, 1999; Arbetter et al., 1999). The present implementation also includes metric terms (Hunke and Dukowicz, 2002). The momentum and stress tensor equations are solved simultaneously and explicitly in a highly efficient parallel manner.

To meet recommendation (2), the energy conserving thermodynamics of Bitz and Lipscomb (1999) was implemented. This thermodynamics model represents the effects of brine pockets explicitly through a temperature and salinity-dependent energy of melting. The vertical temperature is calculated using a prescribed and time-invariant salinity profile. Penetrating shortwave radiation is computed for two spectral bands.

To meet recommendation (3), the ice-thickness distribution of Thorndike et al. (1975) was implemented in a Lagrangian thickness-space form (Bitz, 2000; Bitz et al., 2001). The Lagrangian representation of ice thickness within fixed category limits causes minimal diffusion. Resolving thin ice categories allows for

more realistic ocean/atmosphere heat and momentum exchange, compared to a single ice thickness category. Rafting and ridging due to dynamic convergence are represented using Hibler (1980), which also allows explicit calculation of ice strength used in the dynamics (Rothrock, 1975). Improved lateral and bottom heat exchange was also implemented (McPhee, 1992).

The sea ice model uses the same displaced pole grid as the ocean component to meet recommendations (4) and (5). This removes the singularity of the pole from the computational grid. To meet recommendation (6), the parallel code of Hunke and Lipscomb (2002) was implemented. This code uses a 2D (two dimensional) domain decomposition, effectively dividing the global computational domain into a number of rectangular subdomains, each of which is run on a separate processor. In addition, the thermodynamics and dynamics are time split resulting in further performance enhancement.

To meet recommendation (7), a simple mixed layer ocean model was developed to be used with an active ice model within the coupler framework. The active ice only framework (AIO), with prescribed atmosphere and deep ocean forcing, allows for efficient studies with the sea ice model in uncoupled mode.

In addition to meeting the particular recommendations just listed, the CCSM2 sea ice model has also improved horizontal transport, thickness-space evolution, and surface albedo parameterization. The CSIM1 model horizontal transport was first-order accurate upwind differencing, which is known to be highly diffusive. This results in spurious regional smoothing, especially at coarse resolution (e.g. greater than 1°) near ice edge. In version 2, the second order accurate transport scheme of Smolarkiewicz (1984) was implemented. While the Lagrangian thickness distribution adequately treats ice within each category, it suffers from a tendency to underpopulate categories: a dominant single ice thickness moves through the categories during the seasonal cycle of thickening and thinning, crossing thickness categories in the process. A more accurate way of representing thickness space transport was described by Lipscomb (2001) and was implemented. The method uses incremental linear remapping, resulting in a much smoother thickness distribution. The improvement in the albedo parameterization involved adjusting parameterization values to give better agreement with SHEBA observations (Curry et al., 2001).

The purpose of this document is to describe the basic assumptions, fundamental equations, numerical approximations, exchanged fields with the coupler and output history fields for the CCSM2 sea ice model. The present model is designated CSIM4.

The present document is organized as follows. Section 2 gives an overview of CSIM4. It presents the state variables, fundamental equations and boundary conditions, and summarizes the model physics without numerical and implementation details. Section 3 discusses the time and space discretizations. Section 4 is the largest and most detailed, presenting the specifics on pameterizations and numerical approximations. Where possible, summaries of relevant physical and numerical approximations are given for motivation. Every attempt is made to draw out the important relations between the subcomponents of the sea ice model in order to emphasize its unifying features. The final three sections outline numerical ordering of code, special capabilities, diagnostic output and summarizes CSIM4. Tables of physical constants, a list of acronyms and references are included.

In addition to the supported default physics of CSIM4, there are alternative physics options available. These are conviently summarized in the Appendix. These options include those used in the developmental versions of the model, as well as those which are possible candidates for future versions.

This document describes the physics of CSIM4, but gives some brief discussion on aspects of the model useful in running and in diagnosing its output. For further information on how to obtain and run CSIM4, see the CSIM User's Guide Version 4 (Schramm, 2002). For details on source code structure and its modification, see the CSIM Code Reference Manual Version 4 (Briegleb, 2002).

2 Overview of Sea Ice Model

In this section, an introductory overview of the sea ice model is given. Details on references and numerical approximations can be found in the two sections that follow.

2.1 State Variables

The **state variables** for the sea ice model are listed in Table 1. They are the time dependent or prognostic variables of the sea ice model. Where possible, we use conserved quantities as state variables. The subscript n, $\{n = 0, 1, 2...N\}$ refers to the n^{th} ice thickness category, where N is the total number of categories. For each category, ice thickness lies within the category thickness limits, as described in the following subsection.

Table 1: State Variables (subscript n refers to n^{th} category)

Symbol	Description
A_n	Sea ice area (fraction from 0 to 1)
V_n	Sea ice volume (m^3 m^{-2})
E_n	Sea ice internal energy (J m^{-2})
V_{sn}	Snow volume (m^3 m^{-2})
T_{sn}	Surface temperature of snow/ice (°C)
$\mathbf{u}$	Sea ice velocity (m s^{-1})
σ_{ij}	Stress tensor components (i=1,2; j=1,2) (N m^{-1})

2.2 Fundamental Equations

The **fundamental equations** determine the spatial and temporal evolution of the state variables. We first give a rationale for using an ice thickness distribution before describing these equations.

Many properties of sea ice depend on ice thickness (Thorndike et al., 1975). For example, ice compressive strength, growth rate, surface temperature, turbulent and radiative flux exchange with the atmosphere. Two contrasting phenomena alter the distribution of ice thickness on a yearlong average: accretion and ablation against lead opening and ridging of ice. This competition was elegantly described by (Thorndike et al., 1975): "thermodynamics seeks the mean and dynamics the extremes". The evolution of the thickness distribution is the historical integral of these two continuous processes.

Formally, the thickness distribution is described by the distribution function $g(h, \mathbf{x}, t)$, where h is ice thickness (henceforth we suppress the explicit space and time dependence). $g(h)dh$ is the fraction of area covered by ice of thickness h to $h + dh$, normalized by $\int_0^\infty g(h)dh = 1$, the conservation of total area. The aggregate ice fraction is $A = \int_{0+}^\infty g(h)dh$, while the open water fraction is $A_0 = g(h = 0) = 1 - A$. The cumulative distribution function is $G(h) = \int_0^h g(h)dh$. The average of a quantity F that depends on ice thickness is referred to as the aggregate $\bar{F} = \frac{1}{A}\int_0^\infty F(h)g(h)dh$.

The evolution of g is governed by the distribution equation

$$\frac{\partial g}{\partial t} = -\frac{\partial}{\partial h}(\dot{h}g) + L(h, g) - \nabla \cdot (\mathbf{u}g) + R(h, g, \mathbf{u}) \tag{1}$$

where $\dot{h}$ is the rate of change in ice thickness due to vertical thermodynamic processes, $-\frac{\partial}{\partial h}(\dot{h}g)$ is the change in distribution due to thickness space transport, $L(h, g)$ is the change in distribution due to lateral

melt/formation processes, $-\bigtriangledown\cdot(\mathbf{u}g)$ is the change in distribution due to horizontal advection ($\bigtriangledown$ is the horizontal gradient operator and $\mathbf{u}$ is the smoothed velocity field over the thickness distribution) and $R(h,g,\mathbf{u})$ (ψ in Thorndike et al. (1975)) is a redistribution function due to rafting and ridging processes.

To solve Eq. 1, a discrete set of N ice categories is assumed, delimited by the thicknesses ($\{h_n^*\}, n = 0,1,2...N$) for which $h_0^* = 0$. Thus, Eq. 1 is integrated over the thickness limits for each category, resulting in a discrete set of N equations to be solved for the ice fraction in each category n:

$$A_n = \int_{h_{n-1}^*}^{h_n^*} g(h)dh, \tag{2}$$

where the total (aggregate) ice fraction $A = \sum_{n=1}^{N} A_n$. The first moment of the distribution function is the ice volume $V_n = \int_{h_{n-1}^*}^{h_n^*} hg(h)dh$, and any function F which is linear in the ice thickness (i.e. $F = F_0 + F_1 h$) results in $F_n = F_0 A_n + F_1 V_n$.

There are two known ways to solve Eq. 1. The first assumes thickness is distributed uniformly within each category (Hibler (1980), and Flato and Hibler (1995)). Sea ice growth and melt processes require advection in thickness space, and so this method is known as Eulerian. Such advection is very diffusive unless a large number of categories are employed. It is difficult to resolve vertical temperature profiles in snow and ice (Bitz et al. (2001)) in this Eulerian method.

The second method of solving Eq. 1 assumes ice can vary in thickness within each category, as in Thorndike et al. (1975). This method is free from the diffusion of the Eulerian thickness advection, allowing for a smaller number of categories, as well as the resolution of the vertical temperature profile in snow and ice (Bitz et al. (2001)). It naturally allows the use of ice volume as a prognostic variable. This method is known as Lagrangian, and is the method used for the present sea ice model.

Thus, the fundamental equations for the present sea ice model start with the discrete form of Eq. 1 for the ice fractions A_n, the first moment equations for the ice volume V_n, corresponding equations for the snow volume V_{sn}, equations for the vertically varying ice internal energy (from which the vertical temperature profile and heat transfer are evaluated), equations for the surface temperature required for the vertical heat transfer solution, and finally dynamic equations for the aggregate ice velocity $\mathbf{u}$ needed to evaluate horizontal advection and the ridging terms in the distribution equations.

The fundamental equations are as follows. For the category sea ice fraction and volume:

$$\frac{\partial A_n}{\partial t} = S_{TAn} - \bigtriangledown\cdot(\mathbf{u}A_n) + S_{MAn} \tag{3}$$

$$\frac{\partial V_n}{\partial t} = S_{TVn} - \bigtriangledown\cdot(\mathbf{u}V_n) + S_{MVn} \tag{4}$$

where terms S_T denote sources/sinks due to thermodynamic processes and thickness space transport, while terms S_M denote sources/sinks due to mechanical redistribution. The sea ice thickness h_n is derived from the fraction and volume as $h_n = V_n/A_n$.

To resolve vertical atmosphere/ocean heat exchange, and account as well for internal heat within the ice (i.e. brine pocket heat storage), the ice internal energy E_n (vertically varying) is governed by the conservation equation:

$$\frac{\partial E_n}{\partial t} = S_{TEn} - \bigtriangledown\cdot(\mathbf{u}E_n) + S_{MEn} \tag{5}$$

The internal sea ice energy E_n is proportional to the ice volume, $E_n = q_n V_n$, where the proportionality function q_n (termed the energy of melting) is the internal energy per unit volume (by convention, $q_n < 0$, and therefore $E_n < 0$ also). The effects of brine pockets are represented explicitly through the temperature (T_n) and salinity (S_n) dependent energy of melting $q_n = q_n(T_n, S_n)$. The vertical temperature profile is inferred by solving for T_n in $q_n(T_n, S_n) = E_n/V_n$ over an ice thickness $h_n = V_n/A_n$, using a prescribed salinity profile.

The conservation equation for snow volume V_{sn} is:

$$\frac{\partial V_{sn}}{\partial t} = S_{TVsn} - \nabla \cdot (\mathbf{u} V_{sn}) + S_{MVsn} \tag{6}$$

Snow thickness is derived from $h_{sn} = V_{sn}/A_n$. Snow energy per unit volume is $E_{sn} = q_s V_{sn}$, where the energy of melting of snow q_s is constant.

For each category, the heat equation governing vertical heat transfer over time interval t to t' corresponding to temperatures T_n and T_n' respectively, allowing for temperature and salinity dependent heat capacity c_i, thermal conduction and internal absorption of penetrating solar radiation, is given by:

$$\int_{T_n}^{T_n'} \rho_i c_i dT_n = \int_t^{t'} \left(\frac{\partial}{\partial z} k \frac{\partial T_n}{\partial z} + Q_{SW} \right) dt \tag{7}$$

where sea ice is assumed to have a constant density ρ_i, z is the vertical coordinate within the sea ice, Q_{SW} is the absorbed shortwave flux, and the thermal conductivity k is that for either snow or ice. Modifications to the temperature profile resulting from heat transfer change the ice internal energy according to $E_n = q_n(T_n, S_n)V_n$.

The surface boundary conditions for the vertical heat transfer solution require surface temperature T_{sn} to satisfy the conservation equation

$$\frac{\partial A T_{sn}}{\partial t} = S_{TTsn} - \nabla \cdot (\mathbf{u} A_n T_{sn}) + S_{MTsn}, \tag{8}$$

For momentum conservation, sea ice is assumed to be a two-dimenstional continuum. The sea ice velocity $\mathbf{u}$ and stress tensor σ_{ij} are considered (along with related dynamic quantities) to be representative of the entire ice thickness distribution. Their governing equations are:

$$\bar{m} \frac{\partial \mathbf{u}}{\partial t} = -\bar{m} f \mathbf{k} \times \mathbf{u} + \boldsymbol{\tau}_a + \boldsymbol{\tau}_o + \bar{m} g \nabla H_o + \nabla \cdot \boldsymbol{\sigma} \tag{9}$$

where $\bar{m} = \rho_s V_s + \rho_i V$, the non-linear $\mathbf{u}$ advection terms are ignored as they are negligibly small when the equations are scaled, f is the Coriolis parameter, $\mathbf{k}$ is the local vertical unit vector, $\boldsymbol{\tau}_a$ and $\boldsymbol{\tau}_o$ are air and water stresses respectively, g is the gravitational acceleration, H_o is the sea surface height and $\nabla \cdot \boldsymbol{\sigma}$ is the force per unit area due to internal ice stress, where $\boldsymbol{\sigma}$ is the stress tensor. The stress tensor equations are:

$$\frac{\partial \sigma_{ij}}{\partial t} + \frac{e^2}{2T_{ew}} \sigma_{ij} + \frac{1 - e^2}{4T_{ew}} \sigma_{kk} \delta_{ij} = \frac{P}{2T_{ew} \Delta'} \dot{\epsilon}_{ij} - \frac{P}{4T_{ew}} \delta_{ij} \tag{10}$$

where $(i, j = 1, 2)$ refer to the four components of the stress tensor, e is a constant ratio of major to minor axes of the elliptical yield curve, T_{ew} is a damping time scale for elastic waves, δ_{ij} is the Kronecker delta, P is the ice compressive strength (or mechanical pressure, a function of the thickness distribution), $\dot{\epsilon}_{ij}$ is the rate of strain tensor, in turn a function of velocity gradients, and Δ' is a function of the rate of strain tensor. Note that σ_{ij} is a state variable because of the EVP solution method, which is not necessary for the VP solution method.

2.3 Boundary Conditions

Boundary conditions are represented vertically by atmosphere/ocean forcing, consisting of states and interfacial fluxes (summarized in Table 2), and horizontaly by a lateral no slip condition for $\mathbf{u}$ along coastlines and $\mathbf{u} \rightarrow \mathbf{u_o}$ (i.e. ocean surface current) on the open ocean edge. The atmosphere states are used, along with ice surface temperature and aerodynamic roughness (the latter is a constant), to compute the bulk sensible/latent fluxes and surface stresses (F_{SH}, F_{LH} and $\boldsymbol{\tau}_a$ respectively). The atmosphere to ice flux

Table 2: State Variables and Fluxes Received by Sea Ice Model from the Coupler

Symbol	Description	Units
	Atmospheric States	
z_a	reference height	m
u_a	x direction wind speed at z_a	m s^{-1}
v_a	y direction wind speed at z_a	m s^{-1}
θ_a	potential temperature at z_a	K
T_a	air temperature at z_a	K
q_a	specific humidity at z_a	kg kg^{-1}
ρ_a	air density at z_a	kg m^{-3}
	Atmosphere $\Rightarrow$ ice fluxes	
F_{SWvsdr}	direct, visible downwelling shortwave	W m^{-2}
F_{SWvsdf}	diffuse, visible downwelling shortwave	W m^{-2}
F_{SWnidr}	direct, near infrared downwelling shortwave	W m^{-2}
F_{SWnidf}	diffuse, near infrared downwelling shortwave	W m^{-2}
F_{LWDN}	downwelling longwave	W m^{-2}
F_{RN}	freshwater flux due to rain	kg m^{-2} s^{-1}
F_{SNW}	freshwater flux due to snow (liquid equiv.)	kg m^{-2} s^{-1}
	Ocean States	
T_o	sea surface temperature	K
S_o	sea surface salinity	ppt
u_o	x direction ocean surface current	m s^{-1}
v_o	y direction ocean surface current	m s^{-1}
$(\nabla H_o)_x$	x direction sea surface slope	m m^{-1}
$(\nabla H_o)_y$	y direction sea surface slope	m m^{-1}
	Ocean $\Rightarrow$ ice fluxes	
F_{Qoi}	freezing/melting potential	W m^{-2}

of freshwater due to snow (F_{SNW}) is used to compute snow accumulation ($dh_s/dt = F_{SNW}/\rho_s$). Rain (F_{RN}) is assumed to run off directly into the ocean. Down shortwave and longwave fluxes are $F_{SWDN} = F_{SWvsdr} + F_{SWvsdf} + F_{SWnidr} + F_{SWnidf}$ and F_{LWDN} respectively.

Surface albedo α is a function of spectral interval, snow depth, ice thickness and surface temperature. Of the total absorbed shortwave in the ice ($F_{SW} = F_{SWDN}(1-\alpha)$), a portion ($I_{SW}$) penetrates below the surface layer and is either internally absorbed in the ice (Q_{SW}) or penetrates to the ocean below (F_{SWo}). The net longwave flux at the surface (F_{LW}) is due to surface emission ($\varepsilon\sigma_{sb}T_s^4$) and absorption of down longwave (εF_{LWDN}), where ε is the longwave emissivity and σ_{sb} is the Stefan-Boltzmann constant.

The boundary condition for the heat equation at surface temperature T_s is: $F_{TOP}(T_s) = F_{SW} - I_{SW} + F_{LW} + F_{SH} + F_{LH} + kdT/dz$. If $F_{TOP}(T_{melt}) > 0$, where T_{melt} is the snow/ice melting temperature, then snow/ice melt is computed by: $F_{TOP}(T_s = T_{melt}) = qdh/dt$ as appropriate for either snow (if present) or ice (recall that $q < 0$).

The ocean surface currents $\mathbf{u_o}$ and ice velocity $\mathbf{u}$ are used to compute ocean/ice stress $\boldsymbol{\tau}_o$. The tilt stress is computed from the gradient of the sea surface height.

Ice formation occurs by three processes. Although these processes are distinguished in formation, no distinction is made between ice types. If the freezing/melting potential is such that heat is required by the ocean to maintain the freezing temperature ($F_{Qio} > 0$), then **frazil ice** formation occurs, at a rate $dV_f/dt = F_{Qio}/\rho_i q_f$, where q_f is a heat of melting assuming the ice forms at $T = -1.8°C$ and $S = 4.0$ppt. If the freezing/melting potential indicates ocean heat is available to melt ice ($F_{Qio} < 0$), this heat is partitioned between lateral (F_{SID}) and bottom (F_{BOT}) heat fluxes according to the fraction of absorbed solar energy near the surface and in deeper water. The actual amounts used are limited by mixed layer formulae. The

Table 3: State Variables and Fluxes Sent from Sea Ice Model to the Coupler

Symbol	Description	Units
	Ice States	
A	ice area	
T_s	surface temperature	K
α_{vsdr}	albedo (visible, direct)	
α_{nidr}	albedo (near infrared, direct)	
α_{vsdf}	albedo (visible, diffuse)	
α_{nidf}	albedo (near infrared, diffuse)	
	Ice $\Rightarrow$ atmosphere fluxes	
F_{LH}	latent heat flux	W m^{-2}
F_{SH}	sensible heat flux	W m^{-2}
F_{LWUP}	upwelling longwave	W m^{-2}
F_{EVAP}	evaporated water	kg m^{-2} s^{-1}
τ_{ax}	x direction atmosphere-ice stress	N m^{-2}
τ_{ay}	y direction atmosphere-ice stress	N m^{-2}
	Ice $\Rightarrow$ ocean fluxes	
F_{SWo}	shortwave transmitted to ocean	W m^{-2}
F_{Qio}	heat flux to ocean	W m^{-2}
F_{Wo}	fresh water flux	kg m^{-2} s^{-1}
τ_{ox}	x direction ice-ocean stress	N m^{-2}
τ_{oy}	y direction ice-ocean stress	N m^{-2}
	Diagnostic Fields	
T_{ref}	atmospheric reference temperature (2 m)	K
F_{SW}	ice/ocean absorbed shortwave flux	W m^{-2}

bottom boundary condition is: $F_{BOT} - kdT/dz = qdh/dt$. If bottom ice formation occurs (i.e. $dh/dt > 0$), this ice is termed **congelation ice**. Finally, if sufficient snow h_s overlies ice, the snow-ice interface can be depressed below sea level. Snow below sea level is assumed to be converted into ice at a rate that conserves mass and energy, and is termed **snow-ice**. It is assumed that such conversion occurs without heat or salt exchange with the ocean. Output sea ice states and fluxes are given in Table 3.

2.4 Summary

In summary, Eqs. 1 - 10, subject to atmosphere/ocean boundary conditions, constitute the fundamental equations for the sea ice model. The next two sections present in detail the discretizations, parameterizations and numerical approximations used to solve the fundamental equations. Parameterizations involve evaluating fluxes with the atmosphere and ocean, and calculating the thermodynamic, advective, mechanical and dynamic tendencies in the fundamental equations.

3 Discretization

The fundamental equations are discretized for numerical solution as described in this section. Further details on the discretization can be found in the following section.

3.1 Time

The sea ice model is characterized by a collection of state variables S (Table 1) subject to forcing fields F_{in} (Table 2) over the coupling time step Δt. Let m designate an initial time step and $m+1$ the subsequent time step over a coupling interval. Let V^m represent one of the state variables S at time step m, and V^{m+1} the variable after one coupling time step. The ice model computes V^{m+1} from V^m subject to F_{in} by two half (or time split) steps. The two time split steps are separated by exchange with the coupler.

In the first half, the forcing fields F_{in} received from the coupler are used to compute the ice-atmosphere exchange and the ice vertical thermodynamic response

$$V^{m+1/2} = V^m + \Phi^{m+1/2}(S^m, F_{in}^m, F_{out}^{m+1/2})\Delta t \tag{11}$$

where the tendency function $\Phi^{m+1/2}$ represents the vertical thermodynamic exchange with the atmosphere, while the output fluxes $F_{out}^{m+1/2}$ represent the updating of the ice-atmosphere fluxes. The fields sent to the coupler at this point (Table 3) update only the surface temperature and the ice-atmosphere fluxes, while the ice concentration, albedos and ice-ocean fluxes are unchanged.

The second half time step is

$$V^{m+1} = V^{m+1/2} + \Phi^{m+1}(S^{m+1/2}, F_{in}^m, F_{out}^{m+1})\Delta t \tag{12}$$

where the tendency function Φ^{m+1} represents the rest of the ice physical processes, including lateral thermodynamics, thickness space transport, dynamics and physical space transport, mechanical and thermodynamic redistribution and albedo calculation. The output fluxes F_{out}^{m+1} now are all updated, including the ice-ocean fluxes and albedos. The collection of state variables V^{m+1} in S are thus updated to time step $m+1$. Note that the second half time step makes the initial contribution to other fluxes for the coupling time step.

The sea ice model is time split for improved CCSM computational performance, since once the atmospheric model receives the ice-atmosphere fluxes, it can run in parallel with the second half time step of the sea ice model.

The ice model requires initialization to set grid and mask (land/ocean) information, as well as a restart file with the states S^m and the fluxes $F_{out}^{m+1/2}$ to be sent to the coupler. The model outputs restart files $(S^m, F_{out}^{m+1/2})$ periodically, and accumulates time mean states (S^m) and fluxes $(F_{in}^m, F_{out}^{m+1})$, as well as diagnostic fields, for the output history files.

The time stepping code runs in parallel. All communication between the ice model and the other components is handled via MPI in parallel through the coupler. The ice model also runs parallel internally in a somewhat different manner via MPI for its domain decomposition.

3.2 Thickness

The thickness distribution function $g(h)$ is integrated over N discrete thickness ranges or categories. Presently there are $N = 5$ ice thickness categories in the standard model, but arbitrary N is allowed. These categories are described in the next section. The state variables (listed in Table 1) of sea ice concentration, volume, energy, snow volume and surface temperature are discretized into $n = 1, 2, ...N$ categories. Henceforth, a subscript n will refer to the n^{th} thickness category.

3.3 Vertical

To compute vertical heat conduction through ice, ice thickness is divided into an even number of vertical layers. This requires sea ice internal energy E to vary in the vertical, with two evenly spaced layers in the thinnest ice thickness categories and four in the thickest. Temperatures are computed from E using the

energy of melting and the ice volume in each layer. Internal temperatures are centered within each layer, while conductivities and energy fluxes are represented at layer interfaces. Temperature boundary conditions at the surface and base of ice are taken at the top and bottom interfaces respectively. See Figure 2 in section 4.6 for a diagram on the vertical level structure.

3.4 Horizontal

The horizontal grids used presently for the sea ice model are the POP displaced pole grids, in which the South Pole is typically located at the geographic South Pole, but the North Pole may be located in any northern hemisphere land mass. The CCSM has chosen a grid with the North Pole in central Greenland. The grids are orthogonal curvilinear, so that vectors parallel to increasing longitude and latitude coordinates are perpendicular to one another. Two available resolutions are the standard gx1 (320 longitudes x 384 latitudes, $\sim 1.1^\circ \times 0.94^\circ$), and a coarse gx3 (100 longitudes x 116 latitudes, $\sim 3.6^\circ \times 1.6^\circ$). The grids south of the equator are regular spherical coordinates. Spatial discretization is that of a B-grid (see Figure 1).

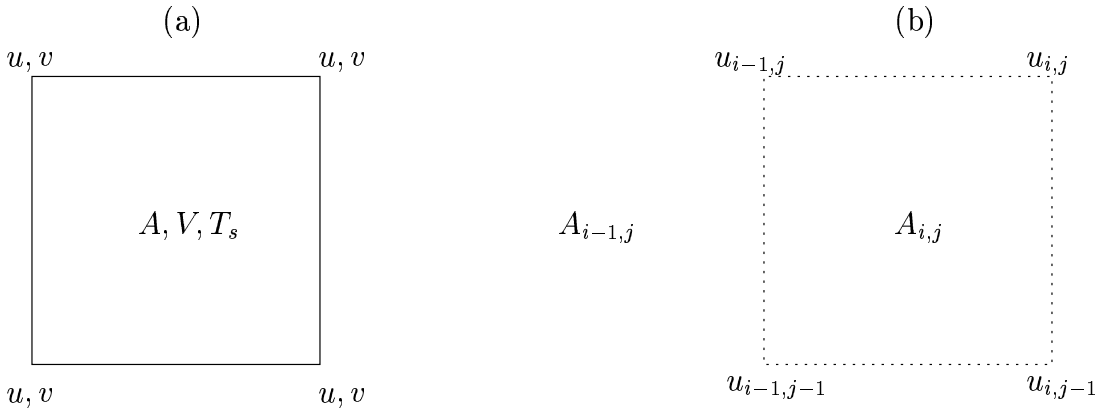

Figure 1: The Arakawa-B grid (a), with horizontal indices (b), used for computation. Shown are the A,V,T_s prognostic fields on the T-grid, while u,v are on the U-grid. Modified from Bitz (2000).

All state variables except ice velocity and stress tensor components are taken at grid box mid-points (a tracer grid termed the T-grid), while velocities at grid box corners (a velocity grid termed the U-grid). The stress tensor, rates of strain and viscosities are defined bilinearly across each grid cell using the values at the corners. This discretization tends to avoid decoupling problems associated with the B-grid.

Grid information is taken from a grid data file read in by the ice model at initialization. The fields on the U-grid are latitude, longitude and angle the grid makes with a geographic latitude line (ULAT, ULON and ANGLE respectively), and fields on the T-grid are the land/ocean mask and T cell widths on north and east sides (tmask, HTN and HTE respectively). tmask gives the land points on the T-grid, and is either 0 (land) or 1 (ocean). umask (on the U-grid) is 0 if any four surrounding tmask points are 0 (i.e. land), and is 1 for points where non-zero ice velocity is possible (if ice is locally present). In other words, umask is zero for all coastal points. dxt and dyt are the T-grid longitudinal and latitudinal widths through cell centers respectively, while dxu and dyu are the analogous for the U-grid. ANGLET χ^t is ANGLE χ^u interpolated

to the T-grid. Specifically:

$$\begin{aligned} dxt_{ij} &= \frac{1}{2}(HTN_{ij} + HTN_{ij-1}) \\ dyt_{ij} &= \frac{1}{2}(HTE_{ij} + HTE_{i-1j}) \\ dxu_{ij} &= \frac{1}{2}(HTN_{ij} + HTN_{i+1j}) \\ dyu_{ij} &= \frac{1}{2}(HTE_{ij} + HTE_{ij+1}) \\ A^t_{ij} &= dxt_{ij}\ dyt_{ij} \\ A^u_{ij} &= \frac{1}{4}(A^t_{ij} + A^t_{i+1j} + A^t_{ij+1} + A^t_{i+1j+1}) \\ \chi^t_{ij} &= \frac{1}{4}(\chi^u_{ij} + \chi^u_{i-1j} + \chi^u_{ij-1} + \chi^u_{i-1j-1}) \end{aligned} \tag{13}$$

where the ij are the grid longitude and latitude indices respectively (see Figure 1), A^t_{ij},A^u_{ij} are the grid box areas on the T-grid and U-grid respectively, and for the χ^t calculation, χ^u values are adjusted if any differ by more than 180°.

3.5 Domain Decomposition

The horizontal computational grid is domain decomposed in two dimensions for parallelization. The global domain of dimensions $imt_{global} \times jmt_{global}$ (for example, the gx1 grid has $imt_{global} = 320$ longitude points and $jmt_{global} = 384$ latitude points) is divided into integral NX longitude by NY latitude subdomains of dimensions $(imt_{local} = imt_{global}/NX + 2n_{ghost} + 1) \times (jmt_{local} = jmt_{global}/NY + 2n_{ghost} + 1)$, where imt_{global}/NX, jmt_{global}/NY must be integers. Each subdomain has a physical portion indexed as $[ilo : ihi, jlo : jhi]$ with n_{ghost} boundary cells outside. Periodic boundary conditions are applied, with boundary routines performing communications between subdomains when running parallel. Global scatter and gather routines distribute information from the global domain to the subdomains and back, respectively.

We note that since the thermodynamic calculations involve one grid point at a time, a purely thermodynamic model integration is independent of the domain decompostion (i.e. the exact values of NX,NY), while the dynamic calculation depends upon domain boundary conditions. Hence an integration with active dynamics is dependent upon the exact values of NX and NY.

4 Parameterizations and Numerical Approximations

Sections 2 and 3 introduced the sea ice model state variables, fundamental equations, boundary conditions and discretizations. In the present section we elaborate on the parameterizations necessary to represent various forcing terms in the fundamental equations and the details of the numerical solutions. For many of the subsections to follow, the processes are described (sometimes implicitly) for a particular thickness category n. For exchange with the coupler, only aggregate quantities (i.e. those summed over the thickness distribution) are used.

4.1 Thickness Distribution

The number of ice thickness categories N used in the ice model results from a trade off between the desire to resolve thin ice that is important in ocean-atmosphere heat exchange and feedback processes against computational cost. Bitz et al. (2001) showed that five thickness categories with adequate thin ice resolution are sufficient to represent the first order effects of an ITD. We therefore chose $N = 5$, with thickness boundaries given in Table 4, based on the category limit formula of Lipscomb (2001). (Note that we also list

the number of vertical levels for each category). While $N = 5$ is a convenient value for climate modeling, it is not hardwired in the code; other values can be used, including $N = 1$. Also, while the category 1 lower limit is 0, for thermodyanmic stability the minimum ice thickness in category 1 is h_{min}. If ice thickness in this category falls below h_{min}, it is reshaped using $h_{min}A_1' = h_1 A_1$.

Table 4: Ice Thickness Distribution (N=5)

n	Range (m)	Levels
0	0	0
1	0^+ - 0.65	2
2	0.65 - 1.39	2
3	1.39 - 2.47	4
4	2.47 - 4.60	4
5	> 4.60	4

In the Lagrangian method of ice thickness distribution used here, there is no process (thermodynamic or dynamic) that absolutely prevents ice from outgrowing its thickness range for a given category. While it is true that the incremental linear remapping used to evaluate thickness space transport in most cases prevents ice from outgrowing its category thickness limits, an occasional adjustment is still necessary, which is termed "thermodynamic redistribution". This process contributes to the thermodynamic source terms S_T in the conservation equations (see section 4.2).

Any category of ice which outgrows its upper thickness limit is combined with the next thickness category. The combination is done preserving ice area, volume, energy and snow volume. Any category of ice which melts below its lower thickness limit, will be combined with the next lower category in a manner similar to outgrowth just described, except for the thinnest ice category. For ice in category 1 that melts below its lower limit, the ice is reshaped so its thickness equals the minimum, with its concentration adjusted to conserve ice volume.

Small amounts of either open water or ice area can be created due to numerical diffusion associated with horizontal advection. To reduce the possiblity of roundoff error corrupting the ice state owing to very small amounts of sea ice, any ice category whose area is less than an adjustable minimum (typically 5×10^{-6}) is added to the nearest ice filled category, if one is available. Small amounts of open water (typically less than 1×10^{-6}) are eliminated by increasing ice concentration equivalently in the thinnest ice category. Any remaining small ice areas in a grid box are set to zero in such a way that ice and snow volume are conserved across the entire hemisphere's ice pack (i.e. renormalization factors are applied across the entire hemispheric ice pack to compensate exactly for setting small ice areas and volumes to zero).

4.2 Thermal Properties

The ice area (A_n) and volume (V_n) were introduced in the previous section for specific ice thickness categories. The ice internal energy (E_n) is proportional to the ice volume:

$$E_n = q_n V_n \tag{14}$$

for the n^{th} category, where the proportionality function q_n is termed the energy of melting. q_n is thus the internal energy of the ice per unit volume. It is derived from the basic thermodynamic relation between the applied heat Q for the given heat capacity of sea ice c_i and the resulting temperature change from T to T':

$$Q = \int_T^{T'} \rho_i c_i dT \tag{15}$$

where the ice density ρ_i is a constant (see Table 10). Treating ice density as a constant is a limitation of the model. During the melt season, a layer of deteriorated ice 5-10 cm thick is often observed at the top surface,

with a density of 500 kg m^{-3} or less. Beneath this deteriorated ice, multiyear ice contains air-filled pores that can reduce its density to 700-800 kg m^{-3} in the upper 30-50 cm (Bitz, 2000). A constant ice density implies that all drained brine pockets are filled with melt water and not air.

The storage of latent heat in brine pockets is accounted for explicitly by using the heat capacity of Bitz and Lipscomb (1999), originally from Ono (1967):

$$c_i(T, S) = c_0 + \frac{L_i \mu S}{T^2} \tag{16}$$

where c_0 (J kg^{-1} $°C^{-1}$) is the heat capacity for pure water ice, L_i (J kg^{-1}) is the latent heat of fusion of ice, S (ppt) is the ice salinity, T (°C) is the temperature, and μ (°C ppt^{-1}) is the empirical constant in the melting temperature (T_{melt}) and salinity relation:

$$T_{melt} = -\mu S. \tag{17}$$

(See Table 10 for a list of physical constants.) For each category n, (15) is evaluated using this heat capacity from temperature T to the melting temperature T_{melt}:

$$q_n(T, S) = -\rho_i c_0 (T_{melt} - T) - \rho_i L_i \left(1 + \frac{\mu S}{T}\right). \tag{18}$$

The quantity q_n is defined to be negative, implying that $|q_n|$ is the amount of energy required to melt a unit volume of sea ice of salinity S and temperature T. With this sign convention, a positive amount of heat $|q_n(T, S)|$ must be applied to raise the ice temperature from T to T_{melt}, resulting in a rise of internal energy from $E_n < 0$ to zero.

For snow, the heat required to change its temperature below melting is small compared to the latent heat of fusion, and thus for simplicity is ignored. Tests show that allowing for internal heat storage in a one-layer snow model makes little difference in the heat transfer and surface temperature simulation for climate. Further, snow is fresh and therefore has zero salinity. Hence, the amount of energy required to melt a unit volume of snow is given by:

$$q_s = -\rho_s L_i \tag{19}$$

where ρ_s is the constant snow density. Note that since q_s is a constant, the snow internal energy is proportional to V_{sn}, so that an explicit snow internal energy is not a state variable. When required, the snow internal energy is computed from:

$$E_{sn} = q_s V_{sn}. \tag{20}$$

The snow/ice surface temperature is an important quantity for determining the heat and mass exchange between the atmosphere and the snow/ice surface. The surface temperature T_{sn} for the n^{th} category varies rapidly with changing forcing conditions, and because it is used as an initial condition for the thermodynamic surface energy calculation, it is treated as a state variable. The area-weighted surface temperature is used for conservation and transport, in both thickness and physical space.

Snow and ice thickness and ice temperature are not state variables, but they can be diagnosed as follows. Ice and snow thickness are computed from the ice area and volume and snow volume, respectively, as:

$$h_n = V_n/A_n \quad h_{sn} = V_{sn}/A_n. \tag{21}$$

Ice temperature can be diagnosed from the energy of melting. As discussed in section 4.6 on vertical heat conduction, the ice is divided vertically into a number of layers. For each layer there is an internal energy and volume. From these an energy of melting (q_n) can be computed for each layer (Eq. 14), and hence a layer temperature from the solution to the quadratic equation (Eq. 18)

$$\rho_i c_0 T^2 - (q_n + \rho_i c_0 T_{melt} + \rho_i L_i) T - \rho_i L_i \mu S = 0. \tag{22}$$

The solution yields one temperature below T_{melt} and another above T_{melt}, which is discarded.

4.3 Input from the Coupler

Fields received by the ice model from the coupler are shown in Table 2. They include atmospheric/oceanic states and fluxes. Atmospheric states must be available to the ice model because with an ice thickness distribution, it is necessary for the ice model, rather than for the coupler (as in CSM1), to compute fluxes over each ice thickness category and aggregate them.

All of the fields received are on the T-grid (see section 3.4). However, the vector fields of surface wind, surface ocean current and tilt are projected onto geographical latitude-longitude directions. These vectors are first rotated to the pop grid directions using a T-grid rotation angle (χ^t) calculated from a U-grid rotation angle (χ^u) provided by a pop grid input dataset. The rotated surface wind is then used on the T-grid to calculate atmosphere/ice fluxes, including stresses (see section 4.5). The resulting atmosphere/ice stress, as well as the ocean surface current and tilt, are then bilinearly interpolated with area weight to the U-grid for use in the dynamics (see section 4.10).

Specifically, let (u_g^t, v_g^t) represent a vector field of components (u, v), where the subscript "g" refers to geographic, and the superscripts "t" and "u" to the T-grid and U-grid respectively. Similarly, let a subscript "p" refer to the POP grid. All the vector fields received from the coupler are then (u_g^t, v_g^t) fields. For these to be useful on the POP grid, they must first be rotated to the POP grid boxes as follows:

$$\begin{aligned}(u_p^t)_{ij} &= (u_g^t)_{ij} cos(\chi_{ij}^t) + (v_g^t)_{ij} sin(\chi_{ij}^t) \\ (v_p^t)_{ij} &= -(u_g^t)_{ij} sin(\chi_{ij}^t) + (v_g^t)_{ij} cos(\chi_{ij}^t)\end{aligned} \tag{23}$$

where (ij) are the longitude/latitude indices of the appropriate grid. The atmosphere winds in the (u_p^t, v_p^t) form can be used to directly compute atmosphere/ice stresses. However, these stresses, as well as the ocean currents and tilts, are required to be on the U-grid for the dynamic calculation. Therefore, the following interpolation from the T-grid to the U-grid is required:

$$\begin{aligned}(u_p^u)_{ij} &= \frac{1}{4}(A_{ij}^t (u_p^t)_{ij} + A_{i+1j}^t (u_p^t)_{i+1j} + A_{ij+1}^t (u_p^t)_{ij+1} + A_{i+1j+1}^t (u_p^t)_{i+1j+1})/A_{ij}^u \\ (v_p^u)_{ij} &= \frac{1}{4}(A_{ij}^t (v_p^t)_{ij} + A_{i+1j}^t (v_p^t)_{i+1j} + A_{ij+1}^t (v_p^t)_{ij+1} + A_{i+1j+1}^t (v_p^t)_{i+1j+1})/A_{ij}^u\end{aligned} \tag{24}$$

where A_{ij}^t is the T-grid box area, and A_{ij}^u is the U-grid box area (see Fig. 1).

The freezing/melting potential F_{Qoi} is calculated in the ocean model and received by the ice model as input. In the ice model, three forms of ice are distinguished: **frazil** (which forms directly in the ocean surface layer), **congelation** (which forms at the ice base), and **snow-ice** (which forms by flooding of snow-covered ice). Frazil ice formation is determined by the ocean model, and the other two by the ice model.

If the ocean surface layer temperature (T_o) falls below freezing (at fixed temperature T_{of}), frazil ice forms such that the heat flux F_{Qoi} restores the ocean temperature to freezing:

$$F_{Qoi} = \rho_o c_o h_o (T_{of} - T_o)/\Delta t \tag{25}$$

where $\rho_o c_o$ is the product of ocean density and heat capacity, h_o is the surface layer thickness, Δt is the coupling time step for the ocean (i.e. the time between exchanges of data with the coupler: one day). If $(T_o < T_{of})$ then $F_{Qoi} > 0$ and frazil ice forms (note that all CCSM fluxes are positive downwards).

The salinity adjustment ΔS in the ocean model due to brine rejection is:

$$\Delta S = (S_{ro} - S_{ri}) F_{Qoi} \Delta t/(\rho_o h_o q_f) \tag{26}$$

where S_{ro} is the constant reference ocean salinity, S_{ri} is the constant reference salinity of sea ice, ρ_o is the constant ocean density, and q_f is the latent heat of sea ice for frazil ice formation. This latent heat is computed from the (positive) ice energy of melting per unit mass (18) with $T = T_{of}$ and $S = 4$ppt. Furthermore, there is no physical reason for the reference salinity of sea ice to depend on the assumed

salinity profile used for the brine pocket parameterization and hence q_n and q_f. Therefore we have not imposed such an unnecessary requirement.

However, it is important to note that in the current configuration, the water flux exchanged between ice and ocean is assumed fresh (i.e. $S_{ri} = 0$). Also, the freezing temperature is T_{of} is kept constant independent of salinity, and the latent heat q_f of frazil ice formation is a strict constant, and identical in the ocean and sea ice models.

The total downwards shortwave flux is the sum of the four components, which are defined in Table 2:

$$F_{SWDN} = F_{SWvsdr} + F_{SWvsdf} + F_{SWnidr} + F_{SWnidf}. \tag{27}$$

For the rest of the document, Δt will represent both the physical and the coupling time step. These do not need to be identical, as in the present code. The time step Δt is one hour.

4.4 Snow and Ice Albedo

Snow and ice albedos are important for computing the absorption of shortwave radiation in the snow/ice system, and hence the snow/ice feedback (Curry et al., 1995). The physics of this absorption and scattering is very complex (Ebert and Curry, 1993; Grenfell et al., 1994), but here it is simplied significantly. The snow and ice albedo formulas are basically those of CSM1, modified to give better agreement with various modeling and observational studies cited below. The albedo depends upon spectral band, snow thickness, ice thickness and surface temperature.

Snow and ice spectral albedos (visible = vs, wavelength $< 0.7\mu m$ and near-infrared = ni, wavelength $> 0.7\mu m$) are distinguished, as both snow and ice spectral reflectivities are significantly higher in the vs band than in the ni band. This two-band separation represents the basic spectral dependence. Thus, we ignore the near-infrared spectral structure, with generally decreasing reflectivity with increasing wavelength (Ebert and Curry, 1993).

The zenith angle dependence of snow and ice is ignored (Ebert and Curry, 1993; Grenfell et al., 1994), and therefore the distinction between downwelling direct and diffuse shortwave radiation. With the addition of a solar elevation angle, an angle dependent albedo could easily be employed. Horizontal variations in snow/ice topography are also ignored, which affect scattering and transmission into the surface through shadowing effects and through variations in the angle of the surface above the horizon.

Snow albedo depends strongly on snow age (i.e. grain size, Grenfell et al. (1994)) and on surface temperature (i.e. melting or non-melting conditions, Ebert and Curry (1993)). Sea ice albedo depends on ice thickness (Allison et al., 1993), as well as the presence of melt ponds (Ebert and Curry, 1993). In addition, snow only partially covers a surface if there are strong topographic variations (Allison et al., 1993).

Here we ignore the dependence of snow albedo on age, but retain the melting/non-melting distinction and thickness dependence. Dry snow spectral albedos are:

$$\begin{aligned} \alpha^s_{vsdf}(dry) &= 0.98 \\ \alpha^s_{nidf}(dry) &= 0.70 \end{aligned}. \tag{28}$$

These values are consistent with those of Grenfell et al. (1994) and Ebert and Curry (1993). In the case of the measurements of Grenfell et al. (1994), these dry snow albedos are closest to clear sky values for low sun and for limited cloud cover, corresponding to the spring-time high values prior to significant melt (Curry et al., 2001). These albedos are only slightly higher than those for late summer conditions with early snow fall under cloudy skies.

To represent melting snow albedos, the surface temperature is used. Springtime warming produces a rapid transition from sub-zero to melting temperatures, while late fall values transition more slowly to sub-zero

conditions. This is approximated by a temperature dependence out to $-1°$C. Let T_{snc} represent the snow/ice surface temperature for category n in °C. If $T_{snc} = T_{sn} - T_{melt} \geq -1°$C then

$$\begin{aligned} \Delta T_s =& T_{snc} + 1.0 \\ \alpha^s_{vsdf}(melt) =& \alpha^s_{vsdf}(dry) - 0.10\Delta T_s \,. \\ \alpha^s_{nidf}(melt) =& \alpha^s_{nidf}(dry) - 0.15\Delta T_s \end{aligned} \tag{29}$$

The lowest albedos at 0°C are .88 and .55 for visible and near-ir respectively, consistent to within $\pm.02$ of Ebert and Curry (1993). If the surface temperature $T_{snc} < -1°$C, the dry snow albedos are used; otherwise the melt albedos are used.

For bare non-melting sea ice, albedo depends on thickness and spectral band. If $h_n < 0.5$ m then

$$\begin{aligned} \alpha_{vsdf}(dry) =& \alpha_o(1 - fh) + \alpha_{vsdf}(thick) fh \\ \alpha_{nidf}(dry) =& \alpha_o(1 - fh) + \alpha_{nidf}(thick) fh \end{aligned} \tag{30}$$

where α_o is the open ocean albedo,

$$fh = min(tan^{-1}(A\ h_i)/tan^{-1}(A\ 0.5), 1.0) \tag{31}$$

$A = 5$, and the thick, dry sea ice albedos are:

$$\begin{aligned} \alpha_{vsdf}(thick) =& 0.78 \\ \alpha_{nidf}(thick) =& 0.36 \end{aligned} \,. \tag{32}$$

which are the asymptotic values for ice thicker than 0.5 m. These expressions represent a crude fit to the data of Allison et al. (1993), with the limiting cases for zero ice thickness that of the open ocean albedo α_o, and for ice thicker than 0.5 m that of the thick ice case of (Ebert and Curry, 1993). The inverse tangent functional form approximates the theoretical dependence of ice albedo on thickness.

For bare melting sea ice, melt ponds can significantly lower the area averaged albedo. This effect is crudely approximated by the following temperature dependence. If $T_{snc} \geq -1°$C, where $T_{snc} = T_{sn} - T_{melt}$, then

$$\begin{aligned} \alpha_{vsdf}(melt) =& \alpha_{vsdf}(dry) - 0.075\Delta T_s \\ \alpha_{nidf}(melt) =& \alpha_{nidf}(dry) - 0.075\Delta T_s \end{aligned} \,. \tag{33}$$

This results in minimum spectral albedos of .705 and .295 for visible and near-ir respectively, or a rough broad band albedo (summertime spectral ratios of visible and near-ir of .53 and .47 respectively) of .512 . As for the case of snow, if the surface temperature $T_{snc} < -1°$C, the dry sea ice albedos are used; otherwise the melt albedos are used.

The horizontal fraction of surface covered with snow is

$$f_{sn} = \frac{h_{sn}}{h_{sn} + 0.02}. \tag{34}$$

This expression is approximately in keeping with snow depth dependence of albedo from (Ebert and Curry, 1993), and from measurements of albedo on snow covered Antarctic sea ice (Allison et al., 1993). We arrived at the value of .02 in the denominator to achieve the best match with SHEBA data.

Combining ice and snow albedos by averaging over the horizontal coverage results in

$$\begin{aligned} \alpha_{vsdfn} =& \alpha_{vsdf}(1 - f_{sn}) + f_{sn}\alpha^s_{vsdf} \\ \alpha_{nidfn} =& \alpha_{nidf}(1 - f_{sn}) + f_{sn}\alpha^s_{nidf} \end{aligned} \,. \tag{35}$$

As noted above, the direct albedos are assumed identical to the diffuse. The final index n is included to signify that these albedos are category dependent.

This crude albedo, when compared with SHEBA measurements (Curry et al., 2001), is able to represent the major albedo regimes of springtime pre-melt dry snow, melting snow cover, dry bare ice, bare ice with melt ponds, and early fall freeze with light snow. However, future versions of the CCSM sea ice model will likely have more explicit physics for these regimes.

For diagnostic purposes, it is useful to have an aggregate broad band surface albedo for the history file (see section 6):

$$\alpha_{bb} = .29\alpha_{vsdr} + .24\alpha_{vsdf} + .31\alpha_{nidr} + .16\alpha_{nidf}. \tag{36}$$

The relative weights are only rough estimates of typical surface flux in each spectral band and incident angle.

4.5 Ice to Atmosphere Flux Exchange

Atmospheric states and downwelling fluxes, along with surface states and properties, are used to compute atmosphere-ice shortwave and longwave fluxes, stress, sensible and latent heat fluxes. Surface states are temperature T_{sn} and albedos α_{vsdrn}, α_{vsdfn}, α_{nidrn}, α_{nidfn} (see section 4.4), while surface properties are longwave emissivity ε and aerodynamic roughness z_i (note that these properties in general vary with ice thickness, but are here assumed constant). Additionally, certain flux temperature derivatives required for the ice temperature calculation are computed, as well as a reference diagnostic surface air temperature.

The following formulae are used for the n^{th} category for the absorbed shortwave fluxes and upwelling longwave flux:

$$F_{SWvsn} = F_{SWvsdr}(1 - \alpha_{vsdrn}) + F_{SWvsdf}(1 - \alpha_{vsdfn}) \tag{37}$$

$$F_{SWnin} = F_{SWnidr}(1 - \alpha_{nidrn}) + F_{SWnidf}(1 - \alpha_{nidfn}) \tag{38}$$

$$F_{SWn} = F_{SWvsn} + F_{SWnin} \tag{39}$$

$$F_{LWUPn} = -\varepsilon\sigma_{sb}T_{sn}^4 + (1 - \varepsilon)F_{LWDN} \tag{40}$$

The downwelling shortwave flux and albedos distinguish between visible ($vs, \lambda < 0.7\mu m$), near-infrared ($ni, \lambda > 0.7\mu m$), direct (dr) and diffuse (df) radiation for each category. Note that the upwelling longwave flux has a reflected component from the downwelling longwave whenever $\varepsilon < 1$.

For the n^{th} category stress components, sensible and latent heat flux, the following bulk formulae are used (Bryan et al., 1996):

$$\tau_{axn} = \rho_a r_{mn} u_n^* u_a \tag{41}$$

$$\tau_{ayn} = \rho_a r_{mn} u_n^* v_a \tag{42}$$

$$F_{SHn} = \rho_a c_a r_{hn} u_n^* (\theta_a - T_{sn}) \tag{43}$$

$$F_{LHn} = \rho_a L_s r_{en} u_n^* (q_a - q_s(T_{sn})) \tag{44}$$

where:

$$q_s(T_{sn}) = (q_1/\rho_a)e^{-q_2/T_{sn}} \tag{45}$$

$$c_a = C_p(1 + C_{pvir}q_s(T_{sn})) \tag{46}$$

$$C_{pvir} = (C_{pwv}/C_p) - 1. \tag{47}$$

$q_s(T)$ is the surface saturation specific humidity for either ice or ocean at temperature T in Kelvins (the values of q_1, q_2 for ice were kindly supplied by Xubin Zeng of the University of Arizona), C_p is the specific heat of dry air and C_{pwv} of water vapor (see Table 10 for values of constants). The exchange coefficients for momentum, sensible and latent heat for each category are r_{mn}, r_{hn}, and r_{en} respectively.

The bulk formulae are based on Monin-Obukhov similarity theory. Among boundary layer scalings, this is the most well tested (Large, 1998). It is based on the assumption that in the surface layer (typically the lowest tenth of the atmospheric boundary layer), but away from the surface roughness elements, only the distance from the boundary and the surface kinematic fluxes are important in the turbulent exchange.

The fundamental turbulence scales that are formed from these quantities are the friction velocity u_n^*, the temperature and moisture fluctuations θ_n^* and q_n^* respectively, and the Monin-Obukhov length scale L_n:

$$u_n^* = r_{mn} V_{mag} \tag{48}$$

$$\theta_n^* = r_{hn}(\theta_a - T_{sn}) \tag{49}$$

$$q_n^* = r_{en}(q_a - q_s(T_{sn})) \tag{50}$$

$$L_n = u_n^{*3}/(\kappa F_n) \tag{51}$$

with

$$V_{mag} = max(1.0, \sqrt{u_a^2 + v_a^2}), \tag{52}$$

to prevent zero or small fluxes under quiescent wind conditions, κ is von Karman's constant (0.4), and F_n is the bouyancy flux, defined as:

$$F_n = \frac{u_n^*}{g}\{\frac{\theta_n^*}{\theta_{vn}} + \frac{q_n^*}{z_v^{-1} + q_a}\} \tag{53}$$

with g the gravitational acceleration and the virtual potential temperature $\theta_{vn} = \theta_a(1 + z_v q_a)$ where $z_v = \rho_{wv}/\rho_a - 1$.

Similarity theory holds that the vertical gradients of mean horizontal wind, potential temperature and specific humidity are universal functions of stability parameter $\zeta = z/L$, where z is height above the surface (ζ is positive for a stable surface layer and negative for an unstable surface layer). These universal similarity functions are determined from observations in the atmospheric boundary layer (Hogstrom, 1988) though no single form is widely accepted. Integrals of the vertical gradient relations result in the familiar logarithmic mean profiles, from which the exchange coefficients can be defined, where $\zeta_n = z_a/L_n$:

$$r_{mn} = r_0\{1 + \frac{r_0}{\kappa}(ln(z_a/z_{ref}) - \chi_m(\zeta_n))\}^{-1} \tag{54}$$

$$r_{hn} = r_0\{1 + \frac{r_0}{\kappa}(ln(z_a/z_{ref}) - \chi_h(\zeta_n))\}^{-1} \tag{55}$$

$$r_{en} = r_{hn} \tag{56}$$

with the neutral coefficient r_0 over ice:

$$r_0 = \frac{\kappa}{ln(z_{ref}/z_i)}, \tag{57}$$

and over ocean:

$$r_0 = (.0027/V_{mag} + .000142 + .0000764 V_{mag})^{1/2} \tag{58}$$

where the flux profile functions (integrals of the similarity functions mentioned above) for momentum m and heat/moisture h are:

$$\chi_m(\zeta_n) = \chi_h(\zeta_n) = -5\zeta_n \tag{59}$$

for stable conditions ($\zeta_n > 0$). For unstable conditions ($\zeta_n < 0$):

$$\chi_m(\zeta_n) = ln\{(1 + X_n(2 + X_n))(1 + X_n^2)/8\} - 2tan^{-1}(X_n) + 0.5\pi \tag{60}$$

$$\chi_h(\zeta_n) = 2ln\{(1 + X_n^2)/2\} \tag{61}$$

with

$$X_n = (max((1 - 16\zeta_n)^{1/2}), 1.)^{1/2}. \tag{62}$$

The stability parameter ζ_n is a function of the turbulent scales and thus the fluxes, so an iterative solution is necessary. The coefficients are initialized with their neutral value r_0, from which the turbulent scales, stability, and then flux profile functions can be evaluated. This order is repeated for five interations to ensure convergence to an acceptible solution.

The surface temperature derivatives required by the ice temperature calculation are evaluated as:

$$\frac{dF_{LWUPn}}{dT_{sn}} = -4\varepsilon\sigma_{sb}T_{sn}^3 \tag{63}$$

$$\frac{dF_{SHn}}{dT_{sn}} = -\rho_a c_a r_{hn} u_n^* \tag{64}$$

$$\frac{dF_{LHn}}{dT_{sn}} = -\rho_a L_s r_{en} u_n^* \frac{dq_s(T_{sn})}{dT_{sn}} \tag{65}$$

where the small temperature dependencies of c_a, the exchange coefficients r_{hn} and r_{en} and velocity scale u_n^* are ignored.

For diagnostic purposes, an air temperature (T_{REFn}) at the reference height of $z_{2m} = 2m$ is computed, making use of the stability and momentum/sensible heat exchange coefficients. Defining $b_m = \kappa/r_{mn}$, and $b_h = \kappa/r_{hn}$, we have:

$$ln_m = ln\{(1 + z_{2m}/z_a)(e^{b_m} - 1)\} \tag{66}$$

$$ln_h = ln\{(1 + z_{2m}/z_a)(e^{b_m - b_h} - 1)\}. \tag{67}$$

For stable conditions ($\zeta_n > 0$)

$$f_{int} = (ln_m - (z_{2m}/z_a)(b_m - b_h))/b_h \tag{68}$$

and for unstable conditions ($\zeta_n < 0$)

$$f_{int} = (ln_m - ln_h)/b_h \tag{69}$$

where f_{int} is bounded by 0 and 1. The resulting reference temperature is:

$$T_{refn} = T_{sn} + (T_a - T_{sn}) f_{int}. \tag{70}$$

4.6 Vertical Heat Conduction

Vertical heat conduction follows Maykut and Untersteiner (1971) and Bitz and Lipscomb (1999). This section is also drawn from Bitz (2000) with modifications to match the notation used in this report, and with minor modifications for assumptions unique to this model.

To represent the vertical transfer of heat through the ice, we allow the ice internal energy (Eq. 14) to vary with level z, where z is vertical depth measured positive downwards from the ice/atmosphere interface. The number of layers of ice (L) depends on the category, with the thinnest two categories (see Table 4) having two equally spaced layers and the thicker three categories having four, with each layer thickness $\Delta h_n = h_n/L$ where h_n is from Eq. 21. The internal energy for each layer can be solved for an equivalent layer temperature (Eq. 22). Vertical heat transfer is then calculated for ($l = 1...L$) vertical layers in the sea ice and one layer of overlying snow. A staggered vertical grid is used, with temperature and salinity defined at layer midpoints and conductivity defined at layer interfaces. Layers at the top and bottom are referred to as surface layers, and those away from the surfaces as interior layers. See Figure 2 for a diagram on the vertical level structure. In this section, the superscript is reserved for the time index m, and the category index n is implied; the subscript s on T denotes the surface and the subscript 0 denotes the snow layer.

The vertical salinity profile is represented by

$$S(w) = 1.6\left\{1 - \cos\left(\pi w^{\frac{0.407}{0.573+w}}\right)\right\} \tag{71}$$

with the normalized coordinate w calculated for each category as

$$w = z/h, 0 \le w \le 1 \tag{72}$$

and where the ice thickness h is diagnosed from Eq. (21). This results in a profile that varies from 0 ppt at ice surface increasing to 3.2 ppt at ice base. Snow thickness h_s is diagnosed from Eq. (21). Note that the salinity profile is independent of category.

The heat content change over the time interval t to t' corresponding to temperatures T and T', respectively, allowing for temperature dependent heat capacity, thermal conduction and internal absorption of penetrating solar radiation, is given by:

$$\int_T^{T'} \rho_i c_i dT = \rho_i c_0 (T' - T) \left(1 + \frac{L_i \mu S}{c_0 T' T}\right) = \int_t^{t'} \left(\frac{\partial}{\partial z} k \frac{\partial T}{\partial z} + Q_{SW}\right) dt \tag{73}$$

where c_i is from Eq (16), Q_{SW} is the absorbed shortwave flux, and the thermal conductivity k is either that for snow or ice. For snow, $k = k_s$ is a constant, while for ice:

$$k(S,T) = k_{fi} + \frac{\beta S}{T} \tag{74}$$

where k_{fi} and β are empirical constants from Untersteiner (1961). Q_{SW} is given by:

$$Q_{SW} = -\frac{d}{dz}\{I_{0vs} e^{-\kappa_{vs} z} + I_{0ni} e^{-\kappa_{ni} z}\} \tag{75}$$

and I_{0vs}, I_{0ni} are the absorbed shortwave radiation in the visible and near-ir that penetrates the surface, respectively, given by:

$$I_{0vs} = 0.70 F_{SWvsn}(1 - f_{sn}) \tag{76}$$

$$I_{0ni} = 0.0 \tag{77}$$

where f_{sn}, the horizontal fraction of surface covered by snow, is given by Eq. 34. It is assumed that no shortwave radiation penetrates the snow covered surface. The spectral extinction coefficients are κ_{vs} and κ_{ni} for the visible and near-infrared bands respectively (Gary Maykut, personal communication). For the purposes of computing the penetration factors (.70 and .0) for the visible and near-ir radiation respectively, a surface layer of 5 cm thick was assumed. However, for the surface energy balance calculation (see section 4.6.1) the surface layer thickness is not explicitly used. Note that there is no distinction made between direct or diffuse shortwave: in effect, we assume shortwave radiation penetrating the surface is diffuse.

The heat equation is discretized using a backwards-Euler, space-centered scheme. Using the staggered grid with T_l representing the layer temperature and k_l representing conductivity at the layer interfaces, for interior layers we have

$$\rho_i c_0 (T_l^{m+1} - T_l^m) \left(1 + \frac{L_i \mu S_l}{c_0 T_l^{m+1} T_l^m}\right) = \frac{\Delta t}{\Delta h^m} \left(k_{l+1}^m \frac{T_{l+1}^{m+1} - T_l^{m+1}}{\Delta h^m} - k_l^m \frac{T_l^{m+1} - T_{l-1}^{m+1}}{\Delta h^m} + I_l^m\right), \tag{78}$$

where $\Delta h^m = h^m / L$, the conductivity is

$$k_l^m = k\left(\frac{S_l + S_{l+1}}{2}, \frac{T_l^m + T_{l+1}^m}{2}\right), \tag{79}$$

and the absorbed solar radiation is

$$I_l^m = I_{0vs}(e^{-\kappa_{vs} l \Delta h^m} - e^{-\kappa_{vs}(l+1)\Delta h^m}) + I_{0ni}(e^{-\kappa_{ni} l \Delta h^m} - e^{-\kappa_{ni}(l+1)\Delta h^m}). \tag{80}$$

See Figure 2 for a diagram on the vertical level structure.

For a purely implicit backward scheme, k should be evaluated at the $m+1$ time level. However, when k is evaluated at time level m, experiments show that the solution is stable and converges to the same solution one gets when evaluating k at $m+1$.

The discrete heat equation for the surface layers is modified slightly from Eq. 78 to maintain second-order accuracy for $\partial T / \partial z$. The equation for the bottom layer ($l = L$) is

$$\begin{aligned} &\rho_i c_0 (T_L^{m+1} - T_L^m) \left(1 + \frac{L_i \mu S_L}{c_0 T_L^{m+1} T_L^m}\right) = \\ &\frac{\Delta t}{\Delta h^m} \left(3 k_{L+1} \frac{T_b - T_L^{m+1}}{\Delta h^m} - \frac{1}{3} k_{L+1} \frac{T_b - T_{L-1}^{m+1}}{\Delta h^m} - k_L^m \frac{T_L^{m+1} - T_{L-1}^{m+1}}{\Delta h^m} + I_L^m\right), \end{aligned} \tag{81}$$

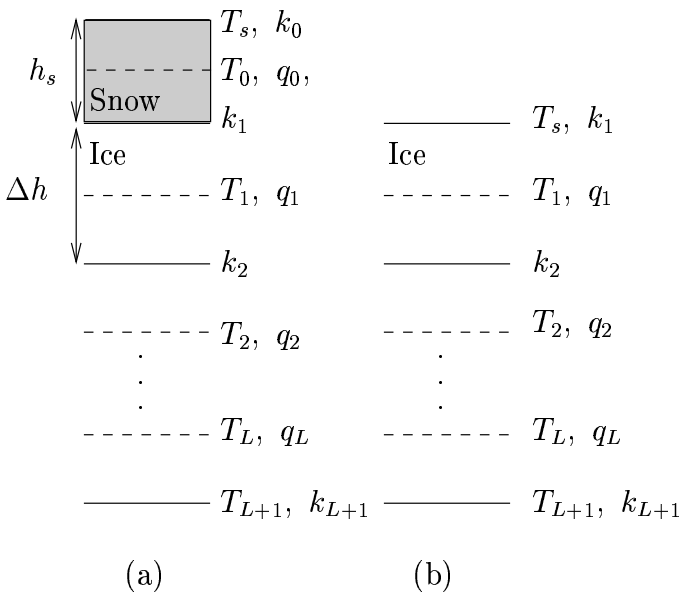

Figure 2: Vertical grid of the sea ice (a) when snow is present and (b) when the ice is snow free; Δh is the thickness of an ice layer and h_s is the thickness of the snow layer. The surface temperature in either case is T_s. Modified from Bitz (2000).

where the $L+1$ interface in contact with the underlying ocean is assumed to be at temperature $T_b = T_{of}$, and where the conductivity is simply $k_{L+1} = k(S_b, T_b)$. The equations for the top surface depend on the surface conditions, of which there are four possibilities, as outlined in Table 5. If the snow depth is too

Table 5: Top Surface Boundary Cases

	snow accumulated	melting
case I	yes	no
case II	no	no
case III	yes	yes
case IV	no	yes

small, numerical solutions are unreliable, and hence the insulating effects of snow are ignored for depths below h_{smin}.

4.6.1 Surface boundary conditions

Freshwater fluxes from the atmosphere are received by the ice model in the form of rain F_{RN} and snow F_{SNW} (see Table 2). Presently, the rain is assumed to run off into the ocean without modification to the snow and ice, and adds to the fresh water flux into the ocean F_{Wo} (see Table 3). Unless otherwise noted, all fluxes have an implied time step index m.

Snow (see Eq. 21) is assumed to accumulate on the surface as:

$$h_{sn}^{m+1/2} = h_{sn}^{m} + F_{SNW}\Delta t/\rho_s. \tag{82}$$

The boundary condition at the ice surface results from a balance of fluxes

$$F_{TOPn}(T_{sn}) = F_{SWvsn} - I_{0vs} + F_{SWnin} - I_{0ni} + \varepsilon F_{LWDN} - \varepsilon\sigma_{sb}T_{sn}^4 + F_{SHn} + F_{LHn} + k_n \left.\frac{dT_n}{dz}\right|_{z=0}, \quad (83)$$

where z is the vertical depth measured downwards from the top ice interface,.

If $F_{TOPn}(T_{melt}) \geq 0$ then $T_{sn} = T_{melt}$ and surface melting when snow is present proceeds according to

$$F_{TOPn}(T_{sn}) = q_s \frac{dh_{sn}}{dt}. \quad (84)$$

When no snow is present surface melting proceeds according to

$$F_{TOPn}(T_{sn}) = q_n(T_n, S)\frac{dh_n}{dt}, \quad (85)$$

where T_n and S are the ice temperature and salinity of the top ice layer, respectively. The boundary condition at the ice bottom is

$$F_{BOT} - k_n \frac{\partial T_n}{\partial z} = q_n(T_n, S)\frac{dh_n}{dt} \quad (86)$$

where F_{BOT} is the heat flux from the ocean (see section 4.7), k_n is the ice thermal conductivity, and T_n,S are the temperature and salinity of the bottom ice layer, respectively.

4.6.2 Case I: Snow accumulated with no melting

The discrete heat equation for the uppermost layer (i.e, the snow layer) is

$$\rho_s c_s (T_0^{m+1} - T_0^m) = \frac{\Delta t}{h_s^m}\left[k_1^m \frac{T_1^{m+1} - T_0^{m+1}}{(\Delta h^m + h_s^m)/2} - \alpha k_s \frac{T_0^{m+1} - T_s^{m+1}}{h_s^m} - \beta k_s \frac{T_1^{m+1} - T_s^{m+1}}{h_s^m}\right]. \quad (87)$$

The heat equation solver is formulated for the general case where the heat capacity of snow c_s may be specified, although it is taken to be 0. The parameters α and β are defined to give second-order accurate spatial differencing for $\partial T/\partial z$ across the changing layer spacing at the snow/ice boundary;

$$\begin{aligned} \alpha &= \frac{h_s^m + \Delta h^m/2}{h_s^m/2}\ \frac{2}{h_s^m + \Delta h^m} h_s^m \\ \beta &= \frac{-h_s^m/2}{h_s^m + \Delta h^m/2}\ \frac{2}{h_s^m + \Delta h^m} h_s^m. \end{aligned} \quad (88)$$

The conductivity at the snow–ice interface is found by equating conductive fluxes above and below the interface;

$$k_1^m = \frac{2k_s k(S_1, T_1^m)}{h_s^m k(S_1, T_1^m) + \Delta h^m k_s}\ \frac{h_s^m + \Delta h^m}{2}. \quad (89)$$

Because T_s is below melting, a flux boundary condition is used, and an additional equation is required in the coupled set:

$$F_o(T_s^{m+1}) + \alpha k_s \frac{T_0^{m+1} - T_s^{m+1}}{h_s^m} + \beta k_s \frac{T_1^{m+1} - T_s^{m+1}}{h_s^m} = 0, \quad (90)$$

where $F_o(T_s^{m+1})$ is the sum of all terms on the right-hand side of Eq. 83 except $k\partial T/\partial z$. The net surface flux $F_o(T_s^{m+1})$ is approximated as linear in T_s^{m+1}; thus

$$F_o(T_s^{m+1}) \sim F_o(T_s^m) + \left.\frac{\partial F_o}{\partial T_s}\right|_{T_s^m} (T_s^{m+1} - T_s^m). \quad (91)$$

with

$$\left.\frac{\partial F_o}{\partial T_s}\right|_{T_s^m} = \left.\frac{\partial F_{LWUP}}{\partial T_s}\right|_{T_s^m} + \left.\frac{\partial F_{SH}}{\partial T_s}\right|_{T_s^m} + \left.\frac{\partial F_{LH}}{\partial T_s}\right|_{T_s^m} \quad (92)$$

To simplify our set of equations, we define

$$\hat{c}_l^{m+1} = \rho_i \left(c_0 + \frac{L_i \mu S}{T_l^{m+1} T_l^m} \right), \tag{93}$$

where the hat implies that $\hat{c}_l^{m+1}$ depends on T_l^m as well as on T_l^{m+1}, and

$$\chi_l^{m+1} = \frac{\Delta t}{\Delta h^m} \frac{1}{\hat{c}_l^{m+1}}. \tag{94}$$

Also, let

$$k_l = \frac{k_l^m}{\Delta h^m}. \tag{95}$$

for $l \geq 2$ and

$$k_0 = \frac{k_s}{h_s^m} \tag{96}$$

$$k_1 = \frac{k_1^m}{(\Delta h^m + h_s^m)/2} \tag{97}$$

and suppress the index m for I_l^m, so that for interior layers ($l = 1...L-1$),

$$T_l^{m+1} - T_l^m = \chi_l^{m+1} \left[k_{l+1}(T_{l+1}^{m+1} - T_l^{m+1}) - k_l(T_l^{m+1} - T_{l-1}^{m+1}) + I_l \right] \tag{98}$$

and at the bottom layer

$$\begin{aligned} T_L^{m+1} - T_L^m = \chi_L^{m+1} \Big[& 3k_b(T_b - T_L^{m+1}) - \frac{1}{3} k_b (T_b - T_{L-1}^{m+1}) \\ & - k_L(T_L^{m+1} - T_{L-1}^{m+1}) + I_L \Big] \end{aligned} \tag{99}$$

where $k_b = k_{L+1}/\Delta h^m$. The equation describing the snow layer is written

$$\rho_s c_s (T_0^{m+1} - T_0^m) = \frac{\Delta t}{h_s^m} \left[k_1(T_1^{m+1} - T_0^{m+1}) - \alpha k_0 (T_0^{m+1} - T_s^{m+1}) - \beta k_0 (T_1^{m+1} - T_s^{m+1}) \right]. \tag{100}$$

Finally, the flux boundary condition becomes

$$F_o(T_s^m) + \left. \frac{\partial F_o}{\partial T_s} \right|_{T_s^m} (T_s^{m+1} - T_s^m) = -\alpha k_0 (T_0^{m+1} - T_s^{m+1}) - \beta k_0 (T_1^{m+1} - T_s^{m+1}). \tag{101}$$

The complete set of coupled equations for case I can be written with all of the terms that explicitly depend on temperature at the $m+1$ time step gathered on the right-hand side:

$$\begin{aligned} -F_o(T_s^m) + \left. \frac{\partial F_o}{\partial T_s} \right|_{T_s^m} T_s^m &= T_s^{m+1} \left(\left. \frac{\partial F_o}{\partial T_s} \right|_{T_s^m} - \alpha k_0 - \beta k_0 \right) \\ &\quad + T_0^{m+1} \alpha k_0 + T_1^{m+1} \beta k_0 \\ \rho_s c_s T_0^m &= T_s^{m+1} \left(-\frac{\Delta t}{h_s^m} \right) (\alpha k_0 + \beta k_0) \\ &\quad + T_0^{m+1} \left(\rho_s c_s + \frac{\Delta t}{h_s^m} (\alpha k_0 + k_1) \right) \\ &\quad + T_1^{m+1} \frac{\Delta t}{h_s^m} (\beta k_0 - k_1) \\ T_l^m + \chi_l^{m+1} I_l &= T_{l-1}^{m+1} (-\chi_l^{m+1} k_l) \\ &\quad + T_l^{m+1} (1 + \chi_l^{m+1} k_l + \chi_l^{m+1} k_{l+1}) \\ &\quad + T_{l+1}^{m+1} (-\chi_l^{m+1} k_{l+1}) \\ T_L^m + \chi_L^{m+1} I_L + \frac{8}{3} \chi_L^{m+1} k_b T_b &= T_{L-1}^{m+1} \left(-\frac{1}{3} \chi_L^{m+1} k_b - \chi_L^{m+1} k_L \right) \\ &\quad + T_L^{m+1} (1 + 3\chi_L^{m+1} k_b + \chi_L^{m+1} k_L). \end{aligned} \tag{102}$$

These equations are subsequently related to the following abbreviated form

$$\begin{aligned} r_s &= T_s^{m+1} b_s + T_0^{m+1} c_s + T_1^{m+1} d_s \\ r_0 &= T_s^{m+1} a_0 + T_0^{m+1} b_0 + T_1^{m+1} c_0 \\ r_1 &= T_0^{m+1} a_1 + T_1^{m+1} b_1 + T_2^{m+1} c_1 \\ &\vdots \\ r_L &= T_{L-1}^{m+1} a_L + T_L^{m+1} b_L. \end{aligned} \tag{103}$$

The first two rows can be combined to eliminate the coefficient on T_1^{m+1} in the first row, allowing the set to be written in tridiagonal form:

$$r = \begin{bmatrix} r_s c_0 - r_0 d_s \\ r_0 \\ r_1 \\ \vdots \end{bmatrix} \quad A = \begin{bmatrix} b_s c_0 - a_0 d_s & c_s c_0 - b_0 d_s & & \\ a_0 & b_0 & c_0 & \\ & a_1 & b_1 & c_1 \\ & & & \ddots \end{bmatrix} \quad T = \begin{bmatrix} T_s^{m+1} \\ T_0^{m+1} \\ T_1^{m+1} \\ \vdots \end{bmatrix}. \tag{104}$$

Because the matrix A depends on χ_l^{m+1}, which in turn depends on T_l^{m+1}, the system of equations is solved iteratively. An initial guess is used for the temperature dependence of χ_l^{m+1}, and then χ_l^{m+1} is updated successively after each iteration. Under most conditions the method approaches a solution in less than four iterations with a maximum error tolerance of ΔT_{err} for T_l with an initial guess of $T_l^{m+1} = T_l^m$.

4.6.3 Case II: Snow free with no melting

Nearly the same method applies when the ice is snow free, except one less equation is needed to describe the evolution of the temperature profile. The equation for the uppermost ice layer is written

$$\begin{aligned} &\rho_i c_0 (T_1^{m+1} - T_1^m) \left(1 + \frac{L_i \mu S_1}{c_0 T_1^{m+1} T_1^m}\right) \\ &\quad = \frac{\Delta t}{\Delta h^m} \left(k_2^m \frac{T_2^{m+1} - T_1^{m+1}}{\Delta h^m} - 3k_1^m \frac{T_1^{m+1} - T_s^{m+1}}{\Delta h^m} + \frac{1}{3} k_1^m \frac{T_2^{m+1} - T_s^{m+1}}{\Delta h^m} + I_1^m\right), \end{aligned} \tag{105}$$

where $k_1^m = k(S_1, T_1^m)$. After the definitions from Eqs. 93–95 are applied, Eq. 105 becomes

$$T_1^{m+1} - T_1^m = \chi_1^{m+1} \left[k_2 (T_2^{m+1} - T_1^{m+1}) - 3k_1 (T_1^{m+1} - T_s^{m+1}) + \frac{1}{3} k_1 (T_2^{m+1} - T_s^{m+1}) + I_1^m\right]. \tag{106}$$

The flux boundary condition follows after linearizing $F_o(T_s^{m+1})$ in T_s^{m+1}:

$$F_o(T_s^m) + \left.\frac{\partial F_o}{\partial T_s}\right|_{T_s^m} (T_s^{m+1} - T_s^m) = -3k_1 (T_1^{m+1} - T_s^{m+1}) + \frac{1}{3} k_1 (T_2^{m+1} - T_s^{m+1}). \tag{107}$$

The complete set of coupled equation includes Eqs. 102 for layers 2 to L with the following two equations for the surface and upper ice layer:

$$\begin{aligned} -F_o(T_s^m) + \left.\frac{\partial F_o}{\partial T_s}\right|_{T_s^m} T_s^m &= T_s^{m+1} \left(\left.\frac{\partial F_o}{\partial T_s}\right|_{T_s^m} - k_1 \frac{8}{3}\right) + T_1^{m+1} 3k_1 + T_2^{m+1} (-k_1/3) \\ T_1^m + \chi_1^{m+1} I_1^m &= T_s^{m+1} \left(-\chi_1^{m+1} k_1 \frac{8}{3}\right) \\ &\quad + T_1^{m+1} (1 + \chi_1^{m+1} k_2 + 3\chi_1^{m+1} k_1) \\ &\quad + T_2^{m+1} (-\chi_1^{m+1} k_2 - \frac{1}{3} \chi_1^{m+1} k_1), \end{aligned} \tag{108}$$

which can be written

$$\begin{aligned} r_s &= T_s^{m+1} b_s + T_1^{m+1} c_s + T_2^{m+1} d_s \\ r_1 &= T_s^{m+1} a_1 + T_1^{m+1} b_1 + T_2^{m+1} c_1. \end{aligned} \tag{109}$$

These two equations can be combined to eliminate the coefficient on T_2^{m+1}, allowing the set to be written in tridiagonal form:

$$r = \begin{bmatrix} r_s c_1 - r_1 d_s \\ r_1 \\ r_2 \\ \vdots \end{bmatrix} \quad A = \begin{bmatrix} b_s c_1 - a_1 d_s & c_s c_1 - b_1 d_s & & \\ a_1 & b_1 & c_1 & \\ & a_2 & b_2 & c_2 \\ & & & \ddots \end{bmatrix} \quad T = \begin{bmatrix} T_s^{m+1} \\ T_1^{m+1} \\ T_2^{m+1} \\ \vdots \end{bmatrix}. \tag{110}$$

As for case I, this system of equations must be solved iteratively.

4.6.4 Case III: Snow accumulated with melting

Case III describes melting conditions in the presence of a snow layer at the surface. Here a temperature boundary condition is used, which simplifies the solution because the first row in Eqs. 102 is not needed and $T_s = T_{melt}$ in the second row. Hence the complete set of coupled equations is identical to Eqs. 102 for layers 1 to L, with the addition of an equation for the snow layer,

$$\rho_s c_s T_0^m + T_{melt} \frac{\Delta t}{h_s} (\alpha + \beta) k_0 = T_0^{m+1} \left[\rho_s c_s + \frac{\Delta t}{h_s} (k_1 + \alpha k_0) \right] - T_1^{m+1} \frac{\Delta t}{h_s} (k_1 - \beta k_0). \tag{111}$$

This set of equations can be written in tridiagonal form, without the need to eliminate any terms, as was required in cases I and II. However, the solution must still be iterated.

4.6.5 Case IV: No snow with melting

Like case III, case IV describes melting conditions, but here the sea ice is snow free. Hence, the first two rows of Eqs. 102 are not needed, and $T_s = T_{melt}$ for $l = 1$. The set of coupled equations comprises those from Eqs. 102 for layers 2 to L and the following equation for layer 1:

$$T_1^m + \chi_1^{m+1} I_1^m + T_{melt} \chi_1^{m+1} k_1 \frac{8}{3} = T_1^{m+1} \left(1 + \chi_1^{m+1} k_2 + 3 \chi_1^{m+1} k_1 \right) + T_2^{m+1} \left(-\chi_1^{m+1} k_2 - \frac{1}{3} \chi_1^{m+1} k_1 \right). \tag{112}$$

As in case III, this set of equations can immediately be written in the tridiagonal form and solved iteratively.

4.6.6 Freezing and melting at the top and bottom surfaces

The energy of melting of snow is a constant, given by Eq. 19, while the energy of melting for each layer l of sea ice depends on the temperature and salinity (T_l and S_l, respectively) of the layer according to Eqs. 17 and 18:

$$q_l = -\rho_i c_0 (-\mu S_l - T_l) - \rho_i L_i \left(1 + \frac{\mu S_l}{T_l} \right). \tag{113}$$

The energy balance at the top and bottom surfaces determines the melt and growth rates of the sea ice. From the top surface flux balance in Eq. 83, if $F_{\mathrm{TOP}}(T_{melt}) \geq 0$, then the upper surface is fixed at the melting temperature and F_{TOP} is used for melting, according to

$$\delta h_s|_{\mathrm{melt}} = \frac{F_{\mathrm{TOP}}(T_{melt}) \Delta t}{q_s} \tag{114}$$

where $\delta h_s|_{\rm melt}$ is the change in snow thickness due to melt; if the snow layer is completely melted, then

$$\delta h|_{\rm melt} = \frac{F_{\rm TOP}(T_{melt})\Delta t}{q_1}, \tag{115}$$

where $\delta h|_{\rm melt}$ is the change in the top layer thickness due to ice melt, and q_s and q_1 are the energy of melting of the snow and the top layer of the ice, respectively. Snow and ice melt water is assumed to drain to the ocean below without any effect on the intervening snow and ice.

Sublimation occurs when $F_{LH} < 0$ (regardless of T_s), according to

$$\delta h_s|_{\rm evap} = -\frac{F_{LH}\Delta t}{(q_s - \rho_s L_v)} \tag{116}$$

if there is snow at the upper surface, where $\delta h_s|_{\rm evap}$ is the change in snow thickness due to evaporation, and

$$\delta h|_{\rm evap} = -\frac{F_{LH}\Delta t}{(q_1 - \rho_i L_v)} \tag{117}$$

if the ice is snow free, where $\delta h|_{\rm evap}$ is the change in the top layer ice thickness due to evaporation. The same set of equations applies when $F_{LH} > 0$ for condensation on the ice or snow.

The bottom-surface energy balance is (see section 4.7)

$$\delta h|_{\rm basal} = \frac{(F_{BOT} - k\frac{\partial T}{\partial z})\Delta t}{q_b}, \tag{118}$$

where $\delta h|_{\rm basal}$ is the change in the lowest ice layer thickness due to basal freezing or melting, F_{BOT} is the heat supplied to the ice from the underlying ocean,

$$k\frac{\partial T}{\partial z} = 3k_b\frac{T_b - T_L^{m+1}}{\Delta h^m} - \frac{1}{3}k_b\frac{T_b - T_{L-1}^{m+1}}{\Delta h^m} \tag{119}$$

accurate to second order, where the subscript "b" refers to ice base (i.e. $k_b = k_{L+1}$), and

$$q_b = \begin{cases} q_L; & \delta h|_{basal} < 0 \\ -\rho_i c_0(-\mu S_b - T_b) - \rho_i L_i\left(1 + \frac{\mu S_b}{T_b}\right); & \delta h|_{basal} > 0. \end{cases} \tag{120}$$

$\delta h|_{\rm basal} > 0$ represents formation of congelation ice, and is treated as a (negative) fresh water flux to the ocean; while $\delta h|_{\rm basal} < 0$ represents basal ice melting which is added to the fresh water flux to the ocean (see next section).

Snow to ice conversion is allowed. This occurs if the snow layer overlying the sea ice becomes thick enough to depress the snow-ice interface below freeboard (the ocean surface). The interface height is:

$$z_{int} = h - (\rho_s h_s + \rho_i h)/\rho_o. \tag{121}$$

If $z_{int} < 0$, then an amount of snow equal to $-z_{int}\rho_i/\rho_s$ is removed from the snow layer and added to the ice. It is assumed that ocean water floods the depressed snow, and then converts it into ice of thickness $-z_{int}$. The energy of melting of the newly formed ice is: $q_{flood} = q_s\rho_i/\rho_s$. Note that such conversion is assumed to occur with no heat or salt exchange with the ocean. The energy of melting of the ice and snow layers needs to be adjusted when the layer spacing changes after growth/melt, evaporation/sublimation, and flooding (see Figure 3). The adjusted energy of melting is

$$q_l' = \begin{cases} \sum_{k=1}^{L} w_{k,1}q_k - q_{flood}\frac{z_{int}}{\Delta h'}; & l = 1 \\ \sum_{k=1}^{L} w_{k,l}q_k; & 1 < l < L \\ \sum_{k=1}^{L} w_{k,L}q_k + q_b\ \max(\frac{\delta h|_{\rm basal}}{\Delta h'}, 0); & l = L. \end{cases} \tag{122}$$

where $w_{k,l}$ are weights computed from the relative overlap of layer l with each layer k from the old layer spacing and $\Delta h'$ is the new layer spacing.

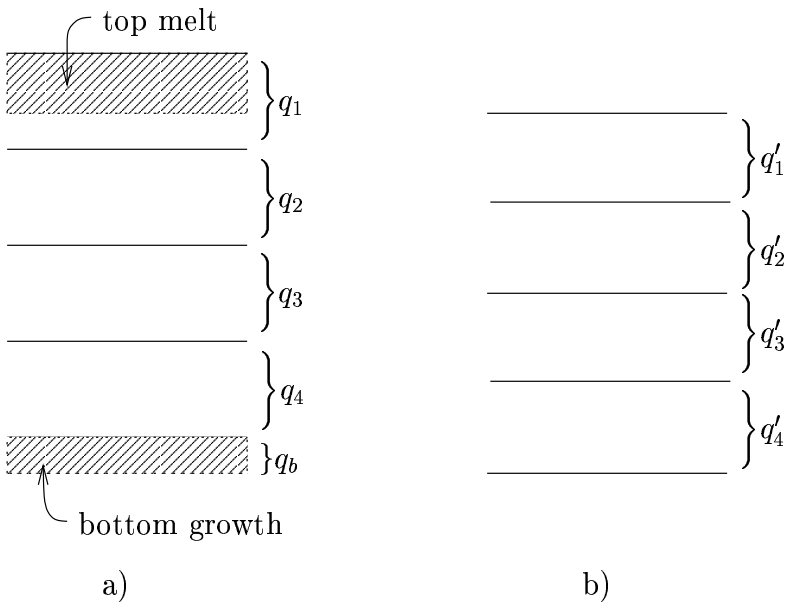

Figure 3: Diagram showing energy content before (a) and after (b) changing the layer spacing for an ice model with four vertical layers that experiences melt at the top surface and growth at the bottom surface. From Bitz (2000)

4.6.7 Flux exchange with the underlying ocean

The shortwave flux transmitted to the ocean for the n^{th} category is:

$$F_{SWon} = \{I_{0vs}e^{-\kappa_{vs}h_n} + I_{0ni}e^{-\kappa_{ni}h_n}\}_n \tag{123}$$

(see Eq. 75 and following).

During ice melt, a fraction of the heat available from the ocean ($F_{Qoi} < 0$), is used, and the ice model must give the actual heat used to the ocean model. The heat used by the ice model in melt includes that used to melt the ice basally and laterally. For the n^{th} category we have:

$$F_{Qion} = \{F_{BOT} + F_{SID}\}_n \tag{124}$$

(see next section).

For the fresh water flux F_{Wo}, recall that three types of ice formation are distinguished: **frazil** (which forms directly in the ocean surface layer), **congelation** (which forms at ice base), and **snow-ice** (which forms by flooding of snow covered ice). Frazil ice is formed in the ocean model as previously described (see section 4.3). The amount of frazil ice given to the ice model is implied in the freezing/melting potential ($F_{Qoi} > 0$). Therefore, there is no explicit water flux from the ocean to the ice model in this case. However, when the ice melts, the melt water is passed back to the ocean. Congelation ice forms in the ice model at ice base. Therefore, the water exchange with the ocean must include both formation and melt. Snow-ice is an internal transformation in the ice model itself, and need not be included in the fresh water flux to the ocean.

The fresh water flux to the ocean for category n is:

$$F_{Won} = A_n F_{RN} + \{-\rho_i \delta h_t - \rho_i \delta h_b - \rho_s \delta h_s + R_{side}(\rho_i V + \rho_s V_s)\}_n / \Delta t. \tag{125}$$

with AF_{RN} is that due to rain on ice assumed to drain directly to the ocean, δh_t is the change in the top ice thickness due to surface melt and evaporation, δh_b is the change in the basal ice thickness due to

congealation ice formation and melt, δh_s is the change in surface snow depth due to melting and evaporation, and $R_{side}(\rho_i V + \rho_s V_s)$ is the ice and snow amount melted by lateral thermodynamic processes (see next section).

4.7 Lateral Formation and Melt

In this section, we evaluate the contribution of the lateral formation/melt term $L(h, g)$. Lateral formation and melt occurs depending on the sign of the freezing/melting potential F_{Qoi} (see section 4.3).

For **positive** F_{Qoi} values, frazil ice formation occurs. In this case, the lower boundary condition flux F_{BOT}=0, and the ocean temperature is T_{of}. A volume of frazil ice $V_f = F_{Qoi}\Delta t/q_f\rho_i$ is formed, where q_f is the constant latent heat of frazil ice formation (Eq. 18 evaluated at $T = T_{of}$ and $S = 4$ ppt). It is assumed that such frazil ice formation occurs either in open water, or in the thinnest ice category. If open water exists (i.e. $A_0 > 0$), ice of thickness $h_0^* = V_f/A_0$ is assumed to form of area $A_0' = A_0$, unless $h_0^* < h_{min}$, for which the area is adjusted to $A_0' = V_f/h_{min}$. If no open water exists (i.e. $A_0 = 0$), then $A_0' = 0$ is assumed. In either case, the thinnest category n_f such that $A_{n_f} > 0$ is found, and frazil ice is added to this category such that:

$$\begin{aligned} A'_{n_f} &= A_{n_f} + A'_0 \\ V_{n_f} &= V_{n_f} + V_f \\ T_{sn_f} &= (T_{sn_f} A_{n_f} + T_{new} A'_0)/A'_{n_f} \\ A_{n_f} &= A'_{n_f} \end{aligned} \tag{126}$$

where $T_{new} = min\{T_o, 0.5(T_a + T_{of})\}$. For each level z:

$$E_n(z) = E_n(z) + V_f q_f / L \tag{127}$$

where L is the number of vertical layers of ice and q_f is the (positive) heat of formation of frazil ice.

For **negative** F_{Qoi} values, heat is available to melt ice. This flux is partitioned into heat available for side melt and bottom melt based on first assuming F_{Qoi} is dominated by shortwave radiation, and then assuming shortwave radiation absorbed in the ocean surface layer above the mean ice thickness causes side melting and below it causes basal melting. For the mean ice thickness $\bar{h} = V/A$, where V and A are the aggregate ice volume and area respectively (see section 4.8):

$$\begin{aligned} f_{bot} &= Re^{-\bar{h}/\zeta_1} + (1 - R)e^{-\bar{h}/\zeta_2} \\ f_{sid} &= 1 - f_{bot} \end{aligned} \tag{128}$$

where $R = 0.68$, $\zeta_1 = 1.2\ m^{-1}$, $\zeta_2 = 28\ m^{-1}$ (Paulson and Simpson, 1977) and f_{bot} and f_{sid} are the fractions of bottom and side melt flux available, respectively. Thus the maximum fluxes available for melt are $f_{bot}F_{Qoi}$ and $f_{sid}F_{Qoi}$. The actual amount used for bottom melting, F_{BOT}, is based on boundary layer theory (McPhee, 1992).

$$F_{BOT} = max(-\rho_o c_o c_h u^* \Delta T, f_{bot} F_{Qoi}) \tag{129}$$

where the empirical drag coefficient c_h=0.006, and

$$\Delta T = max(T_o - T_{of}, 0) \tag{130}$$

$$u^* = \sqrt{(\tau_{ox}^2 + \tau_{oy}^2)/\rho_o} \tag{131}$$

with u_{min} the minimum allowed skin friction velocity u^*.

The heat flux for lateral melt is the product of the vertically averaged, aggregate energy of melting of snow and ice ($E_{tot} = \rho_s L_s V_s + \sum_{n=1}^{N} \sum_{n=1}^{L_n} q_{nl} V_n / L_n$, where q_{nl} is the energy of melting for layer l, and L_n is the number of layers of sea ice for category n) with the interfacial melting rate M_a and the total floe perimeter p_f per unit floe area A_f. The interfacial melting rate is taken from the empirical expression of

Maykut and Perovich (1987) based on Marginal Ice Zone Experiment observations: $M_a = m_1 \Delta T^{m_2}$, where $m_1 = 1.6 \times 10^{-6}$m s^{-1} deg^{m_2} and $m_2 = 1.36$. The lead-ice perimeter depends on the ice floe distribution and geometry. For a mean floe diameter d and number of floes n_f, $p_f = n_f \pi d$ and the floe area $A_f = \eta_{lm} d^2$ (Rothrock and Thorndike (1984) and Bitz (2000)). Thus the heat flux for lateral melt is $E_{tot}(p_f/A_f)M_a$, so that the actual amount used is:

$$F_{SID} = max(\frac{E_{tot}\pi}{\eta_{lm} d} m_1 \Delta T^{m_2}, f_{sid} F_{Qoi}) \tag{132}$$

where $\eta_{lm} = 0.66$ (Rothrock and Thorndike (1984)). Based partially on tuning and partially on the results of floe distribution measurements, the mean floe diameter of d=300 m was chosen. The ice area, volume, snow volume, and ice energy are all reduced by side melt in time Δt by the fraction $R_{side} = |\frac{F_{SID}\Delta t}{E_{tot}}|$.

The heat flux available that is actually used by the ice model is:

$$F_{Qio} = F_{BOT} + F_{SID} \tag{133}$$

4.8 Output to the Coupler

Aggregate states and fluxes over the ice distribution are computed for exchange with the coupler and for history output. Table 3 lists the states and fluxes which are sent to the coupler. The general aggregate equation for an arbitrary field $(\{X_n\}, n = 1, ...N)$ is;

$$X = \frac{1}{A} \sum_{n=1}^{N} X_n A_n \tag{134}$$

where A is aggregate ice concentration.

Note that the ice-ocean stress in the ice dynamics is an implied aggregate; so there is no aggregate equation for it.

For the atmosphere/ice stress, the computed values on the T-grid in the ice model are rotated from the pop grid onto the geographical latitude/longitude directions before being sent to the coupler. Similarly, the ocean/ice stress on the U-grid is first bilinearly interpolated to the T-grid, and then reprojected onto the geographical latitude/longitude directions. In this manner, all vector fields exchanged with the coupler are on the T-grid and projected onto geographical latitude/longitude directions.

Specifically, the following U-grid to T-grid interpolation is required. Note that (u, v) represents a vector field for which the subscripts "g" and "p" refers to geographic and POP grids respectively, and the superscripts "t"and "u" to the T-grid and U-grid respectively.

$$\begin{aligned}
(u_p^t)_{ij} &= \frac{1}{4}(A_{ij}^u (u_p^u)_{ij} + A_{i-1j}^u (u_p^u)_{i-1j} + A_{ij-1}^u (u_p^u)_{ij-1} + A_{i-1j-1}^u (u_p^u)_{i-1j-1})/A_{ij}^t \\
(v_p^t)_{ij} &= \frac{1}{4}(A_{ij}^u (v_p^u)_{ij} + A_{i-1j}^u (v_p^u)_{i-1j} + A_{ij-1}^u (v_p^u)_{ij-1} + A_{i-1j-1}^u (v_p^u)_{i-1j-1})/A_{ij}^t
\end{aligned} \tag{135}$$

where A_{ij}^u is the U-grid box area, and A_{ij}^t is the T-grid box area (see Fig. 1).

Then, the vector components (u_p^t, v_p^t) are rotated back to the geographic grid orientation by:

$$\begin{aligned}
(u_g^t)_{ij} &= (u_p^t)_{ij} cos(\chi_{ij}^t) - (v_p^t)_{ij} sin(\chi_{ij}^t) \\
(v_g^t)_{ij} &= (u_p^t)_{ij} sin(\chi_{ij}^t) + (v_p^t)_{ij} cos(\chi_{ij}^t)
\end{aligned} \tag{136}$$

where (ij) are the longitude/latitude indices of the appropriate grid.

4.9 Linear Remapping

In this section we evaluate the first right-hand side term in the distribution equation (Eq. 1) due to thermodynamic processes, which can be thought of as a transport in thickness space:

$$\frac{\partial g}{\partial t} = -\frac{\partial}{\partial h}(\dot{h}g) \tag{137}$$

where $\dot{h} = dh/dt$. To evaluate this term we use the linear remapping method of Lipscomb (2001). The method is similar to the 1D version of the incremental remapping algorithm of Dukowicz and Baumgardner (2000).

The linear remapping method uses the integral form of the distribution equation. Integrating the above thickness space transport equation between $h^*_{n-1}(t)$ and $h^*_n(t)$, where the boundary thicknesses are time dependent (i.e. following the motion), results in

$$\int_{h^*_{n-1}(t)}^{h^*_n(t)} \frac{\partial g}{\partial t} dh + \int_{h^*_{n-1}(t)}^{h^*_n(t)} \frac{\partial}{\partial h}(\dot{h}g) dh = 0. \tag{138}$$

Evaluating the second term yields

$$\int_{h^*_{n-1}(t)}^{h^*_n(t)} \frac{\partial}{\partial h}(\dot{h}g) dh = g(h^*_n) \left.\frac{dh^*}{dt}\right|_n - g(h^*_{n-1}) \left.\frac{dh^*}{dt}\right|_{n-1}. \tag{139}$$

The integrated transport equation can be rewritten as

$$\frac{d}{dt} \int_{h^*_{n-1}(t)}^{h^*_n(t)} g(h) dh = 0, \tag{140}$$

or using Eq. 2

$$\frac{dA_n}{dt} = 0. \tag{141}$$

This equation can be interpreted in a Lagrangian sense as a conservation equation, where the time dependent limits are the boundaries of the Lagrangian volume following the motion in thickness space. Differentiating the volume ($V_n = A_n h_n$) with time we have

$$\frac{dV_n}{dt} = A_n \frac{dh_n}{dt}. \tag{142}$$

The linear remapping method involves first calculating the new Lagrangian boundaries h^{*m+1}_n, linearly approximating the distribution function in the n^{th} category $g_n(h)$, and finally transferring ice area and volume in order to restore the original thickness boundaries. $g(h)$ is approximated by a series of linear piecewise continuous functions, and ice is transferred in small increments between categories.

The original ice thickness in category n is h^m_n. After the thermodynamic (both vertical and lateral) changes to ice thickness are computed, the new ice thickness is h^{m+1}_n. Let the growth rate of ice thickness in category n be $f_n = \dot{h}_n = (h^{m+1}_n - h^m_n)/\Delta t$. The $m+1$ growth rates at h^{*m}_n are estimated by interpolating between neighboring values of f_n:

$$f^*_n = f_n + \frac{(f_{n+1} - f_n)}{(h^m_{n+1} - h^m_n)}(h^{*m}_n - h^m_n) \tag{143}$$

The new boundary locations are then: $h^{*m+1}_n = h^{*m}_n + f^*_n \Delta t$. Note that in principle the boundaries can shift any distance, but we require here that $h^{m+1}_{n-1} < h^{*m+1}_n < h^{m+1}_{n+1}$.

If any category has no ice (i.e. $A_n = 0$), while an adjacent category does ($A_{n+1} \neq 0$), the boundary is adjusted by the same amount as the thickness in the non-zero category: $h^{*m+1}_n = h^{*m}_n + f^*_{n+1} \Delta t$.

We approximate each Lagrangian volume linearly as $g_n(h) = g_{0n} + g_{1n}h$. To evaluate the coefficients $\{g_{0n}, g_{1n}\}$, we make use of the area and volume constraints, the requirement of a positive distribution function, and the minimum and maximum boundary conditions. The area and volume constraints are

$$\int_{h_{n-1}^{*m}}^{h_n^{*m}} g(h)dh = \int_{h_{n-1}^{*m+1}}^{h_n^{*m+1}} g(h)dh = A_n^m \tag{144}$$

$$\int_{h_{n-1}^{*m+1}}^{h_n^{*m+1}} hg(h)dh = A_n^m h_n^{m+1} \tag{145}$$

Note that the area is conserved following the motion (i.e A_n^m is a constant) but the volume changes to $A_n^m h_n^{m+1}$.

Let us redefine the n^{th} category boundaries at time step $m+1$ as $h_L = h_{n-1}^{*m+1}$ and $h_R = h_n^{*m+1}$ (henceforth we drop the time and category indices). A positive linear function is constructed such that the area and volume integrals over the Lagrangian volume are satisfied. We transform variables from h to η (a relative coordinate): for each Lagrangian volume $\eta = h - h_L$ and $\eta_n = h_n - h_L$ so that $g(\eta) = g_0 + g_1\eta$, where η ranges from 0 to $\eta_R = h_R - h_L$. Note that the h_n in $\eta_n = h_n - h_L$ is the $m+1$ value h_n^{m+1}.

$$A_n = \int_0^{\eta_R} g(\eta)d\eta = \frac{1}{2}{\eta_R}^2 g_1 + \eta_R g_0 \tag{146}$$

$$A_n h_n = \int_0^{\eta_R} (\eta + h_L)(g_1\eta + g_0)d\eta = h_L A_n + \frac{1}{3}{\eta_R}^3 g_1 + \frac{1}{2}{\eta_R}^2 g_0 \tag{147}$$

We have two linear equations for g_{0n} and g_{1n} for the n^{th} category

$$\frac{1}{2}{\eta_R}^2 g_{1n} + \eta_R g_{0n} = A_n \tag{148}$$

$$\frac{1}{3}{\eta_R}^3 g_{1n} + \frac{1}{2}{\eta_R}^2 g_{0n} = A_n\eta_n \tag{149}$$

which have the solution

$$g_{1n} = \frac{12A_n}{{\eta_R}^3}(\eta_n - \frac{\eta_R}{2}) \tag{150}$$

$$g_{0n} = \frac{6A_n}{{\eta_R}^2}(\frac{2\eta_R}{3} - \eta_n). \tag{151}$$

Note that the sign of g_{1n} is determined by $\eta_n - \frac{\eta_R}{2} = h_n - h_L - \frac{h_R - h_L}{2} = h_n - \frac{1}{2}(h_L + h_R)$. When h_n is greater than the Lagrangian midpoint, the slope is positive; when it is less, it is negative.

As g is linear, its maximum and minimum lie at the boundaries $\eta = 0$ and $\eta = \eta_R$

$$g(0) = \frac{6A_n}{{\eta_R}^2}(\frac{2\eta_R}{3} - \eta_n) \tag{152}$$

and

$$g(\eta_R) = \frac{6A_n}{{\eta_R}^2}(\eta_n - \frac{\eta_R}{3}). \tag{153}$$

For $g(\eta)$ to be positive, both boundary values must be positive. $g(0)$ is less than zero when $(\frac{2\eta_R}{3} - \eta_n) < 0$, or $\eta_n > \frac{2\eta_R}{3}$, and $g(\eta_R)$ is less than zero when $\eta_n < \frac{\eta_R}{3}$, i.e. whenever η_n lies outside the central third of the Lagrangian thickness range. As just noted, whenever h_n is greater than the range mid point, the slope $g_{1n} > 0$; if it is greater than $h_L + \frac{2}{3}(h_R - h_L)$, the slope is so great that the minimum value at $g(0)$ falls below zero; and conversely for $h_n < h_L + \frac{1}{3}(h_R - h_L)$, for which the slope becomes so negative as to require $g(\eta_R)$ to be less than zero.

For the case when h_n falls in the first third of the Lagrangian thickness range, we redefine the upper limit to h'_R as: $h_n = h_L + \frac{1}{3}(h'_R - h_L)$ or $h'_R = 3h_n - 2h_L$ and set $g = 0$ between h'_R and h_R. Similarly, when h_n lies in

the upper third of the Lagrangian thickness range, the lower limit is redefined to h'_L as: $h_n = h'_L + \frac{2}{3}(h_R - h'_L)$ or $h'_L = 3h_n - 2h_R$ and set $g = 0$ between h_L and h'_L. In either case, the solutions for g_{0n} and g_{1n} can still be used as long as the appropriate boundaries are defined.

Once $g(h)$ is constructed for each category, the thickness distribution is remapped to the original category boundaries by transferring the appropriate area ΔA_n and volume ΔV_n. If the displaced boundary h_n^{*m+1} has moved to the right, then:

$$\begin{aligned} \Delta A_n^{m+1} &= \int_{h_n^{*m}}^{h_n^{*m+1}} g_n(h)dh \\ \Delta V_n^{m+1} &= \int_{h_n^{*m}}^{h_n^{*m+1}} h g_n(h)dh \end{aligned} \tag{154}$$

If the displaced boundary has moved to the left, the limits of integration are reversed.

The thinnest (i.e. $n = 1$) and thickest (i.e. $n = N$) categories have special minimum and maximum boundary conditions respectively. For category 1, if sea ice is growing in open water at a positive rate f_0, shift h_1^* to the right by $f_0 \Delta t$. If sea ice is not growing in open water, approximate the growth rate as $f_0 = f_1$. If $f_0 < 0$, reduce the ice area by the integral of $g(h)$ from 0 to $-f_0 \Delta t$, leaving the ice volume fixed, as ice volume cannot cross the left boundary. For the right boundary, h_N^* varies with h_N. As $g(h)$ is linear, setting $h_N^* = 3h_N - 2h_{N-1}^*$ ensures $g(h_N^*) = 0$.

Snow volume, internal energy of ice and surface temperature are affected by thickness space transport as follows. Assuming that within each category snow depth varies linearly with ice thickness, the snow volume transport is proportional to the ice volume transport (see section 2.2). The internal energy of ice is $E_n = q_n V_n$, where q_n is the energy of melting of ice, a function of ice temperature and salinity. The internal energy of ice is proportional to the volume of ice, so that the new internal energy at $m+1$ is $E_n^{m+1} = q_n^{m+1} V_n^{m+1}$, where q_n^{m+1} is the $m+1$ energy of melting after the vertical thermodynamic heat transfer has been computed. The surface temperature T_{sn}^m changes with area due to thickness space transport.

4.10 Velocity

Pack ice is composed of rigid ice floes, ranging in size from order 1 m to greater than 10 km. The characteristics of motion for the pack ice are discontinuous slippage near shore, near rigid motion under considerable wind forcing (i.e. nearly rate-independent stress), small or zero tensile strength for both uniaxial and two dimensional dilation, and high compressive strength.

To model this material, the resolved sea-ice is considered to be a highly fractured, closely packed, isotropic medium in which inter-floe forces are contact stresses. The resolved spatial scales are considered to be much larger than the scale of inhomogeneities (i.e. floes). We consider only aggregate ice motion (across the ITD) in each grid box. Thus, we model sea-ice as a two dimensional continuum, whose momentum conservation is described by

$$\bar{m}\frac{\partial \mathbf{u}}{\partial t} = -\bar{m} f \mathbf{k} \times \mathbf{u} + \boldsymbol{\tau}_a + \boldsymbol{\tau}_o + \bar{m} g \nabla H_o + \nabla \cdot \boldsymbol{\sigma} \tag{155}$$

where $\bar{m}$ is the total mass of snow and ice per unit area given by

$$\bar{m} = \rho_s \sum_{n=1}^{N} V_{sn} + \rho_i \sum_{n=1}^{N} V_n, \tag{156}$$

the non-linear $\mathbf{u}$ advection terms are ignored as they are negligibly small when the equations are scaled, f is the Coriolis parameter, $\mathbf{k}$ is the local vertical unit vector, $\boldsymbol{\tau}_a$ and $\boldsymbol{\tau}_o$ are forces due to air and water stresses respectively, g is the gravitational acceleration (for this section only), H_o is the sea surface slope and $\nabla \cdot \boldsymbol{\sigma}$ is the force due to internal ice stress.

The air-ice stress $\boldsymbol{\tau}_a$ is described in section 4.5 and its aggregate equations in section 4.8. The ocean-ice stress $\boldsymbol{\tau}_o$ can be written in the form of a nonlinear drag law

$$\boldsymbol{\tau}_o = \rho_o c_d |\mathbf{u}_o - \mathbf{u}|(\mathbf{u}_o - \mathbf{u}) \tag{157}$$

where c_d is the ocean-ice drag coefficient, ρ_o is the density of seawater and $\mathbf{u}_o$ is the surface ocean current. Note that while the drag coefficient c_d does vary with ice thickness for actual ice floes, here we assume it to be constant.

The internal stress tensor $\boldsymbol{\sigma}$ is a linear vector function of a vector argument, which gives the internal force on the material for a specified direction. The general constitutive law for sea-ice relates the stress to the rate of strain, and generally includes elastic (linear and reversible) and plastic (non-linear and irreversible) components.

The CSM1 sea ice model assumes a cavitating fluid rheology, in which both elastic, shear and tensile stresses are ignored (Bettge et al., 1996), and the ocean-ice stress is linearized. The model suffers numerical grid convergence difficulties near the North Pole (Weatherly et al., 1998). The cavitating fluid rheology is useful in some circumstances, but is limited especially due to lack of shear stresses. A more realistic and generally accepted rheology is the viscous-plastic, or VP (Hibler, 1979; Kreyscher et al., 2000).

The VP rheology derives from the general stress-strain relation for viscous fluids

$$\sigma_{ij} = 2\eta\dot{\epsilon}_{ij} + (\zeta - \eta)\dot{\epsilon}_{kk}\delta_{ij} - \frac{P}{2}\delta_{ij} \tag{158}$$

where the stress tensor is σ_{ij} (i, j = component indices), the compressive strength P, δ_{ij} is the Kronecker delta and the rate of strain tensor is

$$\dot{\epsilon}_{ij} = \frac{1}{2}\left(\frac{\partial u_i}{\partial x_j} + \frac{\partial u_j}{\partial x_i}\right), \tag{159}$$

the total linear rate of strain (divergence) is $\dot{\epsilon}_{kk} = \dot{\epsilon}_{11} + \dot{\epsilon}_{22}$ and $\dot{\epsilon}_{12} = \dot{\epsilon}_{21}$ is the shear rate of strain component. ζ and η are bulk (i.e. linear) and shear viscosities respectively. The general form of this plastic rheology satisfies the condition that the deformational part of the plastic stress tensor vanishes for constant $\mathbf{u}$ and that for solid body rotation no stress is produced. For the viscous flow to be dissipative both ζ and η must be positive.

The **plastic** assumption is that the flow obeys an idealized plastic behavior, namely, that stressed ice is motionless until a yield stress is obtained, after which the flow is irreversible and rate independent. The principal stress states for plastic deformation lie on the yield curve specified by a normalized convex yield function, while the (irreversible) deformation is given by the normal flow rule.

The VP rheology assumes an elliptical yield curve of specified ratio of major to minor axes e. In terms of the stress and strain rate (or deformation) invariants, obtained by diagonalizing and transforming the symmetric stress (σ_I,σ_{II}) and rate of strain tensors ($\dot{\epsilon}_I$,$\dot{\epsilon}_{II}$) into pure compression (I) and shear (II) components, we have the yield function

$$Y(\sigma_I, \sigma_{II}) = \frac{\left(\sigma_I + \frac{P}{2}\right)^2}{\left(\frac{P}{2}\right)^2} + \frac{\sigma_{II}^2}{\left(\frac{P}{2e}\right)^2} = 1 \tag{160}$$

which is chosen to lie in the lower left quadrant of principal stress space, corresponding to no tensile stress but with finite compressional and shear stresses (the latter if e is relatively small). With the normal flow rule $\dot{\epsilon}_I = \lambda\frac{\partial Y}{\partial \sigma_I}$, and $\dot{\epsilon}_{II} = \lambda\frac{\partial Y}{\partial \sigma_{II}}$, the unknown λ can be computed, resulting in

$$\sigma_I = \zeta\dot{\epsilon}_I - P/2 \tag{161}$$

$$\sigma_{II} = \eta\dot{\epsilon}_{II} \tag{162}$$

$$\zeta = P/2\Delta \tag{163}$$

$$\eta = \zeta/e^2 \tag{164}$$

where

$$\dot{\epsilon}_I = \frac{\partial u}{\partial x} + \frac{\partial v}{\partial y} \tag{165}$$

$$\dot{\epsilon}_{II} = \{(\frac{\partial u}{\partial x} - \frac{\partial v}{\partial y})^2 + (\frac{\partial u}{\partial y} + \frac{\partial v}{\partial x})^2\}^{\frac{1}{2}} \tag{166}$$

(Stern et al., 1995), and

$$\Delta = \left[\dot{\epsilon}_I^2 + \dot{\epsilon}_{II}^2/e^2\right]^{1/2}. \tag{167}$$

In the limit of zero strain rate (i.e. rigid solid with no deformation), the viscosities become infinite. To regularize this behavior, the viscosities are bounded for sufficiently small strain rates so that the sea ice moves as a linear viscous fluid undergoing slow creep. Minimum viscosities are set to prevent non-linear instabilities.

The **elastic viscous plastic** (EVP) rheology (Hunke and Dukowicz 1997) derives from the simple stress-strain relation for small strains: $\sigma_{ij} = E\epsilon_{ij}$, where E (analogous to Young's modulus) is related to ice strength such that it increases as ice strength increases. Writing this relation in terms of rate of strain, and ignoring the non-linear advection as in the momentum equation, gives $\frac{1}{E}\frac{\partial \sigma_{ij}}{\partial t} = \dot{\epsilon}_{ij}$. The stress tensor equation (158) for viscous fluids can be solved in terms of the rate of strain, as

$$\dot{\epsilon}_{ij} = \frac{1}{2\eta}\sigma_{ij} + \frac{(\eta - \zeta)}{4\eta\zeta}\sigma_{kk}\delta_{ij} + \frac{P}{4\zeta}\delta_{ij} \tag{168}$$

Combining these two rates of strain (elastic and plastic) to yield the total rate of strain results in

$$\dot{\epsilon}_{ij} = \frac{1}{E}\frac{\partial \sigma_{ij}}{\partial t} + \frac{1}{2\eta}\sigma_{ij} + \frac{\eta - \zeta}{4\eta\zeta}\sigma_{kk}\delta_{ij} + \frac{P}{4\zeta}\delta_{ij} \tag{169}$$

In the limit $E \to \infty$ this rate of strain equation asymptotes to the pure VP rheology, while for $\eta, \zeta \to \infty$, the purely elastic rheology is recovered. Hence, as $\eta, \zeta \to \infty$ under conditions of very small strain rate, the elastic term controls the solution behavior, and represents a regularization of the VP rheology. Note that the elastic term in the stress tensor equation requires that the stress tensor components become prognostic variables in EVP. This is in contrast to VP for which the stress tensor components are diagnostic. The elastic parameter E is given in terms of the bulk viscosity and a damping time scale for elastic waves T_{ew} and time step Δt

$$E = \zeta/T_{ew} \tag{170}$$

$$T_{ew} = E_0 \Delta t. \tag{171}$$

where E_0 is a constant less than 1. The momentum and stress tensor equations are

$$\bar{m}\frac{\partial u}{\partial t} + c'u - \bar{m}fv = c'u_o + \tau_{ax} - \bar{m}g\frac{\partial H_o}{\partial x} + F_x \tag{172}$$

$$\bar{m}\frac{\partial v}{\partial t} + c'v + \bar{m}fu = c'v_o + \tau_{ay} - \bar{m}g\frac{\partial H_o}{\partial y} + F_y \tag{173}$$

$$\frac{\partial \sigma_{ij}}{\partial t} + \frac{e^2}{2T_{ew}}\sigma_{ij} + \frac{1 - e^2}{4T_{ew}}\sigma_{kk}\delta_{ij} = \frac{P}{2T_{ew}\Delta'}\dot{\epsilon}_{ij} - \frac{P}{4T_{ew}}\delta_{ij} \tag{174}$$

where $c' = \rho_o c_d|\mathbf{u}_o - \mathbf{u}|$ and $\Delta' = max(\Delta, \Delta_{min})$ (which prevents residual ice motion due to spatial variations in P for extremely small or zero rates of strain, where $\Delta_{min} = 10^{-13}AT$, AT is the T-grid area), and the stress divergence terms F_x and F_y are evaluated for a general orthogonal curvilinear coordinate system subject to the contraints that the discretization be dissipative and includes grid curvature effects (see Hunke and Dukowicz (2002)).

It is convenient to introduce the divergence D_D, the horizontal tension D_T and shearing rates D_S defined by:

$$D_D = \dot{\epsilon}_{11} + \dot{\epsilon}_{22} \tag{175}$$

$$D_T = \dot{\epsilon}_{11} - \dot{\epsilon}_{22} \tag{176}$$

$$D_S = 2\dot{\epsilon}_{12}. \tag{177}$$

Letting $\sigma_1 = \sigma_{11} + \sigma_{22}$ and $\sigma_2 = \sigma_{11} - \sigma_{22}$, Eqs. (174) can be alternatively expressed as:

$$\frac{1}{E}\frac{\partial \sigma_1}{\partial t} + \frac{\sigma_1}{2\zeta} + \frac{P}{2\zeta} = D_D \tag{178}$$

$$\frac{1}{E}\frac{\partial \sigma_2}{\partial t} + \frac{\sigma_2}{2\eta} = D_T \tag{179}$$

$$\frac{1}{E}\frac{\partial \sigma_{12}}{\partial t} + \frac{\sigma_{12}}{2\eta} = \frac{1}{2}D_S, \tag{180}$$

where we note that $\sigma_I = \sigma_1/2$, $\sigma_{II} = \sqrt{\sigma_2^2/4 + \sigma_{12}^2}$, $\dot{\epsilon}_I = D_D$, $\dot{\epsilon}_{II} = \sqrt{D_T^2 + D_S^2}$, the above definitions of ζ and η are unchanged, while Δ is:

$$\Delta = \left[D_D^2 + \frac{1}{e^2}\left(D_T^2 + D_S^2\right)\right]^{1/2}. \tag{181}$$

Multiplying the momentum equations by u and v respectively and summing, one can form the kinetic energy equation. Using the product rule, $u_i \frac{\partial \sigma_{ij}}{\partial x_j} = \frac{\partial}{\partial x_j}(u_i \sigma_{ij}) - \sigma_{ij}\frac{\partial u_i}{\partial x_j} = \frac{\partial}{\partial x_j}(u_i \sigma_{ij}) - \sigma_{ij}\dot{\epsilon}_{ij}$, where repeated indices imply summation over $(1,2)$. The area integral of the $\frac{\partial}{\partial x_j}(u_i \sigma_{ij})$ term will vanish on lateral boundaries where $u_i = 0$, or for open ocean where $\sigma_{ij} = 0$. Thus, area integrals of the kinetic energy equation over the ice will result in dissipative internal stresses so long as D, defined by:

$$D = \int \left(\sigma_{11}\dot{\epsilon}_{11} + 2\sigma_{12}\dot{\epsilon}_{12} + \sigma_{22}\dot{\epsilon}_{22}\right) dA,$$

is positive definite. Using the definitions of D_D, D_T and D_S we have:

$$D = \int \left[\frac{1}{2}\sigma_1 D_D + \frac{1}{2}\sigma_2 D_T + \sigma_{12} D_S\right] dA \tag{182}$$

In steady state ($\frac{\partial \sigma}{\partial t} \to 0$), Eqs (178, 179, and 180) reduce to the viscous-plastic constitutive law. Using the steady state forms for σ_1, σ_2 and σ_{12}, D can be written as:

$$D = \frac{1}{2}\int P\left(\Delta - D_D\right) dA \geq 0, \tag{183}$$

which insures that the work done by the internal stress is dissipative. Note that D is a scalar invariant independent of coordinate system.

In an orthogonal, curvilinear coordinate system, u and v represent velocity components along nondimensional coordinates ξ_1 and ξ_2 (0 to 1 across a grid box), with scale factors (the physical lengths of the grid box sides) h_1 and h_2, respectively. The rate of strain components are then:

$$\dot{\epsilon}_{11} = \frac{1}{h_1}\left(\frac{\partial u}{\partial \xi_1} + \frac{v}{h_2}\frac{\partial h_1}{\partial \xi_2}\right) \tag{184}$$

$$\dot{\epsilon}_{22} = \frac{1}{h_2}\left(\frac{\partial v}{\partial \xi_2} + \frac{u}{h_1}\frac{\partial h_2}{\partial \xi_1}\right) \tag{185}$$

$$\dot{\epsilon}_{12} = \frac{1}{2}[\frac{h_1}{h_2}\frac{\partial}{\partial \xi_2}\left(\frac{u}{h_1}\right) + \frac{h_2}{h_1}\frac{\partial}{\partial \xi_1}\left(\frac{v}{h_2}\right)]. \tag{186}$$

Using these expressions in the dissipation D above and integrating by parts, orthogonal curvilinear forms for the stress divergence are derived:

$$F_x = \frac{1}{2h_1h_2}\left[\frac{1}{h_1}\frac{\partial \sigma_1}{\partial \xi_1} + \frac{1}{h_1h_2^2}\frac{\partial}{\partial \xi_1}\left(h_2^2\sigma_2\right) + \frac{2}{h_1^2h_2}\frac{\partial}{\partial \xi_2}\left(h_1^2\sigma_{12}\right)\right] \tag{187}$$

$$F_y = \frac{1}{2h_1h_2}\left[\frac{1}{h_2}\frac{\partial \sigma_1}{\partial \xi_2} - \frac{1}{h_1^2h_2}\frac{\partial}{\partial \xi_2}\left(h_1^2\sigma_2\right) + \frac{2}{h_1h_2^2}\frac{\partial}{\partial \xi_1}\left(h_2^2\sigma_{12}\right)\right]. \tag{188}$$

The discretization of the velocity and stress tensor components is termed the "bilinear discretization" (Hunke and Dukowicz (2002)). For example, the velocity components are expressed in terms of the grid box vertex values and non-dimensional coordinates (0 to 1 across the grid box) as:

$$u(\xi_1,\xi_2) = u^{ne}\xi_1\xi_2 + u^{nw}(1-\xi_1)\xi_2 + u^{sw}(1-\xi_1)(1-\xi_2) + u^{se}\xi_1(1-\xi_2) \quad (189)$$

$$v(\xi_1,\xi_2) = v^{ne}\xi_1\xi_2 + v^{nw}(1-\xi_1)\xi_2 + v^{sw}(1-\xi_1)(1-\xi_2) + v^{se}\xi_1(1-\xi_2). \quad (190)$$

where the four grid box velocities are referred to as ne, nw, sw, se for northeast, northwest, southwest and southeast respectively. Note that velocity is continuous across cell edges (for example, $u_{ij}^{ne} = u_{i+1j}^{nw}$, where ij now represent grid indices). The stress tensor components, associated with velocity gradients through strain rates, are discontinuous, with each cell having four corner values for stress. This method of discretization suppresses B-grid checkerboard solutions, because it is not technically B-grid, since we do not have one grid box center value for the stress tensor components.

The scale factors are evaluated at grid center by averaging the two appropriate sides ($h_1 = \bar{h}_1$, $h_2 = \bar{h}_2$), while scale factor spatial derivatives are simple differences in the grid side lengths ($\partial h_1/\partial\xi_2 = \Delta_2 h_1$, $\partial h_2/\partial\xi_1 = \Delta_1 h_2$). Using the bilinear discretization, the strain rate terms are evaluated as follows:

Divergence

$$D_D^{ne} = \frac{1}{\bar{h}_1\bar{h}_2}\left[\bar{h}_2(u^{ne}-u^{nw}) + \Delta_1 h_2 u^{ne} + \bar{h}_1(v^{ne}-v^{se}) + \Delta_2 h_1 v^{ne}\right]$$

$$D_D^{nw} = \frac{1}{\bar{h}_1\bar{h}_2}\left[\bar{h}_2(u^{ne}-u^{nw}) + \Delta_1 h_2 u^{nw} + \bar{h}_1(v^{nw}-v^{sw}) + \Delta_2 h_1 v^{nw}\right]$$

$$D_D^{se} = \frac{1}{\bar{h}_1\bar{h}_2}\left[\bar{h}_2(u^{se}-u^{sw}) + \Delta_1 h_2 u^{se} + \bar{h}_1(v^{ne}-v^{se}) + \Delta_2 h_1 v^{se}\right]$$

$$D_D^{sw} = \frac{1}{\bar{h}_1\bar{h}_2}\left[\bar{h}_2(u^{se}-u^{sw}) + \Delta_1 h_2 u^{sw} + \bar{h}_1(v^{nw}-v^{sw}) + \Delta_2 h_1 v^{sw}\right]$$

Tension

$$D_T^{ne} = \frac{1}{\bar{h}_1\bar{h}_2}\left[\bar{h}_2(u^{ne}-u^{nw}) - \Delta_1 h_2 u^{ne} - \bar{h}_1(v^{ne}-v^{se}) + \Delta_2 h_1 v^{ne}\right]$$

$$D_T^{nw} = \frac{1}{\bar{h}_1\bar{h}_2}\left[\bar{h}_2(u^{ne}-u^{nw}) - \Delta_1 h_2 u^{nw} - \bar{h}_1(v^{nw}-v^{sw}) + \Delta_2 h_1 v^{nw}\right]$$

$$D_T^{se} = \frac{1}{\bar{h}_1\bar{h}_2}\left[\bar{h}_2(u^{se}-u^{sw}) - \Delta_1 h_2 u^{se} - \bar{h}_1(v^{ne}-v^{se}) + \Delta_2 h_1 v^{se}\right]$$

$$D_T^{sw} = \frac{1}{\bar{h}_1\bar{h}_2}\left[\bar{h}_2(u^{se}-u^{sw}) - \Delta_1 h_2 u^{sw} - \bar{h}_1(v^{nw}-v^{sw}) + \Delta_2 h_1 v^{sw}\right]$$

Shearing

$$D_S^{ne} = \frac{1}{\bar{h}_1\bar{h}_2}\left[\bar{h}_1(u^{ne}-u^{se}) - \Delta_2 h_1 u^{ne} + \bar{h}_2(v^{ne}-v^{nw}) - \Delta_1 h_2 v^{ne}\right]$$

$$D_S^{nw} = \frac{1}{\bar{h}_1\bar{h}_2}\left[\bar{h}_1(u^{nw}-u^{sw}) - \Delta_2 h_1 u^{nw} + \bar{h}_2(v^{ne}-v^{nw}) - \Delta_1 h_2 v^{nw}\right]$$

$$D_S^{se} = \frac{1}{\bar{h}_1\bar{h}_2}\left[\bar{h}_1(u^{ne}-u^{se}) - \Delta_2 h_1 u^{se} + \bar{h}_2(v^{se}-v^{sw}) - \Delta_1 h_2 v^{se}\right]$$

$$D_S^{sw} = \frac{1}{\bar{h}_1\bar{h}_2}\left[\bar{h}_1(u^{nw}-u^{sw}) - \Delta_2 h_1 u^{sw} + \bar{h}_2(v^{se}-v^{sw}) - \Delta_1 h_2 v^{sw}\right]$$

For the divergence of the stress tensor, we note that for the ne corner of grid box ij, there are contributions from the four surrounding grid boxes (i.e. northeast corner of ij, southeast corner of $ij+1$, northwest corner

of $i+1j$ and the southwest corner of $i+1j+1$). The terms below show these contributions to the stress divergence for the northeast corner of grid box ij. Hence, for the contributions of each grid box, the corner designations of σ are relative to that box.

Contribution of the σ_1 term to F_1

$$\frac{1}{\bar{h}_1\bar{h}_2}\left\{\left[-\frac{\bar{h}_2}{4}\left(\frac{1}{3}\left(\sigma_1^{ne}+\sigma_1^{nw}\right)+\frac{1}{6}\left(\sigma_1^{se}+\sigma_1^{sw}\right)\right) - \frac{\Delta_1 h_2}{2}\left(\frac{1}{9}\sigma_1^{ne}+\frac{1}{18}\left(\sigma_1^{nw}+\sigma_1^{se}\right)+\frac{1}{36}\sigma_1^{sw}\right)\right]_{ij}\right.$$
$$+\left[\frac{\bar{h}_2}{4}\left(\frac{1}{3}\left(\sigma_1^{ne}+\sigma_1^{nw}\right)+\frac{1}{6}\left(\sigma_1^{se}+\sigma_1^{sw}\right)\right) - \frac{\Delta_1 h_2}{2}\left(\frac{1}{9}\sigma_1^{nw}+\frac{1}{18}\left(\sigma_1^{sw}+\sigma_1^{ne}\right)+\frac{1}{36}\sigma_1^{se}\right)\right]_{i+1j}$$
$$+\left[-\frac{\bar{h}_2}{4}\left(\frac{1}{3}\left(\sigma_1^{se}+\sigma_1^{sw}\right)+\frac{1}{6}\left(\sigma_1^{ne}+\sigma_1^{nw}\right)\right) - \frac{\Delta_1 h_2}{2}\left(\frac{1}{9}\sigma_1^{se}+\frac{1}{18}\left(\sigma_1^{ne}+\sigma_1^{sw}\right)+\frac{1}{36}\sigma_1^{nw}\right)\right]_{ij+1}$$
$$\left.+\left[\frac{\bar{h}_2}{4}\left(\frac{1}{3}\left(\sigma_1^{se}+\sigma_1^{sw}\right)+\frac{1}{6}\left(\sigma_1^{ne}+\sigma_1^{nw}\right)\right) - \frac{\Delta_1 h_2}{2}\left(\frac{1}{9}\sigma_1^{sw}+\frac{1}{18}\left(\sigma_1^{nw}+\sigma_1^{se}\right)+\frac{1}{36}\sigma_1^{ne}\right)\right]_{i+1j+1}\right\}$$

Contribution of the σ_1 term to F_2

$$\frac{1}{\bar{h}_1\bar{h}_2}\left\{\left[-\frac{\bar{h}_1}{4}\left(\frac{1}{3}\left(\sigma_1^{ne}+\sigma_1^{se}\right)+\frac{1}{6}\left(\sigma_1^{nw}+\sigma_1^{sw}\right)\right) - \frac{\Delta_2 h_1}{2}\left(\frac{1}{9}\sigma_1^{ne}+\frac{1}{18}\left(\sigma_1^{nw}+\sigma_1^{se}\right)+\frac{1}{36}\sigma_1^{sw}\right)\right]_{ij}\right.$$
$$+\left[-\frac{\bar{h}_1}{4}\left(\frac{1}{3}\left(\sigma_1^{nw}+\sigma_1^{sw}\right)+\frac{1}{6}\left(\sigma_1^{ne}+\sigma_1^{se}\right)\right) - \frac{\Delta_2 h_1}{2}\left(\frac{1}{9}\sigma_1^{nw}+\frac{1}{18}\left(\sigma_1^{sw}+\sigma_1^{ne}\right)+\frac{1}{36}\sigma_1^{se}\right)\right]_{i+1j}$$
$$+\left[\frac{\bar{h}_1}{4}\left(\frac{1}{3}\left(\sigma_1^{ne}+\sigma_1^{se}\right)+\frac{1}{6}\left(\sigma_1^{nw}+\sigma_1^{sw}\right)\right) - \frac{\Delta_2 h_1}{2}\left(\frac{1}{9}\sigma_1^{sw}+\frac{1}{18}\left(\sigma_1^{ne}+\sigma_1^{sw}\right)+\frac{1}{36}\sigma_1^{nw}\right)\right]_{ij+1}$$
$$\left.+\left[\frac{\bar{h}_1}{4}\left(\frac{1}{3}\left(\sigma_1^{nw}+\sigma_1^{sw}\right)+\frac{1}{6}\left(\sigma_1^{ne}+\sigma_1^{se}\right)\right) - \frac{\Delta_2 h_1}{2}\left(\frac{1}{9}\sigma_1^{sw}+\frac{1}{18}\left(\sigma_1^{nw}+\sigma_1^{se}\right)+\frac{1}{36}\sigma_1^{ne}\right)\right]_{i+1j+1}\right\}$$

Contribution of the σ_2 term to F_1

$$\frac{1}{\bar{h}_1\bar{h}_2}\left\{\left[-\frac{\bar{h}_2}{4}\left(\frac{1}{3}\left(\sigma_2^{ne}+\sigma_2^{nw}\right)+\frac{1}{6}\left(\sigma_2^{se}+\sigma_2^{sw}\right)\right) + \frac{\Delta_1 h_2}{2}\left(\frac{1}{9}\sigma_2^{ne}+\frac{1}{18}\left(\sigma_2^{nw}+\sigma_2^{se}\right)+\frac{1}{36}\sigma_2^{sw}\right)\right]_{ij}\right.$$
$$+\left[\frac{\bar{h}_2}{4}\left(\frac{1}{3}\left(\sigma_2^{ne}+\sigma_2^{nw}\right)+\frac{1}{6}\left(\sigma_2^{se}+\sigma_2^{sw}\right)\right) + \frac{\Delta_1 h_2}{2}\left(\frac{1}{9}\sigma_2^{nw}+\frac{1}{18}\left(\sigma_2^{sw}+\sigma_2^{ne}\right)+\frac{1}{36}\sigma_2^{se}\right)\right]_{i+1j}$$
$$+\left[-\frac{\bar{h}_2}{4}\left(\frac{1}{3}\left(\sigma_2^{se}+\sigma_2^{sw}\right)+\frac{1}{6}\left(\sigma_2^{ne}+\sigma_2^{nw}\right)\right) + \frac{\Delta_1 h_2}{2}\left(\frac{1}{9}\sigma_2^{se}+\frac{1}{18}\left(\sigma_2^{ne}+\sigma_2^{sw}\right)+\frac{1}{36}\sigma_2^{nw}\right)\right]_{ij+1}$$
$$\left.+\left[\frac{\bar{h}_2}{4}\left(\frac{1}{3}\left(\sigma_2^{se}+\sigma_2^{sw}\right)+\frac{1}{6}\left(\sigma_2^{ne}+\sigma_2^{nw}\right)\right) + \frac{\Delta_1 h_2}{2}\left(\frac{1}{9}\sigma_2^{sw}+\frac{1}{18}\left(\sigma_2^{nw}+\sigma_2^{se}\right)+\frac{1}{36}\sigma_2^{ne}\right)\right]_{i+1j+1}\right\}$$

Contribution of the σ_2 term to F_2

$$\frac{1}{\bar{h}_1\bar{h}_2}\left\{\left[\frac{\bar{h}_1}{4}\left(\frac{1}{3}\left(\sigma_2^{ne}+\sigma_2^{se}\right)+\frac{1}{6}\left(\sigma_2^{nw}+\sigma_2^{sw}\right)\right) - \frac{\Delta_2 h_1}{2}\left(\frac{1}{9}\sigma_2^{ne}+\frac{1}{18}\left(\sigma_2^{nw}+\sigma_2^{se}\right)+\frac{1}{36}\sigma_2^{sw}\right)\right]_{ij}\right.$$
$$+\left[\frac{\bar{h}_1}{4}\left(\frac{1}{3}\left(\sigma_2^{nw}+\sigma_2^{sw}\right)+\frac{1}{6}\left(\sigma_2^{ne}+\sigma_2^{se}\right)\right) - \frac{\Delta_2 h_1}{2}\left(\frac{1}{9}\sigma_2^{nw}+\frac{1}{18}\left(\sigma_2^{sw}+\sigma_2^{ne}\right)+\frac{1}{36}\sigma_2^{se}\right)\right]_{i+1j}$$
$$+\left[-\frac{\bar{h}_1}{4}\left(\frac{1}{3}\left(\sigma_2^{ne}+\sigma_2^{se}\right)+\frac{1}{6}\left(\sigma_2^{nw}+\sigma_2^{sw}\right)\right) - \frac{\Delta_2 h_1}{2}\left(\frac{1}{9}\sigma_2^{sw}+\frac{1}{18}\left(\sigma_2^{ne}+\sigma_2^{sw}\right)+\frac{1}{36}\sigma_2^{nw}\right)\right]_{ij+1}$$
$$\left.+\left[-\frac{\bar{h}_1}{4}\left(\frac{1}{3}\left(\sigma_2^{nw}+\sigma_2^{sw}\right)+\frac{1}{6}\left(\sigma_2^{ne}+\sigma_2^{se}\right)\right) - \frac{\Delta_2 h_1}{2}\left(\frac{1}{9}\sigma_2^{sw}+\frac{1}{18}\left(\sigma_2^{nw}+\sigma_2^{se}\right)+\frac{1}{36}\sigma_2^{ne}\right)\right]_{i+1j+1}\right\}$$

Contribution of the σ_{12} term to F_1

$$\frac{1}{\bar{h}_1\bar{h}_2}\left\{\left[-\frac{\bar{h}_1}{2}\left(\frac{1}{3}\left(\sigma_{12}^{ne}+\sigma_{12}^{se}\right)+\frac{1}{6}\left(\sigma_{12}^{nw}+\sigma_{12}^{sw}\right)\right)\right.\right. \quad + \quad \Delta_2 h_1\left(\frac{1}{9}\sigma_{12}^{ne}+\frac{1}{18}\left(\sigma_{12}^{nw}+\sigma_{12}^{se}\right)+\frac{1}{36}\sigma_{12}^{sw}\right)\Big]_{ij}$$

$$+\left[-\frac{\bar{h}_1}{2}\left(\frac{1}{3}\left(\sigma_{12}^{nw}+\sigma_{12}^{sw}\right)+\frac{1}{6}\left(\sigma_{12}^{ne}+\sigma_{12}^{se}\right)\right) \quad + \quad \Delta_2 h_1\left(\frac{1}{9}\sigma_{12}^{nw}+\frac{1}{18}\left(\sigma_{12}^{sw}+\sigma_{12}^{ne}\right)+\frac{1}{36}\sigma_{12}^{se}\right)\right]_{i+1j}$$

$$+\left[\frac{\bar{h}_1}{2}\left(\frac{1}{3}\left(\sigma_{12}^{ne}+\sigma_{12}^{se}\right)+\frac{1}{6}\left(\sigma_{12}^{nw}+\sigma_{12}^{sw}\right)\right) \quad + \quad \Delta_2 h_1\left(\frac{1}{9}\sigma_{12}^{sw}+\frac{1}{18}\left(\sigma_{12}^{ne}+\sigma_{12}^{sw}\right)+\frac{1}{36}\sigma_{12}^{nw}\right)\right]_{ij+1}$$

$$\left.+\left[\frac{\bar{h}_1}{2}\left(\frac{1}{3}\left(\sigma_{12}^{nw}+\sigma_{12}^{sw}\right)+\frac{1}{6}\left(\sigma_{12}^{ne}+\sigma_{12}^{se}\right)\right) \quad + \quad \Delta_2 h_1\left(\frac{1}{9}\sigma_{12}^{sw}+\frac{1}{18}\left(\sigma_{12}^{nw}+\sigma_{12}^{se}\right)+\frac{1}{36}\sigma_{12}^{ne}\right)\right]_{i+1j+1}\right\}$$

Contribution of the σ_{12} term to F_2

$$\frac{1}{\bar{h}_1\bar{h}_2}\left\{\left[-\frac{\bar{h}_2}{2}\left(\frac{1}{3}\left(\sigma_{12}^{ne}+\sigma_{12}^{nw}\right)+\frac{1}{6}\left(\sigma_{12}^{se}+\sigma_{12}^{sw}\right)\right)\right.\right. \quad + \quad \Delta_1 h_2\left(\frac{1}{9}\sigma_{12}^{ne}+\frac{1}{18}\left(\sigma_{12}^{nw}+\sigma_{12}^{se}\right)+\frac{1}{36}\sigma_{12}^{sw}\right)\Big]_{ij}$$

$$+\left[\frac{\bar{h}_2}{2}\left(\frac{1}{3}\left(\sigma_{12}^{ne}+\sigma_{12}^{nw}\right)+\frac{1}{6}\left(\sigma_{12}^{se}+\sigma_{12}^{sw}\right)\right) \quad + \quad \Delta_1 h_2\left(\frac{1}{9}\sigma_{12}^{nw}+\frac{1}{18}\left(\sigma_{12}^{sw}+\sigma_{12}^{ne}\right)+\frac{1}{36}\sigma_{12}^{se}\right)\right]_{i+1j}$$

$$+\left[-\frac{\bar{h}_2}{2}\left(\frac{1}{3}\left(\sigma_{12}^{se}+\sigma_{12}^{sw}\right)+\frac{1}{6}\left(\sigma_{12}^{ne}+\sigma_{12}^{nw}\right)\right) \quad + \quad \Delta_1 h_2\left(\frac{1}{9}\sigma_{12}^{se}+\frac{1}{18}\left(\sigma_{12}^{ne}+\sigma_{12}^{sw}\right)+\frac{1}{36}\sigma_{12}^{nw}\right)\right]_{ij+1}$$

$$\left.+\left[\frac{\bar{h}_2}{2}\left(\frac{1}{3}\left(\sigma_{12}^{se}+\sigma_{12}^{sw}\right)+\frac{1}{6}\left(\sigma_{12}^{ne}+\sigma_{12}^{nw}\right)\right) \quad + \quad \Delta_1 h_2\left(\frac{1}{9}\sigma_{12}^{sw}+\frac{1}{18}\left(\sigma_{12}^{nw}+\sigma_{12}^{se}\right)+\frac{1}{36}\sigma_{12}^{ne}\right)\right]_{i+1j+1}\right\}$$

Eqns. 172, 173, 178, 179 and 180 are solved simultaneously over elastic time step $\Delta t_e = \Delta t/N_e < T_{ew} < \Delta t$ where N_e is the number of elastic subcycle time steps. The left hand side terms are treated implicitly, the right hand side terms explicitly, and the rate of strain $\dot{\epsilon}_{ij}$ and Δ are updated each elastic time step. The definition of the elastic parameter E in terms of the bulk viscosity, as well as the updating of the rate of strain tensor each elastic time step, eliminates any linearization error associated with viscosities which are lagged over the time step.

4.11 Advection

Horizontal advection in Eqs. 3-6,8 is evaluated following Smolarkiewicz (1983). The transport scheme is known as the Multidimensional Positive Definite Advection Transport Algorithm, or MPDATA (note that the scheme also works for negative definite scalars).

To illustrate the transport scheme, consider the one dimensional case for uniform flow of a positive definite scalar ψ:

$$\frac{\partial \psi}{\partial t} = -\frac{\partial}{\partial x}(u\psi). \tag{191}$$

The CSM1 sea ice model uses an upwind scheme to evaluate the transport (Bettge et al., 1996). This scheme is retained as an option in CSIM4. For a staggered grid of resolution Δx, upwind advection over time Δt from step m to $m+1$ is

$$\psi_i^{m+1} = \psi_i^m - \{F(\psi_i^m, \psi_{i+1}^m, u_{i+\frac{1}{2}}^m) - F(\psi_{i-1}^m, \psi_i^m, u_{i-\frac{1}{2}}^m)\} \tag{192}$$

where i is the spatial grid index and F is the interfacial flux between grid points i and $i+1$, given by (dropping the $m's$)

$$F(\psi_i, \psi_{i+1}, u) = \{(u+|u|)\psi_i + (u-|u|)\psi_{i+1}\}\frac{\Delta t}{2\Delta x} \tag{193}$$

for which u is the interface velocity between i and $i+1$ (i.e. $u_{i+\frac{1}{2}}$). To ensure ${\psi_i}^m$ remains positive definite when u is divergent, $\frac{|u|\Delta t}{\Delta x}$ must be ≤ 0.5.

The upwind scheme has strong implicit diffusion. Performing a Taylor expansion to second order for uniform flow

$$\psi_i^{m+1} = \psi_i^m + \frac{\partial \psi_i^m}{\partial t}\Delta t + \frac{1}{2}\frac{\partial^2 \psi_i^m}{\partial t^2}\Delta t^2 \tag{194}$$

$$\psi_{i+1}^m = \psi_i^m + \frac{\partial \psi_i^m}{\partial x}\Delta x + \frac{1}{2}\frac{\partial^2 \psi_i^m}{\partial x^2}\Delta x^2 \tag{195}$$

$$\psi_{i-1}^m = \psi_i^m - \frac{\partial \psi_i^m}{\partial x}\Delta x + \frac{1}{2}\frac{\partial^2 \psi_i^m}{\partial x^2}\Delta x^2, \tag{196}$$

approximating the second time derivative as $\frac{\partial^2 \psi_i}{\partial t^2} = u^2 \frac{\partial^2 \psi_i}{\partial x^2}$, then the upwind expression becomes

$$\frac{\partial \psi}{\partial t}|_i^m = -\frac{\partial}{\partial x}(u\psi)|_i^m + \frac{\partial}{\partial x}\{0.5(|u|\Delta x - u^2\Delta t)\frac{\partial \psi}{\partial x}\}|_i^m, \tag{197}$$

where $k_{impl} = 0.5(|u|\Delta x - u^2\Delta t)$ is the implicit diffusion coefficient. Let the time and length scales for diffusion be T_d and L_d, respectively (hence $k_{impl} = L_d^2/T_d$). For typical values of $u = 0.2\ ms^{-1}$, $\Delta t = 1\ hr$ and $\Delta x = 100\ km$, the implied diffusive length scale is 300 km over 10 days, during which the flow displacement is only 173 km.

The scheme of Smolarkiewicz (1982,1983,1984) significantly reduces the implicit diffusion by solving the equivalent upwind transport equation

$$\frac{\partial \psi}{\partial t} = -\frac{\partial}{\partial x}(u\psi) - \frac{\partial}{\partial x}(u_d\psi) \tag{198}$$

where the anti-diffusion velocity u' is given by

$$u' = -u_d = \frac{k_{impl}}{\psi}\frac{\partial \psi}{\partial x}. \tag{199}$$

An iterative scheme is suggested, where the initial upwind values of ψ are corrected using the anti-diffusion velocity in an upwind evaluation, which in turn generates implicit diffusion that can be reduced by a second corrective step, and so on.

Thus, the advection scheme is

$$\psi_i^* = \psi_i^m - \{F(\psi_i^m, \psi_{i+1}^m, u_{i+\frac{1}{2}}^m) - F(\psi_{i-1}^m, \psi_i^m, u_{i-\frac{1}{2}}^m)\} \tag{200}$$

$$\psi_i^{m+1} = \psi_i^* - \{F(\psi_i^*, \psi_{i+1}^*, u_{i+\frac{1}{2}}^{\prime m}) - F(\psi_{i-1}^*, \psi_i^*, u_{i-\frac{1}{2}}^{\prime m})\} \tag{201}$$

where the anti-diffusion velocity u' is

$$u_{i+\frac{1}{2}}^{\prime m} = \frac{0.5(|u_{i+\frac{1}{2}}^m|\Delta x - {u_{i+\frac{1}{2}}^m}^2\Delta t)}{\psi^*}\frac{\partial \psi^*}{\partial x} \tag{202}$$

and the second step is repeated several times. As long as the velocities satisfy the stability criterion, successive diffusion velocities (hence the implicit diffusion coefficient) reduce in magnitude.

We can estimate the reduction in the implicit diffusion coefficient. The first (i.e. Δx) term in the coefficient is dominant. Let the typical change in ψ^* over Δx be f. Then, after m iterations we have a $(f/2)^{m/2}$ reduction in diffusive length scale. In the worst case where $f = 1$ (i.e. a step function), after $m = 3$ iterations the length scale will be reduced by about 0.35, to about Δx in the above example after 10 days. For the more realistic case of $f = 0.20$, the reduction after $m = 3$ iterations is by a factor of 0.032, much less than Δx in the above example. Smolarkiewicz (1984) recommends $m = 3$.

In two dimensions, the antidiffusion velocities are

$$u' = -u_d = 0.5(|u|\Delta x)\frac{1}{\psi}\frac{\partial \psi}{\partial x} - \frac{0.5u\Delta t}{\psi}\{\frac{\partial}{\partial x}(u\psi) + \frac{\partial}{\partial y}(v\psi)\} \tag{203}$$

$$v' = -v_d = 0.5(|v|\Delta x)\frac{1}{\psi}\frac{\partial \psi}{\partial y} - \frac{0.5v\Delta t}{\psi}\{\frac{\partial}{\partial x}(u\psi) + \frac{\partial}{\partial y}(v\psi)\}. \tag{204}$$

It is possible that because of quasi-stable conditions a positive definite field after transport will have some very small negative values, and conversely for negative definite fields. If this occurs, the values out of range are zeroed.

The transport calculation proceeds first for the surface temperatures (see section 4.2). First, the product $-A_nT_{sn}$ is transported making sure it is positive definite, then the ice concentrations A_n, the ice volumes V_n, the snow volumes V_{sn} and the sea ice internal energies E_n. After the transport of A_n, the final surface temperatures are retrieved from the transported $-A_nT_{sn}$ by division. Any resulting temperatures above 0°C are set to zero.

For the upwind transport scheme, the ice divergence is relatively simple to compute from $\mathbf{u}$. However, because the Smolarkiewicz scheme requires iteration, an exact expression of the ice divergence cannot be computed from the velocity field. Instead we can compute it consistently from the area change by transport. The ice area is normalized so that prior to transport

$$\sum_{n=0}^{N} A_n^m = 1, \tag{205}$$

but after transport it is

$$\sum_{n=0}^{N} A_n^{m+1} = 1 - \dot{\epsilon}_I' \Delta t. \tag{206}$$

Note the prime on $\dot{\epsilon}_I'$ denotes the ice divergence computed from Eq. (206) rather than simply $\bigtriangledown \cdot \mathbf{u}$. Mechanical distribution immediately follows the transport with the explicit purpose of returning the total ice plus open water area back to unity.

4.12 Mechanical Redistribution

Mechanical redistribution of ice thickness due to rafting and ridging processes is treated in this section. Specifically, the redistribution function R of Eq. 1 (ψ in (Thorndike et al., 1975)) is parameterized, and then used to evaluate the S_M source/sink terms in Eqs. 3-7. For example, the integral of R over the n^{th} category gives the ice fraction source

$$S_{MAn} = \int_{h_n^*}^{h_{n+1}^*} R(h, g, \mathbf{u}) dh. \tag{207}$$

The redistribution function R depends on the the ice thickness h, the distribution function $g(h)$, and the velocity field $\mathbf{u}$, specifically the invariants of the strain rate tensor (see section 4.10). These invariants are the divergence $\dot{\epsilon}_I$ and the shear $\dot{\epsilon}_{II}$. These two invariants are also used in terms of magnitude $|\dot{\epsilon}| = (\dot{\epsilon}_I^2 + \dot{\epsilon}_{II}^2)^{1/2}$ and strain rate angle $\theta = \tan^{-1}(\dot{\epsilon}_{II}/\dot{\epsilon}_I)$. (Note that $\theta = 0°$ refers to pure divergence, $\theta = 45°$ uniaxial extension, $\theta = 90°$ pure shear, $\theta = 135°$ to uniaxial compression, and $\theta = 180°$ pure convergence).

Two strong constraints on the redistribution follow from the first two moments of the distribution equation, corresponding to area and volume conservation:

$$\int_0^{h_{max}} R dh = \dot{\epsilon}_I' \tag{208}$$

$$\int_0^{h_{max}} hRdh = 0. \tag{209}$$

The first follows from the conservation of total area, since the import or export of area ($\dot{\epsilon}_I'$) must be balanced by a redistribution. The second follows from the requirement that mechanical redistribution cannot change the ice volume.

The parameterization of lead opening and mechanical redistribution follows from the theoretical formulation of Thorndike et al. (1975):

$$R = |\dot{\epsilon}|[\alpha_0(\theta)\delta(h) + \alpha_r(\theta)w_r(h,g)], \tag{210}$$

where $\delta(h)$(the delta function) is the opening mode, and $w_r(h,g)$ is the ridging mode. Note that the conservation of area requires:

$$\int_0^{\infty} w_r(h,g)dh = -1. \tag{211}$$

The coefficients $|\dot{\epsilon}|\alpha_0(\theta)$ and $|\dot{\epsilon}|\alpha_r(\theta)$ are known as the lead opening and closing rates, respectively, and they are related such that their difference equals the ice divergence, $|\dot{\epsilon}|\alpha_0(\theta) - |\dot{\epsilon}|\alpha_r(\theta) = \dot{\epsilon}_I'$.

Two aspects of the mechanical redistribution must be considered: the relation between the distribution function and the deformation/compressive strength used in the ice dynamics, and the redistribution source terms in the conservation equations.

For the first, we follow an energetics argument by Rothrock (1975). The deformational work done on the ice is equated to known sinks of energy in ridge building:

$$\sigma_I\dot{\epsilon}_I + \sigma_{II}\dot{\epsilon}_{II} = R_{pot} + R_{fric} \tag{212}$$

where R_{pot} is the rate of mechanical production of gravitational potential energy per unit area, and R_{fric} is the rate of frictional energy loss per unit area. We write

$$\sigma_I\dot{\epsilon}_I + \sigma_{II}\dot{\epsilon}_{II} = (1 + \frac{R_{fric}}{R_{pot}})R_{pot} = ZR_{pot} \tag{213}$$

where Z is the ratio of total energy dissipated to potential energy gain. Ice thickness h has potential energy relative to sea level of $P_e = C_{pe}h^2$, where $C_{pe} = \frac{1}{2}\frac{\rho_i}{\rho_o}(\rho_o - \rho_i)g$ (here g is the gravitational acceleration). Integrating over the entire thickness distribution results in the total potential energy

$$P_e = C_{pe}\int_0^{\infty} h^2 g(h)dh \tag{214}$$

The rate of gain of P_e is

$$\frac{dP_e}{dt} = C_{pe}\int_0^{\infty} h^2\frac{dg(h)}{dt}dh. \tag{215}$$

From the distribution equation, using $\bigtriangledown \cdot \mathbf{u}g = g\bigtriangledown\cdot\mathbf{u} + \mathbf{u}\cdot\bigtriangledown g$:

$$\frac{dg}{dt} = -\frac{\partial}{\partial h}(\dot{h}g) + L(h,g) - g\bigtriangledown\cdot\mathbf{u} + R. \tag{216}$$

Thus the total rate of change of potential energy is

$$\frac{dP_e}{dt} = -\int_0^{\infty} h^2\frac{\partial}{\partial h}(\dot{h}g)dh + \int_0^{\infty} h^2 L(h,g)dh - P_e\bigtriangledown\cdot\mathbf{u} + \int_0^{\infty} h^2 Rdh. \tag{217}$$

The first two terms on the right hand side refer to gain/loss due to thermodynamic and thickness transport processes, the third to large scale divergence, while the last term is due to mechanical redistribution. Using Eq. 210 for R we have

$$R_{pot} = |\dot{\epsilon}|\alpha_r(\theta)C_{pe}\int_0^{\infty} h^2 w_r(h,g)dh. \tag{218}$$

We can therefore define

$$P = ZC_{pe} \int_0^\infty h^2 w_r(h, g) dh \tag{219}$$

so that

$$\sigma_I \dot{\epsilon}_I + \sigma_{II} \dot{\epsilon}_{II} = |\dot{\epsilon}| \alpha_r(\theta) P \tag{220}$$

where P is the compressive strength used in the dynamics (equation(163)).

Further, from the viscous/plastic relations of σ_I and σ_{II} in terms of $\dot{\epsilon}_I$ and $\dot{\epsilon}_{II}$, and the bulk/shear viscosity definitions (see section 4.10), we have:

$$\sigma_I \dot{\epsilon}_I + \sigma_{II} \dot{\epsilon}_{II} = \zeta \dot{\epsilon}_I^2 - \frac{P}{2} \dot{\epsilon}_I + \eta \dot{\epsilon}_{II}^2 \tag{221}$$

or

$$\sigma_I \dot{\epsilon}_I + \sigma_{II} \dot{\epsilon}_{II} = P |\dot{\epsilon}| \{ \frac{1}{2|\dot{\epsilon}|} (\Delta - \dot{\epsilon}_I) \tag{222}$$

so that the ridging mode $\alpha_r(\theta)$ in terms of the strain rate angle is

$$\alpha_r(\theta) = -\frac{1}{2} cos(\theta) + \frac{1}{2} \sqrt{cos^2(\theta) + \frac{sin^2(\theta)}{e^2}} \tag{223}$$

$$|\dot{\epsilon}| \alpha_r(\theta) = \frac{1}{2} (\Delta - \dot{\epsilon}_I'). \tag{224}$$

which is the result for the elliptical yield curve with aspect ratio e found by Hibler (1980). Note the use of $\dot{\epsilon}_I'$ in the final result, which is the divergence computed from Eq. 206.

Flato and Hibler (1995) separated the expression in Eq. 224 into the sum of two terms representing the energy dissipation from ridge building by shear and convergence:

$$|\dot{\epsilon}| \alpha_r(\theta) = C_s \frac{1}{2} (\Delta - |\dot{\epsilon}_I'|) - \min(\dot{\epsilon}_I', 0), \tag{225}$$

with the factor C_s added so the shearing component can be altered by varying C_s between 0 (all energy dissipation by shear is lost to sliding) and 1 (all energy dissipation by shear is used to build ridges). Equations 224 and 225 are equivalent when $C_s = 1$. The experiments of Flato and Hibler (1995) indicate that $C_s = 0.5$ is appropriate to produce the concentrations of ridged ice observed in the Arctic. However, Bitz et al. (2001) found that a coupled model tended to predict too much ridged ice with $C_s = 0.5$. Bitz et al. tested the model with $C_s = 0$ and found better agreement with observations. Unfortunately, the parameter C_s depends on e and P, and none of these values is well constrained by observations. It is some consolation that Bitz et al. (2001) found that C_s, and hence the precise concentration of ridged ice, has relatively little affect on the *climate* of the Arctic. Our standard model uses a compromise value of $C_s = 0.25$.

The ridging mode is the sum of two distributions describing the ice participating in ridging $a(h)$ and the newly ridged ice $n(h)$, normalized to conserve area and volume:

$$w_r(h) = \frac{-a(h) + n(h)}{\int_0^\infty [a(h) - n(h)] dh}. \tag{226}$$

The ice participating in ridging is found by weighting $g(h)$ by a function $b(h)$ that is designed to make thinner ice more likely to ridge than thicker ice. The newly ridged ice is found by integrating $a(h)$ times the redistribution function $\gamma(h', h)$ over the range of ice thicknesses h' that can contribute to form newly ridged ice of thickness h. Hence,

$$\begin{aligned} a(h) &= b(h) g(h) \\ n(h) &= \int_0^h \gamma(h', h) b(h') g(h') dh'. \end{aligned} \tag{227}$$

Thorndike et al. (1975) argued that a plausible $b(h)$ might depend linearly on the cumulative thickness distribution $G(h) = \int_0^h g(h')dh'$ according to

$$b(G) = \frac{2}{G^*}\left[1 - \frac{G(h)}{G^*}\right] \tag{228}$$

when $G \leq G^*$; otherwise 0 for $G > G^*$, for which G^* is the limiting fraction below which all ridging occurs and is assumed to be 15% as assumed by Thorndike et al. (1975). The redistribution process is parameterized according to Hibler (1980), who constructed a rule for deriving $n(h)$ from $a(h)$ based on observations that constrain ice of thickness h participating in ridging to be linearly distributed between thicknesses $2h$ and $2\sqrt{Kh}$:

$$\gamma(h', h) = \frac{1}{2(K - h')} \tag{229}$$

when $2h' \leq h \leq 2\sqrt{Kh'}$; otherwise 0.

The mechanical redistribution function R_n is the integral of the continuous function (see Eq. 210) over the thickness limits of each category:

$$R_n = \int_{h_n^*}^{h_{n+1}^*} R dh = \delta(h)\left[\dot{\epsilon}_I' + |\dot{\epsilon}|\alpha_r(\theta)\right] + |\dot{\epsilon}|\alpha_r(\theta)W_n, \tag{230}$$

where

$$W_n = \int_{h_n^*}^{h_{n+1}^*} w_r(h)dh. \tag{231}$$

The W_n factors can be separated into two components, participation W_{an} (loss) and redistribution W_{nn} (gain),

$$W_n = -W_{an} + W_{nn}, \tag{232}$$

such that

$$\begin{aligned} W_{an} &= \frac{1}{\omega}\int_{h_n^*}^{h_{n+1}^*} b(h)g(h)dh \\ W_{nn} &= \frac{1}{\omega}\int_{h_n^*}^{h_{n+1}^*}\int_0^{h_{n+1}^*} \gamma(h', h)b(h')g(h')dh'dh \end{aligned} \tag{233}$$

where ω normalizes W_n such that $\sum_{n=0}^N R_n = \dot{\epsilon}_I$. After substituting $g(h)dh = dG$ into the equation for W_{an}, we find

$$W_{an} = \frac{1}{\omega}\int_{\min(G^*, G_n)}^{\min(G^*, G_{n+1})} b(G)dG, \tag{234}$$

where $G_n = \sum_{p=0}^n A_p$, with $G_{-1} = 0$. Finally we express W_{an} as a function of the auxiliary function Y_n:

$$W_{an} = \frac{1}{\omega}(Y_n - Y_{n+1}), \quad \text{where} \quad Y_n = [1 - \frac{G_n}{G^*}]^2 \tag{235}$$

when $G_n \leq G^*$; otherwise 0 for $G_n > G^*$. In Eq. 233, W_{nn} is evaluated by first changing the order of integration and then expanding the outer integral into a sum of integrals over the categories:

$$W_{nn} = \frac{1}{\omega}\sum_{p=0}^{n+1}\int_{h_p^*}^{h_{p+1}^*}\int_{h_n^*}^{h_{n+1}^*} \gamma(h', h)dh\ b(h')g(h')dh'. \tag{236}$$

Taking $\int_{h_n^*}^{h_{n+1}^*} \gamma(h', h)dh$ outside of the remaining integral we have

$$W_{nn} = \frac{1}{\omega}\sum_{p=0}^{n+1}\Gamma_{pn+1}\int_{h_n^*}^{h_{n+1}^*} b(h')g(h')dh' = \frac{1}{\omega}\sum_{p=0}^{n+1} W_{ap}\Gamma_{pn+1}. \tag{237}$$

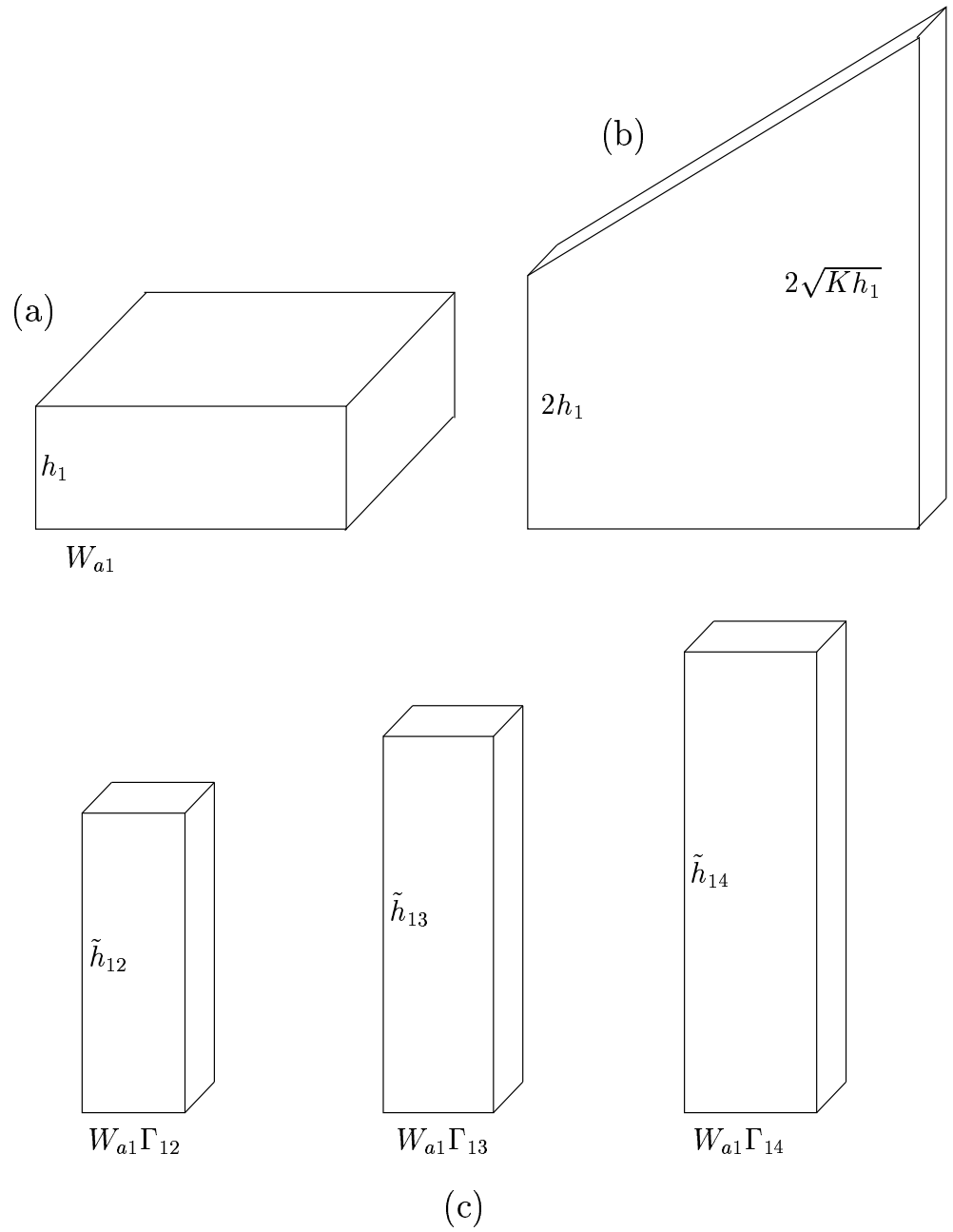

Figure 4: Example showing mechanical redistribution for a concentration W_{a1} of ice in category 1 with thickness h_1 that participates in ridging (a). Conceptually, this ice ridges into a continuous distribution whose thickness is linearly distributed between $2hh_1$ and $2\sqrt{Kh_1}$ (b). In practice, the model is discrete, so the ridged ice is redistributed into a few discrete thickness categories (c). In this example, the newly ridged ice will join categories 2, 3, and 4. Modified from Bitz (2000).

The discrete distributor Γ_{pn+1} is computed as in the method of Hibler (1980) from

$$\Gamma_{pn+1} = \int_{h_n^*}^{h_{n+1}^*} \gamma(h_p, h)dh = \frac{\min(2\sqrt{Kh_p}, h_{n+1}^*) - \max(2h_p, h_n^*)}{2(K - h_p)}, \tag{238}$$

when $2h_p < h_n^*$ or $2\sqrt{Kh_p} > h_{n+1}^*$; otherwise $\Gamma_{pn+1} = 0$. In general, ice from any category may participate in ridging provided that the cumulative distribution of ice up to that category is less than G^* (see Figure 4). The final equation for S_{MAn} is:

$$S_{MAn} = |\dot{\epsilon}|\alpha_r(\theta) \left[-W_{an} + \sum_{p=1}^{n+1} W_{ap}\Gamma_{pn+1} \right]. \tag{239}$$

Because the volume of the ice and snow is influenced by ridging, the volume of the ice and snow must be redistributed as well as the ice concentration. The ice participating in ridging reduces the volume in category n proportional to $h_n W_{an}$. The ice that ridges into category n increases the volume proportional to $\sum_{p=1}^{n+1} \tilde{h}_{pn+1} W_{an}\Gamma_{pn+1}$, which is summed over the p categories that ridge into category n. The thickness of this newly ridged ice $\tilde{h}_{pn+1}$ is uniquely determined by conservation of volume and the discrete distributor. For simplicity, we assume the snow thickness redistribution process is independent of the category that receives the newly ridged ice and snow. Hence, the snow thickness would be the same on top of each ridged ice category. The rate of change of the ice and snow volumes due to mechanical redistribution is

$$\begin{aligned} S_{MVn} &= |\dot{\epsilon}|\alpha_r(\theta) \left[-h_n W_{an} + \sum_{p=1}^{n+1} \tilde{h}_{pn+1} W_{ap}\Gamma_{pn+1} \right] \\ S_{MVsn} &= |\dot{\epsilon}|\alpha_r(\theta) \left[-h_{sn} W_{an} + \sum_{p=1}^{n+1} \tilde{h}_{spn+1} W_{ap}\Gamma_{pn+1} \right], \end{aligned} \tag{240}$$

where

$$\begin{aligned} \tilde{h}_{pn+1} &= \frac{1}{2}\left[\max\left(2h_p, h_n^*\right) + \min\left(2\sqrt{Kh_p}, h_{n+1}^*\right) \right] \\ \tilde{h}_{spn+1} &= h_{sp}\frac{h_p + \sqrt{Kh_p}}{h_p}. \end{aligned} \tag{241}$$

Conservation of energy requires a redistribution of internal energy as well. We assume that mechanical redistribution does not mix energy vertically. Again it may be helpful to think of the vertical dimension broken into a fixed number of layers, where energy is redistributed layer by layer. Hence, redistribution transfers heat only from the upper layer of one category to another and so on. Consistent with the redistribution of ice and snow volume, we find

$$\begin{aligned} S_{MEn} &= |\dot{\epsilon}|\alpha_r(\theta) \left[-q_n h_n W_{an} + \sum_{p=1}^{n+1} q_p \tilde{h}_{pn+1} W_{ap}\Gamma_{pn+1} \right] \\ S_{MESn} &= |\dot{\epsilon}|\alpha_r(\theta) \left[-q_s h_{sn} W_{an} + \sum_{p=1}^{n+1} q_{sp} \tilde{h}_{spn+1} W_{ap}\Gamma_{pn+1} \right]. \end{aligned} \tag{242}$$

The ridged ice will have the same vertical temperature profile as the ice which has participated in ridging.

Finally, the surface temperature is also affected by mechanical redistribution:

$$S_{MTsn} = |\dot{\epsilon}|\alpha_r(\theta) \left[-T_{sn} W_{an} + \sum_{p=1}^{n+1} T_{sp} W_{ap}\Gamma_{pn+1} \right]. \tag{243}$$

With the redistribution of surface temperature, the ridged ice will have the same surface temperature as the ice that participates in ridging.

Using the definitions above, the mechanical pressure P is:

$$P = ZC_{pe} \sum_{n=1}^{N} \left[-h_n^2 W_{an} + \sum_{p=1}^{n+1} \tilde{h}_{pn+1}^2 W_{ap} \Gamma_{pn+1} \right]. \tag{244}$$

Based on the work of Hopkins and Hibler (1991) and Flato and Hibler (1995), we let $Z = 17$.

Table 6: Ocean Fields Required for Mixed Layer

Symbol	Description	Units
h_o	mixed layer depth	m
S_o	salinity	o/oo
u_o	x direction surface velocity	m s^{-1}
v_o	y direction surface velocity	m s^{-1}
$(\nabla H_o)_x$	x direction surface slope	m m^{-1}
$(\nabla H_o)_y$	y direciton surface slope	m m^{-1}
F_{Qdp}	deep heat flux	W m^{-2}

5 Special Capabilities

There are a few special configurations of the ice model that can be chosen either by setting internal input ice parameters, or by setting the run scripts for the other components accordingly. More information can be found in the separate CSIM User's Guide Version 4. Some aspects of three special configurations are discussed as follows.

5.1 Active Ice Only (AIO) Framework

The ice model can be run through the coupler but with other components prescribed in a framework called Active Ice Only (AIO). Thus, in AIO mode the ice model communicates via the coupler with other components in the same manner as it would in a fully coupled run. The user need only insure that the other components are data models (i.e. prescribed). However, because of the way ice and ocean are coupled, the ice-ocean heat exchange in the data ocean model is independent of ice state. Therefore the sea ice model has an option to run with a simple ocean mixed layer model that is part of the sea ice component, as described in the next section.

5.2 Ocean Mixed Layer

For maximum flexibility in studies of sea-ice/mixed layer interactions, an ocean mixed layer formulation is included within the sea ice model. The mixed layer prognostic variable is ocean temperature T_o, determined by the thermodynamic equation:

$$\rho_o c_o h_o \frac{\partial T_o}{\partial t} = F_{SW} + F_{LW} + F_{SH} + F_{LH} + F_{Qio} - F_{Qdp}. \tag{245}$$

where ρ_o, c_o, h_o are the ocean mass density, heat capacity and mixed layer depth respectively, $F_{LW} = F_{LWDN} - F_{LWUP}$, F_{Qio} is the available mixed layer heat flux used by the sea ice model as shown in section 4.7, and F_{Qdp} is the sub-mixed layer, or deep heat flux. Note that the fluxes include contributions from both open water and sea ice. The required monthly mean input data are the mixed layer depth, salinity (presently not used), ocean currents, sea surface slopes and the deep heat flux, as shown in Table 6. The ocean currents and tilt are used in the sea ice dynamic calculation. All of these data are supplied on a monthly basis from either an observational and/or a model source. For model data, the mean monthly surface temperatures and surface heat fluxes from a model run can be used. The deep heat flux F_{Qdp}, which represents seasonal sub-mixed layer heat storage/release and oceanic heat transport, is computed from the monthly data as:

$$F^k_{Qdp} = -\rho_o c_o h^k_o \left(\frac{T^{k+1}_o - T^{k-1}_o}{2\Delta t_k} \right) + F^k_{SW} + F^k_{LW} + F^k_{SH} + F^k_{LH} + F^k_{Qio} \tag{246}$$

for the k^{th} month (k = 1, 2, ..., 12), and the required data are shown, with Δt_k = mean month time. The monthly data (if necessary) must be spatially interpolated to the sea ice model grid, and be formatted as an external netCDF file, containing the monthly fields shown in Table 6. Once read in, these monthly data are linearly interpolated in time to the sea ice model time step (therefore allowing for seasonal variation only).

For a time step m with initial temperature T_o^m, the mixed layer temperature forecast equation is:

$$T_o^{'m+1} = T_o^m + \Delta t \left(F_{SW}^m + F_{LW}^m + F_{SH}^m + F_{LH}^m + F_{Qio}^m \right) / \rho_o c_o h_o \tag{247}$$

where we first evaluate the exchange between the mixed layer and the atmosphere/ice above, in order to limit possible loss of mixed layer heat to the deep heat source when the mixed layer temperature is at freezing (see below). F_{SW}^m is computed from:

$$F_{SW}^m = F_{SWDN}^m (1 - \alpha_o)(1 - A^m) + F_{SW_o}^m A^m \tag{248}$$

where α_o is a constant ocean surface albedo, $F_{SW_o}^m$ is the shortwave flux that penetrates the ice to be absorbed in the underlying ocean, and A^m is the sea ice fraction. The fluxes F_{LWUP}^m, F_{SH}^m and F_{LH}^m are computed over the open ocean using the ocean mixed layer temperature and surface properties, and then weighted by the open ocean fraction.

If $T_o^{'m+1} < T_{of}$, where T_{of} is the freezing temperature of the ocean, and $F_{Qdp} > 0$ (implying heat loss to the deep ocean), then the heat exchange is limited by the fraction f (constrained so $f \geq 0$) given by: $f = (T_o^m - T_{of})/(T_{oc} - T_{of})$, where $T_{oc} = 0°\mathrm{C}$, $F_{Qdp}^* = f F_{Qdp}$, and deep exchange is evaluated by:

$$T_o^{m+1} = T_o^{'m+1} - F_{Qdp}^* \Delta t / \rho_o c_o h_o. \tag{249}$$

Frazil ice heat flux (>0) or melt potential (<0) is then evaluated as:

$$F_{Qoi} = \rho_o c_o h_o \frac{(T_{of} - T_o^{m+1})}{\Delta t} \tag{250}$$

as in the ocean model (see section 4.3). If $T_o^{m+1} < T_{of}, T_o^{m+1} = T_{of}$, to ensure the mixed layer temperature always remains above freezing.

5.3 Prescribed Ice

For some purposes, it may be useful to run an active atmospheric model with prescribed SST and sea ice properties. This requires computing the ice-atmosphere fluxes within the ice component model as a function of a prescribed ice state, while the ocean-atmosphere fluxes are computed in the usual manner (see Tables 1 and 3).

Concerning the specification of sea ice states, the approach followed is to use observational data where available, and to make some arbitrary but reasonable assumptions about ice states were necessary. The ice concentration is specified from observational data, either the specific year/month or a twelve month climatology. Sea ice volume is specified by setting the ice thickness to 1.5 m in the northern hemisphere and 0.5 m in the southern hemisphere. Snow/ice surface temperature is set equal to the atmospheric air temperature (maximum value 0°C in case the latter is warmer). Assuming a linear vertical temperature gradient from the snow/ice temperature to the freezing temperature at ice base allows evaluation of the sea ice internal energy. The snow volume is specified from a snow cover of twelve monthly values based on SHEBA data, with maximum snow cover 0.33 m and minimum 0.0 m. The southern hemisphere snow cover is from the six month phase shifted northern hemisphere values. Specific time step values for ice concentration and snow cover are linearly interpolated between available monthly means. The sea ice velocities and stress tensors are simply zeroed, and the ice is assumed motionless. Snow/ice albedos are computed directly from the assumed ice thickness, snow cover and surface temperature.

The ice-atmosphere fluxes are evaluated by computing the vertical ice thermodynamics. This calculation uses the above specified ice states as initial conditions for the updated snow/ice temperatures. The ice states are set at each model time step, and any implied changes to snow/ice volume as a result of the thermodynamics calculation are ignored. All lateral thermodynamics, thickness transport, ice dyanmics, advection and mechanical redistribution are also ignored.

6 Overview of the Sea Ice Model Code

A brief overview of the CSIM4 code is given here, to introduce the sea ice model to a potential user. The main tasks of the sea ice code and its relation to the coupler are presented. The actual order of computations, which differs somewhat from the order given in section 4, is discussed. Input datasets and output files are introduced. A complete listing of user options, as well as other aspects of running the sea ice code, can be found in a separate CSIM User's Guide Version 4. A detailed description of the code can be found in an additional CSIM Code Reference Manual Version 4.

6.1 General Structure

The ice model code performs the general tasks of initiating communication with the coupler, initializing the ice state by reading in a restart dataset, reading in grid information from a separate dataset, receiving input states and fluxes from the coupler, performing various ice model calculations, sending output states and fluxes to the coupler, occasionally writing restart and history files, and finally terminating communication with the coupler.

The coupler controls the time stepping tasks for the sea ice model, while internal model options are set by the user through various input parameters. Some of these options (such as ocean mixed layer and prescribed ice) require seperate datasets.

6.2 Order of Computations

The actual order of computations differs from that presented in section 4. The order in the code reflects the requirements of computational efficiency and overall CCSM ordering.

To illustrate the actual order of computations in the sea ice model, we refer again to the distribution equation Eq 1. Into that equation we insert brackets ([]) to show, in the time flow of computations from left to right in the equation, when various coupler or other calculations or input/output is performed, as follows:

$$[Initial]\frac{\partial g}{\partial t} = [C_{in}][\dot{h}][C_{out}] - \frac{\partial}{\partial h}(\dot{h}g) + L(h,g)[\mathbf{u}] - \bigtriangledown \cdot (\mathbf{u}g) + R(h,g,\mathbf{u})[\alpha][Output]. \qquad (251)$$

$[Initial]$ refers to reading in grid information and the sea ice model initial conditions (see next section; restart and initial datasets have same structure). Input/output from the coupler of forcing states and fluxes is designated by $[C_{in}]$ and $[C_{out}]$ respectively. $[\dot{h}]$ refers to the calculation of the vertical thermodynamics along with the ice/atmosphere fluxes. The output to the coupler is done after the vertical thermodynamics to improve load balance, as once the ice-atmosphere fluxes are computed, the atmosphere model can be stepped forward in time parallel with the ice model. Thickness space transport ($-\frac{\partial}{\partial h}(\dot{h}g)$) and lateral thermodynamics ($L(h,g)$) follow the output exchange with the coupler, followed in turn by the calculation of ice velocities ($[\mathbf{u}]$), ice advection ($-\bigtriangledown\cdot(\mathbf{u}g)$), mechanical redistribution ($R(h,g,\mathbf{u})$) and albedos (α). Note that since the lateral thermodynamics (including exchange with underlying ocean) and the albedo calculation follow the send of output to the coupler ($[C_{out}]$), the ice/ocean fluxes and snow/ice albedos are offset by one time step with respect to the ice states and ice/atmosphere fluxes. The albedos are computed last in order to insure that the computation in the atmosphere model of the atmosphere/ice radiative fluxes received on

Table 7: Log Output

Field	Arctic	Antarctic
max cH (m)	8.03225425266130166	9.58834109817763292
total area (km^2)	1.55832393981866352E+07	1.31359497615335882E+07
total ice volume (m^3)	2.20786018559233555E+13	1.53478890145911914E+13
total snw volume (m^3)	2.17290336346162354E+12	4.69722936833253418E+12
max u, v (ms^{-1})	0.31679670285941031	0.39223897146835074
average albedo	0.71055459990319281	0.70681393896051892
arwt rain h2o kg in dt	3.17006796356205261E+11	4.78847982778436737E+10
arwt snow h2o kg in dt	2.57338282670871045E+12	3.37288892640776123E+12
arwt evap h2o kg in dt	-3.72313609236561218E+11	-1.32881931733842285E+12
arwt frzl h2o kg in dt	2.39631833842436230E+12	1.69429453330916382E+11
arwt frsh h2o kg in dt	-1.06491819315876992E+13	1.94703321708546680E+13
arwt ice mass (kg)	2.02460779018817160E+16	1.40740142263801220E+16
arwt snw mass (kg)	7.17058109942335750E+14	1.55008569154973625E+15
arwt tot mass (kg)	2.09631360118240520E+16	1.56240999179298580E+16
arwt tot mass chng(kg)	1.55635762838520000E+13	-1.72089483101840000E+13
arwt water flux	1.55635762838404180E+13	-1.72089483101765703E+13
water flux error	-5.52495163102852028E-16	4.75527392875532042E-16
arwt atm heat flux (W)	-5.05399495812494625E+14	6.48043747524047500E+13
arwt ocn heat flux (W)	-8.57981240938527969E+13	-4.65620142529616938E+14
arwt frzl heat flux(W)	5.67278377599885547E+13	4.29626561770771094E+12
arwt tot enthalpy (J)	-7.00797110852405481E+21	-5.06512061411722946E+21
arwt net heat (J)	-5.14435546236920832E+18	5.68218511797459149E+18
arwt tot enth. chng(J)	-5.33210204460495667E+18	5.67196916992442368E+18
arwt heat error	-2.67904332549809225E-05	-2.01692098342031014E-06

the next time step ($[C_{in}]$) use the **same** albedos as are used for the ice vertical thermodynamic calculation $[\dot{h}]$, thus ensuring energy conservation. Time stepping occurs by cycling between $[Initial]$ and $[Output]$, with an occasional write of output to both log and history files (see following sections).

6.3 Log Files

Diagnostic output to the log files consists of instantaneous hemispheric mean fields at a user selected frequency. Included is the model step number, the date (yyyymmdd, where yyyy is the year, mm the month, and dd the day), along with the renormalization factors for the conservation of ice after minimum values are removed. Then come a list of fields with max values (max cH) and hemispheric area weighted (arwt) values as shown in Table 7. The frequency of diagnostic output can be varied: see the CSIM User's Guide Version 4.

These values are examples from an output for year/month/day 251129 of an AIO run. The 'max cH' field is the maximum ice volume of any point in the respective hemispheric domains. The 'max u,v' show the maximum (positive) u,v values in the respective hemispheric domains.

In addition to the fluxes, energies and masses, there are also two error statistics: a water flux error showing the boundary water flux over the time step against the change of snow/ice water content, as a relative error, and the same for the boundary heat flux compared to the change in internal energy. These show that while the present code conserves mass to within machine accuracy, heat is conserved to no better than 3×10^{-5} relative error. The error in conservation of heat is limited by the number of iterations of the heat equation. Improved accuracy has no significant affect on climate.

6.4 Restart Files

The variables in the restart dataset are the same as those needed to initialize the model. This dataset consists of instantaneous states, ice/ocean fluxes and albedos. The latter two are necessary, as these are offset by one time step with the remaining ice states (as discussed in the previous section). The use of a restart dataset ensures that the sea ice model restarts exactly, so long as the forcing remains unchanged.

Whenever restart datasets are read or written, the sea ice model code writes out some useful global integral information into the log file. The frequency of writing restart files is variable- see the CSIM User's Guide Version 4.

6.5 History Files

There are two groups of fields written to the history file: time-invariant and time dependent. The former are fields related to the horizontal grid, while the latter are prognostic and diagnostic fields from an ice model integration. Table 8 presents a list of the time-invariant fields, while Table 9 lists all prognostic and diagnostic fields.

Table 8: Time-Invariant History Fields

Name	Description	Units
tmask	T grid mask (0 = land, 1 = ocean)	
tarea (A^t)	area of T grid cells	m^2
uarea (A^u)	area of U grid cells	m^2
dxu	U cell grid width longitudinally through middle	m
dyu	U cell grid width latitudinally through middle	m
dxt	T cell grid width longitudinally through middle	m
dyt	T cell grid width latitudinally through middle	m
HTN	T cell width on north side	m
HTE	T cell width on east side	m
ANGLE (χ^u)	angle grid makes with lat line on U grid	radians
ANGLET (χ^t)	angle grid makes with lat line on T grid	radians

Table 9 lists all prognostic and diagnostic fields that can be written to the history file from an ice model integration (see the CSIM User's Guide Version 4 for instructions on how to reduce the number of fields in the history file). The field names and the equivalent variable name used in this document (in parentheses) are shown. Note that some of the fields have non-standard units and names not necessarily consistent with this document. History file format is netCDF. The history file frequency (i.e. how often written) can be either instantaneous (i.e. every time step), daily, monthly, or annual means. A sequence of history files is written during model execution at the desired frequency, all but the instantaneous files are time averaged over the interval between writes (see the CSIM User's Guide Version 4 for more information). There is one exception to time averaging: the normalized principal stress components (sig1 and sig2) are always instantaneous because time average stress states at geographically fixed points are not physically meaningful.

There are four tendency fields included in the history file: two ice volume and two ice area tendencies $[(\partial V/\partial t)_T$, $(\partial V/\partial t)_D]$ and $[(\partial A/\partial t)_T)$, $(\partial A/\partial t)_D]$ respectively. These tendencies are purely diagnostic, and distinguish the effect of thermodynamic processes (vertical and lateral, designated by subscript T) from dynamic processes (advection and rafting/ridging, designated by subscript D). They are computed at every time step, as for example the ice volume change due to thermodynamic processes:

$$(\partial V/\partial t)_T = [V(after\ vertical,\ lateral\ thermodynamics) - V(before)]/dt \tag{252}$$

and similarly for the remaining tendencies.

As noted in section 3, there are two horizontal grids used in the ice model: T-grid (a tracer grid with points at box mid-points), and U-grid (a velocity grid with points at box corners). In the history file, the prognostic and diagnostic fields not related to the dynamics are on the T-grid, while the ice/ocean velocity components and stresses are on the U-grid.

The user may add fields to the history file. The code is modified as follows. The parameter for the number of fields must be increased accordingly, the desired field(s) stored internally in an accumulator array, the field name, units and description specified in data statements in the netCDF write routine, and finally the field(s) included in the appropriate input parameter file (see the CSIM User's Guide Version 4 for more information).

Table 9: Prognostic and Diagnostic History Fields

Name	Description	Units
hi (V)	grid box mean ice thickness	m
hs (V_s)	grid box mean snow thickness	m
Tsfc (T_s)	snow/ice surface temperature	°C
aice (A)	aggregate ice area	%
aice1 (A_1)	ice area (category 1)	%
aice2 (A_2)	ice area (category 2)	%
aice3 (A_3)	ice area (category 3)	%
aice4 (A_4)	ice area (cateogry 4)	%
aice5 (A_5)	ice area (category 5)	%
u (u_i)	x direction ice velocity	cm s^{-1}
v (v_i)	y direction ice velocity	cm s^{-1}
Fswdn (F_{SWDN})	down solar flux	W m^{-2}
Flwdn (F_{LWDN})	down longwave flux	W m^{-2}
snow (F_{SNW})	snow fall rate	cm day^{-1}
rain (F_{RN})	rain fall rate	cm day^{-1}
sst (T_o)	sea surface temperature	°C
sss (S_o)	sea surface salinity	psu
uocn (u_o)	x direction ocean current	cm s^{-1}
vocn (v_o)	y direction ocean current	cm s^{-1}
frzmlt (F_{Qoi})	freezing/melting potential	W m^{-2}

Prognostic and Diagnostic History Fields continued

Name	Description	Units
Fswabs (F_{SW})	absorbed solar flx in snow/ice/ocean	W m^{-2}
albsni (α_{bb})	snow-ice broad band albedo	%
Flat (F_{LH})	latent heat flux	W m^{-2}
Fsens (F_{SH})	sensible heat flux	W m^{-2}
Flwout (F_{LWUP})	outgoing long wave flux	W m^{-2}
evap (F_{EVAP})	evaporative water flux	cm day^{-1}
Tref (T_{REF})	2 m reference air temperature	°C
growb ($\Sigma(\delta h\|_{\rm basal} > 0)_n A_n$)	basal ice growth	cm day^{-1}
frazil ($F_{Qoi}/q_f > 0$)	frazil ice growth	cm day^{-1}
snoice ($\Sigma\|z_{int}\|_n A_n$)	snow-ice conversion	cm day^{-1}
meltb ($\Sigma(\delta h\|_{\rm basal} < 0)_n A_n$)	basal ice melt	cm day^{-1}
meltt ($\Sigma(\delta h\|_{\rm melt} < 0)_n A_n$)	top ice melt	cm day^{-1}
meltl (VR_{side})	lateral ice melt	cm day^{-1}
Fresh (F_{Wo})	fresh water flux ice to ocean	cm day^{-1}
Fhnet (F_{Qio})	net heat flux ice to ocean	W m^{-2}
strairx (τ_{ax})	x direction atm/ice stress	N m^{-2}
strairy (τ_{ay})	y direction atm/ice stress	N m^{-2}
strtltx ($H_{ox} = \bar{m}g\partial H_o/\partial x$)	x direction sea surface tilt stress	N m^{-2}
strtlty ($H_{oy} = \bar{m}g\partial H_o/\partial y$)	y direction sea surface tilt stress	N m^{-2}
strcorx ($+\bar{m}fv_i$)	x direction coriolis stress	N m^{-2}
strcory ($-\bar{m}fu_i$)	y direction coriolis stress	N m^{-2}
strocnx (τ_{ox})	x direction ocean/ice stress	N m^{-2}
strocny (τ_{oy})	y direction ocean/ice stress	N m^{-2}
strintx $(\nabla \cdot \boldsymbol{\sigma})_x$	x direction div internal ice stress tensor	N m^{-2}
strinty $(\nabla \cdot \boldsymbol{\sigma})_y$	y direction div internal ice stress tensor	N m^{-2}
strength (P)	compressive ice strength	N m^{-1}
divu ($\dot{\epsilon}_I$)	strain rate (divergence)	% day^{-1}
shear ($\dot{\epsilon}_{II}$)	strain rate (shear)	% day^{-1}
opening ($\dot{\epsilon}_I + \|\dot{\epsilon}\|C(\theta)$)	lead opening rate	% day^{-1}
sig1 (σ_I)	norm principal stress component 1	
sig2 (σ_{II})	norm principal stress component 2	
dvidtt $(\partial V/\partial t)_T$	ice volume tendency thermodynamics	cm day^{-1}
dvidtd $(\partial V/\partial t)_D$	ice volume tendency dynamics	cm day^{-1}
daidtt $(\partial A/\partial t)_T$	area tendency thermodynamics	% day^{-1}
daidtd $(\partial A/\partial t)_D$	area tendency dynamics	% day^{-1}

7 Summary

The CSIM4 sea ice model addresses several recommendations of the CCSM PCWG made during 1999-2001. Areas of needed improvement in the CCSM sea ice model were:

(1) a plastic rheology with an elliptical yield curve

(2) enhanced sea ice thermodynamics

(3) an ice thickness distribution

(4) elimination of spurious polar convergence near the north pole

(5) an ice model on same grid as the ocean model

(6) an efficient parallel version of the model

(7) and an active ice only framework for testing the ice model.

The CSIM4 sea ice model meets all of these recommendations.

Constants

Table 10: List of Physical Constants

Symbol	Code Symbol	Description	Value
ρ_s	rhos	Density of snow	330 kg m^{-3}
ρ_i	rhoi	Density of ice	917 kg m^{-3}
ρ_o	rhow	Density of seawater	1026 kg m^{-3}
C_p	cp_air	Specific heat of atmosphere dry	1005 J kg^{-1} K^{-1}
C_{pwv}	cpwv	Specific heat of atmosphere water	1810 J kg^{-1} K^{-1}
c_s	cp_sno	Specific heat of snow	0 J kg^{-1} K^{-1}
c_0	cp_ice	Specific heat of fresh ice	2054 J kg^{-1} K^{-1}
c_o	cp_ocn	Specific heat of ocean	4218 J kg^{-1} K^{-1}
z_i	ice_ruf	Aerodynamic roughness of ice	5.0x10^{-4} m
z_{ref}	zref	Reference height for bulk fluxes	10 m
$q_1(ice)$	qqqice	saturation specific humidity const	11637800
$q_2(ice)$	TTTice	saturation specific humidity const	5897.8
$q_1(ocean)$	qqqocn	saturation specific humidity const	627572.4
$q_2(ocean)$	TTTocn	saturation specific humidity const	5107.4
c_d	—	Drag coefficient for water on ice	0.00536
h_{min}	hi_min	Minimum ice thickness for cat 1	0.1 m
h_{smin}	hsmin	Minimum snow depth for heat eqn	0.01 m or 0.00001 m
k_s	ksno	Thermal conductivity of snow	0.31 W m^{-1} K^{-1}
k_{fi}	kice	Thermal conductivity of fresh ice	2.0340 W m^{-1} K^{-1}
β	beta	Thermal conductivity ice constant	0.1172 W m^{-1} ppt^{-1}
u_{min}	—	Minimum ice/ocean friction velocity	0.001ms^{-1}
q_f	qio=-rhoi*Lfus	Frazil ice latent heat of formation	2.9717x10^5 J kg^{-1}
L_i	Lfus	Latent heat of fusion of ice	3.340x10^5 J kg^{-1}
L_s	Lsub	Latent heat of sublimation	2.835x10^6 J kg^{-1}
L_v	Lvap	Latent heat of vaporization	2.501x10^6 J kg^{-1}
T_f	Tffresh	Freezing temperature of freshwater	273.15 K
T_{of}	Tf	Freezing temperature of ocean	-1.8°C
T_{melt}	Timelt,Tsmelt	Melting temperature of top surface	0 °C
ΔT_{err}	T_errmax	Maximum error tolerance	5×10^{-4} °C
μ	depressT	Ocean freezing temperature constant	0.054 °C ppt^{-1}

Constants continued

Symbol	Code Symbol	Description	Value
S_{ro}	ocn_ref_salinity	Ocean frazil ice ref salinity	34.7 ppt
S_{ri}	ice_ref_salinity	Sea ice frazil ice ref salinity	0 ppt
g	gravit	Gravitational acceleration	9.80616 m s^{-2}
σ_{sb}	stefan_boltzmann	Stefan-Boltzmann constant	5.67x10^{-8} W m^{-2} K^{-4}
ε	emissivity	Ice emissivity	0.95
κ_{vs}	kappav	Ice SW visible extinction coeff	1.4 m^{-1}
κ_{ni}	kappan	Ice SW near-ir extinction coeff	17.6 m^{-1}
α_o	albocn	Mixed layer ocean albedo	0.06
E_0	eyc	dynamic constant	0.36
C_s	—	fraction of shear used for ridging	0.225
G^*	gstar	accumulative ice fraction for ridging	0.15
K	cK	max ridged ice thickness constant	100 m
Z	Zfric	ratio tot e diss to pot e gain	17
C_{pe}	cpe	ice/ocn potential energy constant	450 N m^{-3}

List of Acronyms

Symbol	Description
AIO	Active Ice Only- the D configuration of CCSM2 with active ice
CCM	Climate System Model
CCSM	Community Climate System Model
CREL	Cryogenics Research Environmental Laboratory
CSIM	Community Sea Ice Model
CU	University of Colorado
EVP	Elastic Viscous Plastic sea ice dynamics
ITD	Ice Thickness Distribution
netCDF	network Common Data Format data structure
MPDATA	Multidimensional Positive-Definite Advection Transport Algortihm
PCWG	Polar Climate Working Group
POP	Parallel Ocean Program, the CCSM Ocean component model
SHEBA	Surface HEat Budget of the Arctic field program
SST	Sea Surface Temperature
UW	University of Washington
VP	Viscous Plastic sea ice dynamics

Appendix: Non-Default Physics Options

During the development of CSIM4, several physics options were incorporated into the sea ice model. Some of these relate to options not chosen as default, and others are possible candidates for future versions of CSIM. These physics options have been retained for the released version of CSIM4. In this appendix these options are briefly described.

It would be very useful to run CSIM4 in column mode, namely, as a **1D column model** with prescribed inputs (i.e. SHEBA data or other). This would allow efficient testing and validation of the vertical sea ice physics. There is some code to implement this option in the CSIM4 source, but this option has not been thoroughly tested.

An earlier method for evaluating thickness space transport is the **delta scheme** of Bitz (2000); Bitz et al. (2001). This method represents the distribution function $g(h)$ as a sum of delta functions, one for each populated ice thickness category. This physics option has the limitation of underpopulating the ITD, resulting in jumps in properties across category boundaries. The linear remapping scheme in CSIM4 was chosen as default because it represents $g(h)$ in each category as a linear function, and allows for incremental transport between categories, yielding a much smoother representation.

For some initial testing and comparison studies, a physics option of running with **thermodyanmics only** is available. For this option, the dynamics is not computed, and ice velocities are zeroed so that there is no ice advection. This option allows an assessment of sea ice model simulations without dynamics.

The previous version of the sea ice model evaluated the ice strength using the method of Hibler (1979). This **ice strength parameterization** depends only on the mean ice thickness and ice fraction. The scheme in CSIM4 makes use of the ice participating in ridging, but is dependable only if the ITD is well resolved (i.e. has at least five categories). For fewer categories, it is preferable to use the Hibler (1979) expression.

Very high spatial resolution implementations of the EVP dynamics using a reasonable subcycling time step can produce simulations for which the elastic waves useful for regularization are not sufficiently damped. In this case, a physical option of **damping of elastic waves** is available, as in Hunke (2001); Hunke and Lipscomb (2002). The elastic wave damping is enhanced by reducing the ice strength compared to the default in CSIM4. For the resolution and subcycling time steps used in CSIM4, this option is not necessary.

The CSIM4 ridging scheme by default retains snow cover on ridged ice. However, another available physics option is to allow snow on ice participating in ridging to fall into the ocean. This **snow into ocean** option is not well tested, will cause the fresh water budget diagnostics to not be closed, and is not supported.

The previous horizontal advection scheme was upwind, as described in section 4.11. This **upwind advection** is retained as an option in CSIM4. It is useful for assessing the effects of second order as against first order advection. Because of the increased accuracy of the MPDATA advection scheme over the upwind, the former is the default for CSIM4.

References

Allison, I., R. E. Brant and S. G. Warren, 1993: East antarctic sea ice: albedo, thickness distribution, and snow cover. *J. Geophys. Res.*, **98**, 12417–12429.

Arbetter, T. E., J. A. Curry and J. A. Maslanik, 1999: Effects of rheology and ice thickness distribution in a dynamic-thermodynamic sea ice model. *J. Phys. Oceanogr.*, **29**, 2656–2670.

Bettge, T. W., J. W. Weatherly, W. M. Washington, D. Pollard, B. P. Briegleb and W. G. Strand Jr., 1996: *The NCAR CSM Sea Ice Model.* pp. 25, NCAR Technical Note, TN-425+STR.

Bitz, C. M., 2000: *Documentation of a Lagrangian sea ice thickness distribution model with energy-conserving thermodyanmics.* U. of Washington APL-UW TM 4-99.

Bitz, C. M., M. Holland, A. J. Weaver and M. Eby, 2001: Simulating the ice-thickness distribution in a coupled climate model. *J. Geophys. Res.*, **106**, 2441–2464.

Bitz, C. M. and W. H. Lipscomb, 1999: An energy-conserving thermodynamic model of sea ice. *J. Geophys. Res.*, **104**, 15,669–15,677.

Boville, B. A. and P. R. Gent, 1998: The NCAR climate system model, version one. *J. Climate*, **11**, 1115–1130.

Briegleb, B. P., 2002: *CSIM Code Reference Manual.* National Center for Atmospheric Research, http://www.ccsm.ucar.edu/models/ice-csim4.

Bryan, F. O., B. G. Kauffman, W. G. Large and P. R. Gent, 1996: *The NCAR CSM Flux Coupler.* NCAR Technical Note NCAR/TN-424+STR, National Center for Atmospheric Research, Boulder, Colorado.

Curry, J. A., J. Schramm and E. Ebert, 1995: Sea ice-albedo climate feedback mechanism. *J. Climate*, **8**, 240–247.

Curry, J. A., J. L. Schramm, D. K. Perovich and J. O. Pinto, 2001: Applications of sheba/fire data to evaluation of snow/ice albedo parameterizations. *J. Geophys. Res.*, **106**, 15,345–15,355.

Ebert, E. E. and J. A. Curry, 1993: An intermediate one-dimensional thermodynamic sea ice model for investigating ice-atmosphere interactions. *J. Geophys. Res.*, **98**, 10085–10109.

Flato, G. M. and W. D. Hibler, 1992: Modeling pack ice as a cavitating fluid. *J. Phys. Oceanogr.*, **22**, 626–651.

Flato, G. M. and W. D. Hibler, 1995: Ridging and strength in modelling the thickness distribution of Arctic sea ice. *J. Geophys. Res.*, **100**, 18611–18626.

Grenfell, T. C., S. G. Warren and P. C. Mullen, 1994: Reflection of solar radiation by the antarctic snow surface at ultraviolet, visible, and near-infrared wavelengths. *J. Geophys. Res.*, **99**, 18669–18684.

Hibler, W. D., 1979: A dynamic thermodynamic sea ice model. *J. Phys. Oceanogr.*, **9**, 815–846.

Hibler, W. D., 1980: Modeling a variable thickness ice cover. *Mon. Wea. Rev.*, **108**, 1943–1973.

Hogstrom, U., 1988: Non-dimensional wind and temperature profiles in the atmospheric surface layer: a re-evaluation. *Boundary-Layer Meteorol.*, **42**, 55–78.

Hopkins, M. A. and W. D. Hibler, 1991: On the ridging of a thin sheet of lead ice. *Ann. Glaciol.*, **15**, 81–86.

Hunke, E. C., 2001: Viscous-plastic sea ice dynamics with the evp model: Linearization issues. *J. Comp. Phys.*, **170**, 18–38.

Hunke, E. C. and J. K. Dukowicz, 1997: An elastic-viscous-plastic model for sea ice dynamics. *J. Phys. Oceanogr.*, **27**, 1849–1867.

Hunke, E. C. and J. K. Dukowicz, 2002: The elastic-viscous-plastic sea ice dynamics model in general orthogonal curvilinear coordinates on a sphere–incorporation of metric terms. *Mon. Wea. Rev.*, In press.

Hunke, E. C. and W. H. Lipscomb, 2002: *CICE: the Los Alamos sea ice model, documentation and software User's Manual.* T-3 Fluid Dynamics Group, Los Alamos National Laboratory, Tech. Rep. LACC-98-16 v.3.

Hunke, E. C. and Y. Zhang, 1999: A comparison of sea ice dynamics models at high resolution. *Mon. Wea. Rev.*, **127**, 396–408.

Kreyscher, M., M.Harder, P.Lemke and G.M.Flato, 2000: Results of the sea ice model intercomparison project: evaluation of sea ice rheology schemes for use in climate simulation. *J. Geophys. Res.*, **105**, 11299–11320.

Large, W. G., 1998: Ocean modeling and parameterization. in E.P.Chassignet and J. (eds.), editors, *Modeling and parameterizing the ocean planetary boundary layer*, pp. 81–120. Kluwer Academic Publishers, Printed in the Netherlands.

Lipscomb, W. H., 2001: Remapping the thickness distribution in sea ice models. *J. Geophys. Res.*, **106**, 13,989–14,000.

Maykut, G. A. and D. Perovich, 1987: The role of shortwave radiation in the summer decay of a sea ice cover. *J. Geophys. Res.*, **92**, 7032–7044.

Maykut, G. A. and N. Untersteiner, 1971: Some results from a time-dependent thermodynamic model of sea ice. *J. Geophys. Res.*, **76**, 1550–1575.

McPhee, M. G., 1992: Turbulent heat flux in the upper ocean under sea ice. *J. Geophys. Res.*, **97**, 5365–5379.

Ono, N., 1967: Specific heat and heat of fusion of sea ice. in H. Oura, editor, *Physics of Snow and Ice*, Vol. I, pp. 599–610. Institute of Low Temperature Science, Hokkaido, Japan.

Paulson, C. A. and J. J. Simpson, 1977: Irradiance measurements in the upper ocean. *J. Phys. Oceanogr.*, **7**, 952–956.

Rothrock, D. A., 1975: The energetics of the plastic deformation of pack ice by ridging. *J. Geophys. Res.*, **80**, 4514–4519.

Rothrock, D. A. and A. S. Thorndike, 1984: Measuring the sea ice floe size distribution. *J. Geophys. Res.*, **89**, 6477–6486.

Schramm, J. L., 2002: *Community Sea Ice Model (CSIM) User's Guide Version 4.0*. National Center for Atmospheric Research, http://www.ccsm.ucar.edu/models/ice-csim4.

Semtner, A. J., 1976: A model for the thermodynamic growth of sea ice in numerical investigations of climate. *J. Phys. Oceanogr.*, **6**, 379–389.

Smolarkiewicz, P. K., 1983: A simple positive definite advection scheme with small implicit diffusion. *Mon. Wea. Rev.*, **111**, 479–486.

Smolarkiewicz, P. K., 1984: A fully multidimensional positive definite advection scheme with small implicit diffusion. *J. Comput. Phys.*, **54**, 325–362.

Stern, H. L., D. A. Rothrock and R. Kwok, 1995: Open water production in Arctic sea ice: satellite measurements and model parameterizations. *J. Geophys. Res.*, **100**, 20,601–12.

Thorndike, A. S., D. S. Rothrock, G. A. Maykut and R. Colony, 1975: The thickness distribution of sea ice. *J. Geophys. Res.*, **80**, 4501–4513.

Untersteiner, N., 1961: On the mass and heat budget of Arctic sea ice. *Arch. Meteorol. Geophys. Bioklimatol., A*, **12**, 151–182.

Weatherly, J. W., B. P. Briegleb, W. G. Large and J. A. Maslanik, 1998: Sea ice and polar climate in the NCAR CSM. *J. Climate*, **11**, 1472–1486.